

Electron Energy-Loss Spectroscopy Study of Polyatomic
Molecular Systems Under Pyrolytic Conditions

Thesis by

Isaac de Melo Xavier, Junior

In Partial Fulfillment of the Requirements
for the Degree of
Doctor of Philosophy

California Institute of Technology
Pasadena, California

1989

(Submitted September 20, 1988)

This thesis is dedicated to my wife, Ana Corinta, to my son, Bruno,
and to my parents for their love support and patience.

ACKNOWLEDGMENTS

The work contained in this thesis required the cooperation and assistance of many fine people.

I would like to thank my advisor, Professor Aron Kuppermann, for his support during the second half of my stay at Caltech. I would also like to thank my former advisor, the enthusiastic Professor Ahmed H. Zewail, for letting me explore the frontiers of the optical coherent transients; and to Professor Daniel P. Weitekamp for providing deep physical insight into the coherent transient phenomena.

I am in debt to J. Spencer Baskin for his friendship and for his *wise* help during the last five years. I am very thankful to the *easy going* Dr. Kerry N. Walzl for teaching me the nuts and bolts of the EIS and for his friendship. I owe a special thanks for the friendship of *the always happy guy*, Guy Duremberg, *the optimist*, Gabor Faludi and *the tireless*, C. Russ Bowers.

The work presented here would not have been possible were it not for the aid and assistance of the personnel of the chemistry department. I personally thank to Guy Duremberg, Toni Stark, Ray Garcia and Delmer Dill for their cooperation in the construction, design, and maintenance of the instruments used in these studies. Jim Olson, Jim Gangwer and Pavel Stivek deserve thanks for their efforts in keeping the pumping systems in good condition. I owe a great deal to Tom Dunn and Jack Guledjian for the miracles they worked in keeping our electronics operational. I also owe a great deal to Gabor Faludi for building the state of art optical cells.

I wish to thank the other members of the Kuppermann group, both past and present, Maria Arnazzi, Garth Parker, Mary Rodgers, Qiu Jin, Ashraf Ali, Bruno Lepetit, Steve Cuccaro, Paul Hipies, Zhengwei Peng, and Mark Wu, for their collaboration.

I also wish to thank the other members of the Zewail group, both past and present, Edward Sleva, Lutfur Kundkar, Norbert Scherer, Joseph Perry, Peter Felker, Brian Keelan, Jack Syage, Marcos Dantus, Larry Peng, David Semmes, and Fuad Doany, for their collaboration.

I wish to thank our group secretaries, Lena Lenore, Joyce Ferrante, and Laurie Fletcher for their assistance.

I wish to thank my Brazilian friends Kazunori and Yaeko Watari, Rogério and Silvia Livi, Marcílio and Inêz Ferreira for their *amizade*.

I want to acknowledge the financial support from CAPES (Brazilian agency), from the *Universidade Federal de Pernambuco*, and from the Department of Energy (DOE).

Last and certainly most of all, I want to express my love for Ana Corinta and Bruno, and the joy they have brought into my life.

ABSTRACT

The technique of variable-angle, electron energy-loss spectroscopy has been used to study the electronic spectroscopy of the diketene molecule. The experiment was performed using incident electron beam energies of 25 eV and 50 eV, and at scattering angles between 10° and 90°. The energy-loss region from 2 eV to 11 eV was examined. One spin-forbidden transition has been observed at 4.36 eV and three others that are spin-allowed have been located at 5.89 eV, 6.88 eV and 7.84 eV. Based on the intensity variation of these transitions with impact energy and scattering angle, and through analogy with simpler molecules, the first three transitions are tentatively assigned to an $n \rightarrow \pi^*$ transition, a $\pi \rightarrow \sigma^*(3s)$ Rydberg transition and a $\pi \rightarrow \pi^*$ transition.

Thermal decomposition of chlorodifluoromethane, chloroform, dichloromethane and chloromethane under flash-vacuum pyrolysis conditions (900-1100°C) was investigated by the technique of electron energy-loss spectroscopy, using the impact energy of 50 eV and a scattering angle of 10°. The pyrolytic reaction follows a hydrogen-chloride α -elimination pathway. The difluoromethylene radical was produced from chlorodifluoromethane pyrolysis at 900°C and identified by its $\tilde{X}^1A_1 \rightarrow \tilde{A}^1B_1$ band at 5.04 eV.

Finally, a number of exploratory studies have been performed. The thermal decomposition of diketene was studied under flash vacuum pressures (1-10 mTorr) and temperatures ranging from 500°C to 1000°C. The complete decomposition of the diketene molecule into two ketene molecules was achieved at 900°C. The pyrolysis of trifluoromethyl iodide molecule at 1000°C produced an electron energy-loss spectrum with several iodine-atom, sharp peaks and only a small shoulder at 8.37 eV as a possible trifluoromethyl radical feature. The electron energy-loss spectrum of trichlorobromomethane at 900°C mainly showed features from bromine

atom, chlorine molecule and tetrachloroethylene. Hexachloroacetone decomposed partially at 900°C , but showed well-defined features from chlorine, carbon monoxide and tetrachloroethylene molecules. Bromodichloromethane molecule was investigated at 1000°C and produced a congested, electron energy-loss spectrum with bromine-atom, hydrogen-bromide, hydrogen-chloride and tetrachloroethylene features.

TABLE OF CONTENTS

CHAPTER 1: INTRODUCTION	1
References	4
CHAPTER 2: THE THEORY OF ELECTRON IMPACT	5
References	8
CHAPTER 3: EXPERIMENTAL ELECTRON-IMPACT SPECTROSCOPY .	9
References	14
Figures	15
CHAPTER 4: AN ELECTRON-IMPACT SPECTROSCOPY INVESTIGATION OF DIKETENE	18
References	24
Figures	26
CHAPTER 5: STUDY OF GAS-PHASE PRODUCTS FORMED BY FLASH- VACUUM PYROLYSIS OF HALOMETHANES USING ELECTRON ENERGY-LOSS SPECTROSCOPY	33
References	40
Figures	42
CHAPTER 6: EXPLORATORY STUDIES	52
References	57
Figures	59
APPENDIX 1: AN ELECTRON-IMPACT SPECTROSCOPY INVESTIGATION OF CH ₃ AND SOME OF ITS PYROLYTIC PRECURSORS	76
References	86
Figures	88

APPENDIX 2: ELECTRON-IMPACT SPECTROSCOPY OF VARIOUS DIKETONE COMPOUNDS	97
References	110
Figures	113

CHAPTER 1

INTRODUCTION

The studies reported here use the technique called electron energy-loss spectroscopy (EELS) or electron-impact spectroscopy (EIS), both terms being used interchangeably. EIS involves focusing a monoenergetic beam of electrons with initial energy E_o into a gaseous target and then measuring the energy of the scattered electrons at a scattering angle θ . Plotting scattered electron intensity versus energy lost by the incident electrons yields the energy-loss spectrum and is analogous to an optical absorption spectrum. These two types of spectra may be directly compared.

Two advantages over optical spectroscopy are provided by electron-impact spectroscopy: the capability of measuring an entire energy loss or absorption spectrum from the infrared to the vacuum ultraviolet in a single scan without alteration of the instrument and, more importantly, the ability to observe transitions which are forbidden by optical selection rules. A typical energy-loss spectrum spans a transition energy range of about 10 eV. Thus, a single spectrum may include features that result from low-energy excitations, such as vibrational transitions, that would be observed in the infrared region of an optical spectrum as well as features that result from excitation to high-lying electronic states that would be observed in the vacuum ultraviolet region of the optical spectrum. In addition, transition having excitation energy above 10 eV may be as readily observed as those below 10 eV by EIS. In contrast, the absence of window materials that are transparent above about 12 eV (105 nm LiF cut-off) make optical spectroscopy difficult in the high-energy region. The resolution of the electron energy-loss spectrum is substantially poorer than that of an optical spectrum at energies below

the vacuum ultraviolet. In the vacuum ultraviolet region, the resolution for the two techniques are still comparable. In the higher-lying, excited electronic states, vibrational structure is often lacking because of uncertainty principle broadening that is due to the very short lifetimes of these states.¹

The relative intensities of various types of transitions in electron scattering experiments is significantly different from those in optical studies. The principal difference is that the $\Delta S = 0$ selection rule of optical spectroscopy² is relaxed in electron impact. Spin-forbidden transitions that are very weak in optical spectroscopy are typically 0.02 to 0.5 times as intense as optically allowed excitations, at scattering angles greater than 40° and incident energies in the range 20 eV to 60 eV.^{3,4}

The mechanism that relaxes the $\Delta S = 0$ selection rule is known as the exchange excitation. First discussed by Oppenheimer⁵ in 1928, the incident electron is interchanged with a molecular electron. While the exchange process must still conserve the overall spin of the incident, electron-target, molecule system, the molecule may undergo a net spin change of unity, while the scattered electron will have the opposite spin as compared to the incident electron.

The intensities of spin-allowed but electric dipole-forbidden transitions are also enhanced relative to optically allowed excitations in electron scattering. Typically, these transitions are from 0.05 to 0.25 times as intense as optically allowed excitations. In electron scattering, spin-allowed transitions proceed primarily via a direct mechanism in which the incident electron interacts with the target through Coloumbic forces. These Coulomb interactions are believed to distort or polarize the molecular charge distribution and effectively alter the molecular symmetry allowing enhancement of dipole-forbidden transitions.

The different types of excitation mechanisms allow one to extract information regarding the nature of transitions by examining how spectral intensities change

as a function of the scattering angle θ and the incident electron energy E_o . More specifically, what is measured is the differential cross section $\frac{d\sigma}{d\Omega}$ (DCS), that is, the cross section per unit solid angle, for scattering into a given direction defined by the spherical polar angles θ and ϕ . For experiments in the gas phase with randomly oriented, molecules the DCS is independent of ϕ .⁴ Another experimental value of interest is the integral cross section Q , which is the differential cross section integrated over all scattering angles.

The following characteristics have been observed for the differential cross section when associated with various types of transitions.³ A transition that exhibits an approximately isotropic DCS (constant to within a factor of 2 or 3 over the range $\theta = 10^\circ$ to $\theta = 90^\circ$) is due to a spin-forbidden excitation. A transition displaying a strongly forward peaked DCS, which falls off by one to two orders of magnitude as θ increases from 10° to 90° , is due to a fully allowed transition (or elastic scattering peak). A DCS of intermediate behavior is most likely due to a spin-allowed/symmetry-forbidden transition.

REFERENCES

1. J. P. Byrne and I. G. Ross, *Aust. J. Chem.*, **24**, 1107 (1971).
2. S. P. McGlynn, T. Azumi, and M. Kinoshita, *Molecular Spectroscopy of the Triplet State*, Prentice-Hall, New Jersey (1969), p. 10.
3. A. Kuppermann, J. K. Rice, and S. Trajmar, *J. Phys. Chem.*, **72**, 3894 (1968).
4. S. Trajmar, J. K. Rice, and A. Kuppermann, *Adv. Chem. Phys.*, **18**, 15 (1970).
5. J. R. Oppenheimer, *Phys. Rev.*, **32**, 361 (1928).

CHAPTER 2

THE THEORY OF ELECTRON IMPACT

In this chapter, we will present a simple approach that uses potential scattering theory¹ in order to determine the general behavior of the differential cross section for both the direct (Coulomb interaction) and exchange-scattering processes. No attempt will be made for a rigorous derivation of the quantum mechanical formalisms of the electron-molecule scattering at low-impact energies. Detailed theoretical treatment can be found in the reviews on this subject.²⁻⁶

The wave function of the incident electron, when it is far away from the target molecule,⁷ has the form of a plane wave

$$\psi_{inc} = \exp(i\mathbf{k}\cdot\mathbf{r}), \quad (1)$$

where the \mathbf{r} is the electron's position vector and \mathbf{k} its wave-number vector. If the z axis is chosen as the direction of the incident electron, equation (1) becomes

$$\psi_{inc} = \exp(ikz). \quad (2)$$

Now, introducing a central field scattering potential, which interacts with the incident plane wave, the scattered electrons can be thought to emerge from the scattering center as an outgoing spherical wave which, as $r \rightarrow \infty$, has the form

$$\psi_{sc} = f(\theta) \frac{\exp(ikr)}{r}, \quad (3)$$

where $f(\theta)$ is the amplitude for the electron scattering into the direction that makes an angle θ with the direction of the incident electron. The asymptotic behavior of the electron's total wave function is given by

$$\psi = \exp(ikz) + f(\theta) \frac{\exp(ikr)}{r}, \quad (4)$$

and the differential cross section is related to the scattering amplitude by

$$\frac{d\sigma}{d\Omega} = |f(\theta)|^2. \quad (5)$$

By applying the partial wave analysis², it is possible to express the incident wave as a sum of products of radial and angular functions,

$$\exp(ikz) = \sum_{l=0}^{\infty} (2l+1) i^l j_l(kr) P_l(\cos\theta), \quad (6)$$

where j_l is the spherical Bessel function of order l and P_l is the l^{th} Legendre polynomial. One can consider the scattering processes as a distortion of the incident plane wave, which introduces a phase shift η_l in the different angular terms of the incident wave. In this way, the wave function must asymptotically reduce to the form of Equation (4) and the scattering amplitude must be related to this phase shift by

$$f(\theta) = \frac{1}{k} \sum_{l=0}^{\infty} (2l+1) \exp(2\eta_l) \sin(\eta_l) P_l(\cos\theta), \quad (7)$$

and the differential cross section can be written as

$$\frac{d\sigma}{d\Omega} = \frac{1}{4k^2} \left| \sum_{l=0}^{\infty} (2l+1) (\exp(2\eta_l) - 1) P_l(\cos\theta) \right|^2, \quad (8)$$

where each term in the expansion is called a contribution of partial wave l to the differential cross section. If η_l is small, it can be shown that⁴

$$\eta_l \approx -\frac{\pi}{2} \int_0^{\infty} [J_{l+\frac{1}{2}}(kr)]^2 U(r) r dr, \quad (9)$$

where $U(r) = \frac{2\mu}{\hbar^2} V(r)$ is the electron-molecule interaction potential, and $J_{l+\frac{1}{2}}$ is the regular Bessel function.

It is assumed that there exists an effective range r_{max} for which $r^2 U(r)$ never exceeds some finite value, and this can be expressed by the following conditions,

$$r^2|U(r)| \leq a \quad 0 \leq r \leq r_{max} \quad (10a)$$

$$r^2|U(r)| = 0 \quad r_{max} > r. \quad (10b)$$

At low enough impact energy such that $\frac{kr_{max}}{2} \ll 1$, one can use the small argument approximation of $J_{l+\frac{1}{2}}$,⁹ which, applied to Equation (9), gives

$$|\eta_l| < \frac{\pi}{2} \frac{a}{[\Gamma(l + \frac{1}{2})]^2} \int_0^{r_{max}} \left(\frac{kr}{2}\right)^{2l+1} \frac{dr}{r} = \frac{2\pi a}{(2l+1)^3} \left(\frac{kr_{max}}{2}\right)^{2l+1} \frac{1}{[\Gamma(l + \frac{1}{2})]^2} \quad (11)$$

For small η_l , Equation (8) can be written as

$$\frac{d\sigma}{d\Omega} \approx \frac{1}{k^2} \left| \sum_{l=0}^{\infty} (2l+1)\eta_l P_l(\cos\theta) \right|^2. \quad (12)$$

By examining Equation (12), one can observe that for long-range potentials, such as the Coulomb interaction, there will be more partial waves contributing to the differential cross section than for short-range potentials such as those involved in the exchange scattering processes. The inclusion of more Legendre polynomials makes the differential cross section to be more forward-peaked, whereas the exchange processes would produce a more isotropic differential cross section. At low impact-energy (low k), only a few partial waves are included and the differential cross section presents again a more isotropic behavior.

At higher-impact energies, the relation between the optical spectrum and the electron-impact spectrum can be found in the first Born approximation. Using this approach, the optical oscillator strengths can be obtained from electron-scattering measurements.^{6,9} For certain types of symmetry-forbidden processes, calculations have been performed to predict the behavior of the differential cross section.^{10,11}

References

1. S. Trajmar, J. K. Rice, and A. Kuppermann, *Adv. Chem. Phys.*, **18**, 15 (1970).
2. H. S. Massey and E. H. S. Burhop, *Electronic and Ionic Impact Phenomena*, Vol. **1**, Oxford Press, London (1969).
3. A. Messiah, *Quantum Mechanics*, Vol. **2**, Wiley, New York (1961), Chap. 19.
4. N. F. Mott and H. S. Massey, *The Theory of Atomic Collisions*, 3rd ed., Oxford Press, London (1965).
5. E. N. Lassetre and A. Skerbele in *Inelastic Electron Scattering, Methods of Experimental Physics*, Vol. **3**, Academic Press, New York (1974).
6. M. Inokuti, *Rev. Mod. Phys.*, **43**, 297 (1971).
7. E. Merzbacher, *Quantum Mechanics*, 2nd ed., Wiley, New York (1970), Chap. 11.
8. H. S. Massey in *Handbuch Der Physik*, Vol. **36**, S. Flugge, Ed., Springer-Verlag, Berlin (1956), p. 240.
9. R. J. Celotta and R. H. Huebner in *Electron Spectroscopy: Theory, Techniques, and Applications*, Vol. **3**, C. R. Brundle, and A. D. Baker, Eds., Academic Press, New York (197), p. 45.
10. W. A. Goddard III, D. L. Hustis, D. C. Cartwright, and S. Trajmar, *Chem. Phys. Lett.*, **11**, 329 (1971).
11. F. H. Read and G. L. Whiterod, *Proc. Phys. Soc.*, **82**, 435 (1963).

CHAPTER 3

EXPERIMENTAL ELECTRON-IMPACT SPECTROSCOPY

The results presented in this thesis were obtained using the electron-impact spectrometer, which has been described in the Ph.D. theses of C. F. Koerting¹ and K. N. Walzl.² In this chapter we will present a brief description of the spectrometer, including any recent changes.

a) Vacuum system

The vacuum system used in these experiments consists primarily of a 70 liter, stainless steel chamber pumped by a 1500 liter/sec turbomolecular pump (Balzers, TPU 1500). This turbomolecular pump is backed by a 500 liter/min mechanical pump. The main chamber base pressure varies from 5×10^{-8} to 1×10^{-7} Torr. In addition to the main chamber pumping system, two other pumps are mounted on the spectrometer. A 50 liter/sec, turbomolecular pump (Balzers, TPU 050) differentially (with respect to the main chamber) pumps the electron optics, which are enclosed in isolation housings. A 60 liter/min mechanical pump provides the back pumping for the TPU 050 turbo pump. The base pressure of this pumping system after a couple of days of pumping varies from 3×10^{-7} to 8×10^{-7} Torr. The other pump is a gravity-fed, liquid nitrogen cryotrap, which is located above the sample jet source and acts as beam dump. Two orders of magnitude in pressure can be maintained between the electron optics and the main chamber. During a scan the pressure in the optics housing is kept at 9×10^{-7} to 3×10^{-6} Torr.

The entire vacuum system is under the control of an interlock system described by Mosher.³ This system shuts the two turbomolecular pumps in case of an over-

pressure. This interlock system also turns off the filament in the electron gun and the high voltage to the detector in order to prevent damage to these components.

The turbomolecular pumps replaced the two previous, mercury-diffusion pumps. This replacement eliminated the costly liquid nitrogen consumption by the diffusion pump traps and provided a substantial improvement in the scattering chamber's ultimate pressure and in the pumping speed. As a result, after opening the system up to atmospheric pressure, the time needed to bring it back down to the low pressure needed to restart operation, was significantly decreased.

b) Electron optics

The spectrometer and electronics are contained within an RF shielded enclosure providing 100 *dB* attenuation of electromagnetic frequencies in the range of 10 *KHz* to 100 *GHz*. The electron optics in the spectrometer are exposed to a reduced ambient magnetic field of 5 *mG* because of the shielding provided by a 0.050 *inch* thick μ -metal sheath.

The electron optics form the heart of the electron-impact spectrometer since the operational characteristics of the instrument are determined by them. The set of electron optics, used for the experiments reported here, is described by Koerting,¹ Walzl² and Rianda.⁴ Briefly, electrons are emitted from a tungsten filament, focused onto a hemispherical-sector, electron-energy analyzer, energy-selected, and focused onto the target gas. Typical beam currents at the scattering center range from 1 to 20 *nAmp*. Scattered electrons are then focused into a second hemispherical analyzer, energy-analyzed again, and finally focused onto an electron multiplier and detected. The spectrometer resolution, measured as the full width at half-maximum (FWHM) of the elastic peak, is typically 50-100 *meV*. The schematic diagram of the electron optics of our electron-impact spectrometer is shown in Figure 1.

The monochromator is mounted on a rotatable gear wheel and may be turned from -15° to 110° about the rotation axis. The actual scattering angle varies from about -10° to 100° because the analyzer and monochromator lie in a plane 20° with respect to the horizontal.

c) Target source

Two gas-target sources were used for the experiments reported here. The first is a static gas cell consisting of a copper (OFHC) tube, closed on one end, with a 0.060 *inch* wide slot cut 120° around its circumference at 20° with respect to the horizontal and also two 0.060 *inch* holes drilled opposite to the slot at 0° and 55° . These holes allow the electron beam to exit into the analyzer and Faraday cup, respectively. This tube slides onto another copper tube, by which the sample gas is admitted, passing through the center of the rotating table via a rotary seal.

The other gas-target source is an effusive jet produced by a quartz pyrolysis tube shown in Figure 2. This inlet consists of a 0.25 *inch* OD, clear-fused, quartz tube, which is constricted at one end to form a 0.125 *inch* OD, 0.060 *inch* ID, and 0.35 *inch* long capillary tube. The clear-fused quartz (from QSI) has a softening point of $1650^\circ C$.⁵ The pyrolyzer is heated by tantalum-sheathed, double-stranded, tungsten-rhenium alloy wires (manufactured by Semco Inc.) wound over the quartz capillary. The alloy has 26% of tungsten and 5% of rhenium with a maximum recommended working temperature of $2300^\circ C$.⁶ The tantalum sheath has a maximum working temperature of $2400^\circ C$.⁶ The electrical insulator between the wires and the sheath is high-purity, alpha alumina, which has low vapor pressure ($< 10^{-6} Torr$) for its maximum working temperature of $1900^\circ C$.⁷ The heater assembly is wrapped with two layers of 0.005 *inch* tantalum foil, which acts as a radiation shield. Temperatures up to $1100^\circ C$ have been obtained, as measured

by an optical pyrometer, through a quartz window located on the spectrometer's front flange.

We attempted to develop an effusive jet pyrolyzer capable of reaching temperatures above 1100°C under reliable operating conditions. A ceramic tube with similar shape and dimensions to the quartz one was carefully made from an Aremcolox (Grade 502-1400, maximum working temperature of 1427°C^8), machinable, ceramic rod. Grooves were machined into the capillary end in order to fit a double-stranded, tantalum wire heater coil, which was held in place by a cap made of the same machinable ceramic. This cap was externally covered with a 0.1 *inch* tantalum foil shield to minimize the radiation losses. It was expected that this entirely home-built pyrolyzer would get higher temperatures because the heater wires were thicker and less brittle than the tungsten-rhenium alloy wires. However, tests performed at 1100°C showed permanent deformation of the ceramic heater assembly.

d) Data collection system and handling

The detection of electrons is accomplished by a Galileo SEM 4219, Spiraltron, electron multiplier, which is connected to a Mechtronics Nuclear Model 509 NIM preamplifier. A MSC 8001, Z80-based computer acts as a programmable multichannel scaler, which collects the counts from the electron multiplier and stores them in the memory. The computer also sweeps the voltages of the electron energy analyzer while incrementing the storage locations in its memory, resulting in the collection of the spectrum under study. The computer also displays the spectrum being accumulated on an oscilloscope and can plot the spectrum on an X-Y recorder. The spectra accumulated are stored on a diskette for transfer to a mainframe (VAX 11/780) computer where the data are analyzed. The transferred data may be further analyzed by a set of data analysis programs described by

Flicker⁹ and Rianda.⁴ The procedure for using the data analysis programs is described in Appendix 4 of the K. N. Walzl thesis.² The only modification is the use of the laser printer for all the necessary plotting.

References

1. C. F. Koerting, *Ph. D. Thesis* (California Institute of Technology, Pasadena, CA, 1985).
2. K. N. Walzl, *Ph.D. Thesis* (California Institute of Technology, Pasadena, CA, 1987).
3. O. A. Mosher, *Ph.D. Thesis* (California Institute of Technology, Pasadena, CA, 1975).
4. R. Rianda, *Ph.D. Thesis* (California Institute of Technology, Pasadena, CA, 1981).
5. *Catalog 882*, Quartz Scientific Inc., Fairport Harbor (OH), p. 2.
6. *Sempak Catalog 672*, Scientific Engineering and Manufacturing Company Inc., North Hollywood (CA), p. 14.
7. Reference 6, pp. 18-20.
8. *Catalog M12*, Aremco Products Inc., Ossining (NY).
9. W. M. Flicker, *Ph.D. Thesis* (California Institute of Technology, Pasadena, CA, 1976).

Figure Captions

Fig. 1 Schematic diagram of the electron optics that are described in detail by Koerting¹.

Fig. 2 Schematic diagram showing the effusive jet target source. GI: gas inlet, H: tantalum-sheathed, tungsten-rhenium alloy, wire heater, QT: clear-fused, quartz tube, SL: swagelock fitting, TS: tantalum shield.

FIGURE 1

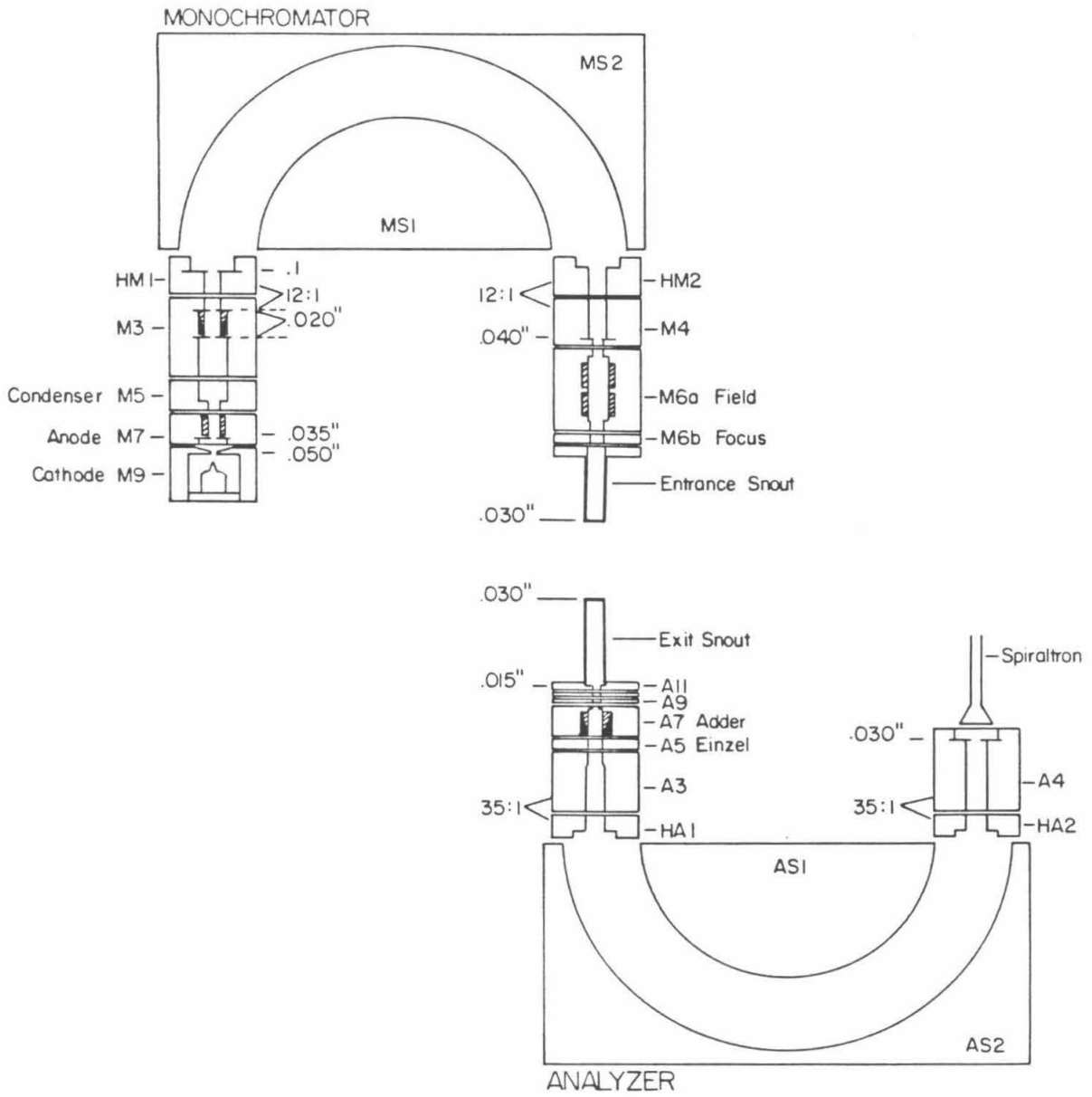
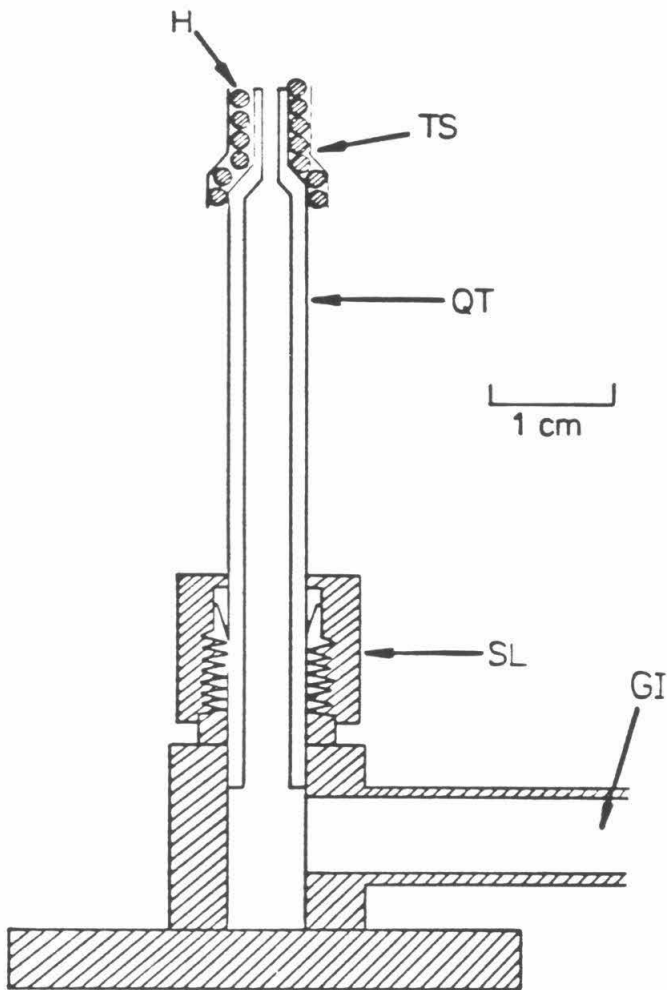


FIGURE 2



CHAPTER 4

Paper 1: *AN ELECTRON-IMPACT SPECTROSCOPY INVESTIGATION
OF DIKETENE*

AN ELECTRON-IMPACT SPECTROSCOPY INVESTIGATION OF DIKETENE¹

I. M. Xavier Jr.², K. N. Walzl³ and A. Kuppermann
Arthur Amos Noyes Laboratory of Chemical Physics,⁴
California Institute of Technology, Pasadena, CA 91125

(Received _____)

Abstract

The electronic spectrum of diketene was investigated by the technique of variable-angle, electron energy-loss spectroscopy, using the impact energies of 25 eV and 50 eV, and varying the scattering angle from 10° to 90°. Transitions have been observed at 4.36 eV, 5.89 eV, 6.88 eV and 7.84 eV. Based on the intensity variation of these transitions with impact energy and scattering angle, and through analogy with simpler molecules, the first three are tentatively assigned to an $n \rightarrow \pi^*$ transition, a $\pi \rightarrow \sigma^*(3s)$ Rydberg transition and a $\pi \rightarrow \pi^*$ transition.

¹ This work was supported in part by the U. S. Department of Energy, Contract No. DE-AM03-76F00767, Project Agreement No. DE-AT03-76ER72004.

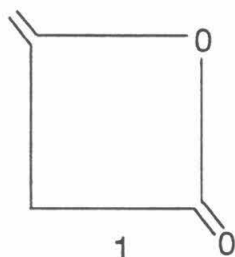
² Work performed in partial fulfillment of the requirements for the Ph.D. degree in Chemistry at the California Institute of Technology.

³ Present address: The Pennsylvania State University, Department of Chemistry, University Park, PA 16802.

⁴ Contribution No.

1. Introduction

Low-energy, variable-angle, electron-impact spectroscopy, which is a useful method for studying both optically forbidden and optically allowed electronic transitions,^{1,2} has been used to investigate the electronic spectrum of diketene. Previous optical studies^{3,4} of diketene have shown only a weak, ultraviolet, absorption band at 313 nm (3.96 eV), but the present work shows four new, higher energy-loss, electronic transitions including a spin-forbidden one. The diketene (4-methyleneoxetan-2-one, **1**) structure⁵ was elucidated by x-ray diffraction in 1952, forty-five years after its first preparation.



The planarity of the four-membered ring has been established by Raman spectroscopy.⁶

Information about the nature of the excited electronic states observed in an electron-impact spectrum can be obtained by studying the dependence of the intensity of each transition on impact energy and scattering angle.^{1,2} Transitions which, in optical spectroscopy, are both electric dipole-allowed and spin-allowed have differential cross sections (DCS) in electron-impact spectroscopy, which are forward-peaked.^{1,2} In contrast, spin-forbidden transitions involving changes in the molecular spin quantum number by ± 1 , such as singlet \rightarrow triplet excitation, have more nearly isotropic DCS in the angular range 10° to 90° .^{1,2} Such transitions occur by the mechanism of electron exchange.⁷ Spin-allowed but electric-dipole-forbidden processes are forward-peaked, but often not as much as fully allowed

transitions.^{8,9} Finally, the optically forbidden processes, and in particular the spin-forbidden ones, become more intense with respect to the optically allowed processes.^{1,2} Another advantage of the electron-impact method is that spectral features in the far ultraviolet are as easily examined as those in the visible and near ultraviolet.

2. Experimental

The electron spectrometer used in this study was similar to one described previously.¹⁰ Briefly, an electron beam is energy-selected by a hemispherical electrostatic energy analyzer (and the associated focusing lenses) and scattered from the target vapor in a scattering box. In this work, the incident-beam current was between 1-10 *nA* and was typically 4 *nA*. Sample pressures were estimated to be between 5-10 *mTorr*. Electron-energy losses were determined at angles between 10°-90° by means of a second electrostatic energy analyzer and detector. The energy-loss spectrum thus obtained is analogous to an optical absorption spectrum, except that optically forbidden processes are much more readily detected.^{1,2}

The spectrometer resolution (as measured by the full width at half-maximum of the elastically scattered feature) varied between 50 and 100 *meV* for all reported spectra and was typically 80 *meV*. Diketene was obtained from Aldrich, and had a stated purity of 98%. All samples were subjected to three liquid nitrogen freeze-pump-thaw cycles and used without further purification.

3. Results and discussion

Figure 1 shows the low-energy-loss part of the electron-impact spectrum of diketene at an impact energy (E_o) of 25 *eV* and scattering angle (θ) of 10°, while

Figure 2 shows the spectrum at the same energy but with $\theta = 90^\circ$. Figures 3 and 4 present the diketene spectrum at $E_o = 50 \text{ eV}$ and with $\theta = 10^\circ$ and $\theta = 90^\circ$, respectively. These figures indicate the presence of four transitions having maximum intensities at 4.36 eV , 5.89 eV , 6.88 eV and 7.84 eV energy loss. In Figures 5 and 6 we display the corresponding differential cross-section curves at the impact energies of 25 eV and 50 eV , obtained by a method previously described.⁸

The most intense feature has a peak intensity at 6.88 eV . From Figures 5 and 6 the elastic peak and the peak at 6.88 eV exhibit an intensity variation of about two orders of magnitude over the angular range, as should fully allowed bands. The transitions at 7.84 eV and 5.89 eV have DCS curves less forward-peaked, but they can still be considered as allowed bands. The DCS of the 4.36 eV transition is nearly isotropic and has the characteristic behavior of a spin-forbidden transition.^{1,11}

No far-ultraviolet spectra of diketene have been reported, in spite of the recent appearance of an extensive review article on this molecule.⁵ In the absence of any calculations for this molecule, we are tentatively assigning these observed transitions of diketene under the qualitative assumptions described below.

Diketene contains two important chromophores: the carbonyl and the ethylene groups. The carbonyl in small monoketones exhibits the well-known (n, π^*) band in the ultraviolet followed by three Rydberg bands $(n, (3s, 3p, 3d))$ in the far-ultraviolet.¹² The (π, π^*) band is expected to be at relatively high-energy loss (possibly as high as 9.0 eV) superimposed by Rydberg bands.^{12,13} The carbon double bond in monoalkenes exhibits an intense (π, π^*) absorption band, which coincides with, or is preceded by, a $(\pi, 3s)$ Rydberg band.¹² In ethylene itself, the Rydberg band is superimposed on the low-frequency wing of the (π, π^*) band,¹⁴ while in highly methylated or fluorinated olefins, the Rydberg $(\pi, 3s)$ becomes the first spectral band and is well separated from the (π, π^*) band.¹²

The observed spectral bands of diketene can be tentatively assigned by analogy to the properties of the isolated carbonyl and ethylene chromophores. In the energy-loss range of this work (3.5-8.5 eV), the spin-forbidden transition at 4.36 eV is the only spectral feature that can be attributed to the carbonyl chromophore. By analogy with previous electron-impact assignments in monoketones,^{13,15} this transition is assigned as $n \rightarrow \pi^*(S - T)$. The other three spin-allowed transitions can be attributed as due to mainly the carbon-carbon, double-bond chromophore. The strongest transition at 6.88 eV is assigned as $\pi \rightarrow \pi^*(S - S)$, based on the electron energy-loss spectroscopy of methyl-substituted ethylenes¹⁶ and fluoroethylenes.¹⁷ The shoulder at 5.89 eV resembles the shoulder on the strongest feature in the energy-loss spectrum of the fluoroethylenes¹⁷ and is assigned as $\pi \rightarrow \sigma^*(3s)$ Rydberg ($S - S$). Finally, the spin-allowed band at 7.84 eV is probably another Rydberg band, similar to those observed in ethylenes.¹⁴

4. Summary

In conclusion, we have used the method of low-energy, variable-angle, electron-impact spectroscopy to study the far-ultraviolet spectrum of diketene. Four new transitions have been observed, including one that is spin-forbidden. Tentative assignment of these transitions was made under qualitative assumptions. We hope that calculations will be available in the near future in order to confirm our expectations.

References

1. A. Kuppermann, J. K. Rice, and S. Trajmar, *J. Phys. Chem.*, **72**, 3094 (1968).
2. S. Trajmar, J. K. Rice, and A. Kuppermann, *Advan. Chem. Phys.*, **18**, 15 (1970).
3. J. D. Roberts, R. Armstrong, R. F. Trimble, and M. Burg, *J. Am Chem. Soc.*, **71**, 843 (1949).
4. M. Calvin, T. T. Magel, and C. D. Hurd, *J. Am. Chem. Soc.*, **63**, 2174 (1941).
5. R. J. Clemens, *Chem. Rev.*, **86**, 241 (1986).
6. J. R. Durig and J. N. Willis Jr., *Spectrochim. Acta*, **22**, 1299 (1966).
7. J. R. Oppenheimer, *Phys. Rev.*, **29**, 433 (1927).
8. O. A. Mosher, W. M. Flicker, and A. Kuppermann, *J. Chem. Phys.*, **62**, 2600 (1975).
9. D. C. Cartwright, W. J. Hunt, W. Williams, S. Trajmar, and W. A. Goddard III, *Phys. Rev.*, **A8**, 2436 (1973).
10. (a) C. F. Koerting, K. N. Walzl, and A. Kuppermann, *Chem. Phys. Lett.*, **109**, 140 (1984); (b) C. F. Koerting, *Ph.D. Thesis* (California Institute of Technology, Pasadena, CA, 1985).
11. A. Kuppermann, W. M. Flicker, and O. A. Mosher, *Chem. Rev.*, **79**, 77 (1979).
12. C. Sandorfy and L. S. Lussier in *Photophysics and Photochemistry in the Vacuum Ultraviolet*, S. P. McGlynn, G. L. Findley and R. H. Huebner, Eds., Reidel, Dordrecht (1985), p. 819.
13. K. N. Walzl, C. F. Koerting, and A. Kuppermann, *J. Chem. Phys.*, **87**, 3796 (1987).
14. A. J. Merer, and R. S. Mulliken, *Chem. Rev.*, **69**, 639 (1969).
15. R. P. Frueholtz, W. M. Flicker, and A. Kuppermann, *Chem. Phys. Lett.*, **38**, 57 (1976).

16. W. M. Flicker, O. A. Mosher, and A. Kuppermann, *Chem. Phys. Lett.*, **36**, 56 (1975).
17. M. J. Coggiola, O. A. Mosher, W. M. Flicker, and A. Kuppermann, *Chem. Phys. Lett.*, **27**, 14 (1974).

Figure Captions

Fig. 1 Electron energy-loss spectrum of diketene at an incident electron energy $E_o = 25 \text{ eV}$ and scattering angle $\theta = 10^\circ$.

Fig. 2 Electron energy-loss spectrum of diketene with $E_o = 25 \text{ eV}$ and $\theta = 90^\circ$.

Fig. 3 Electron energy-loss spectrum of diketene with $E_o = 50 \text{ eV}$ and $\theta = 10^\circ$.

Fig. 4 Electron energy-loss spectrum of diketene with $E_o = 50 \text{ eV}$ and $\theta = 90^\circ$.

Fig. 5 Differential cross sections of diketene as a function of scattering angle at an incident-electron energy of 25 eV for elastic scattering (\square) and for transitions to the excited states lying at 4.36 eV (\circ), 5.89 eV (\triangle), 6.88 eV ($+$), and 7.84 eV (\times) above the ground state.

Fig. 6 Differential cross sections of diketene as a function of scattering angle at an incident-electron energy of 50 eV for elastic scattering (\square) and for transitions to the excited states lying at 4.36 eV (\circ), 5.89 eV (\triangle), 6.88 eV ($+$), and 7.84 eV (\times) above the ground state.

FIGURE 1

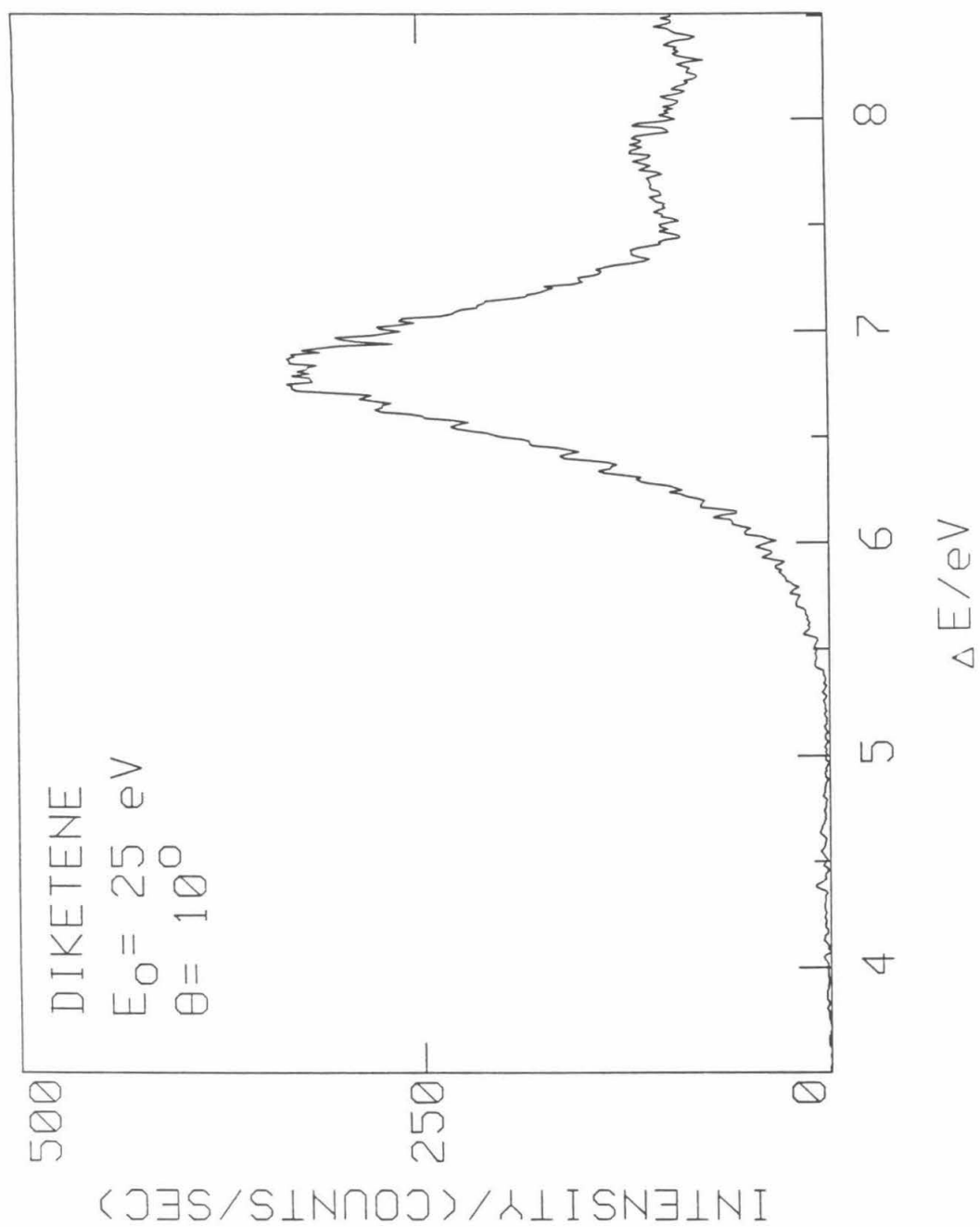


FIGURE 2

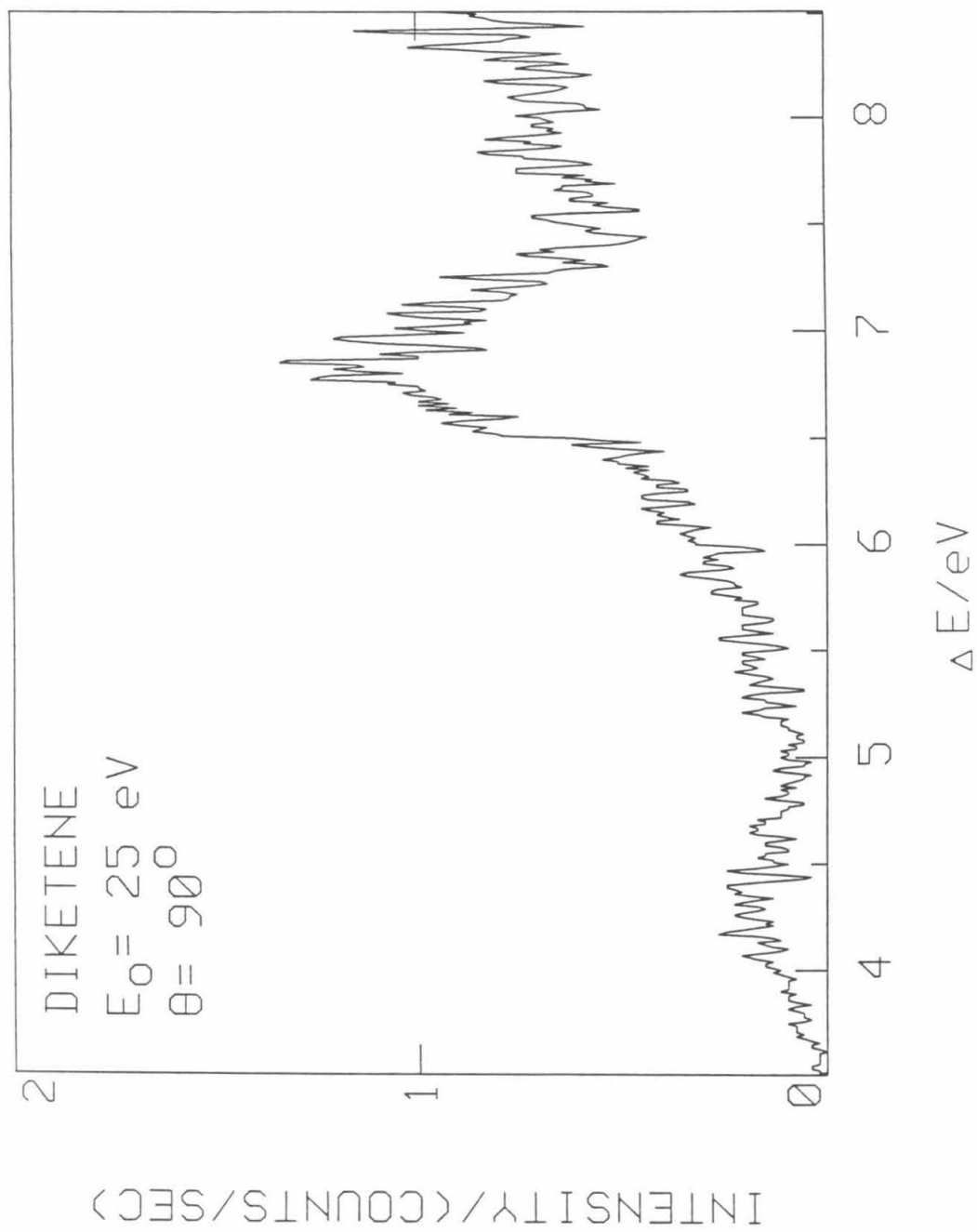


FIGURE 3

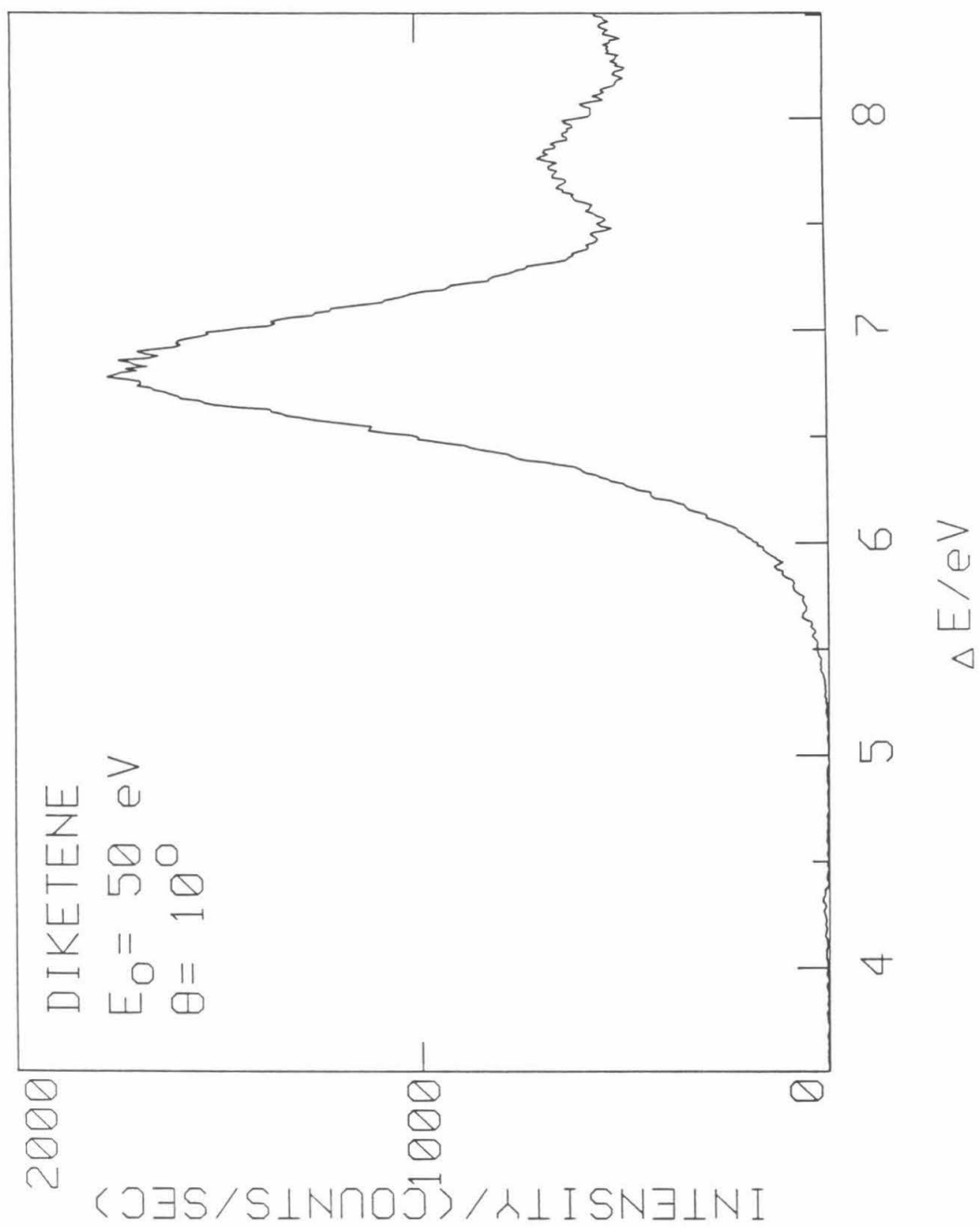


FIGURE 4

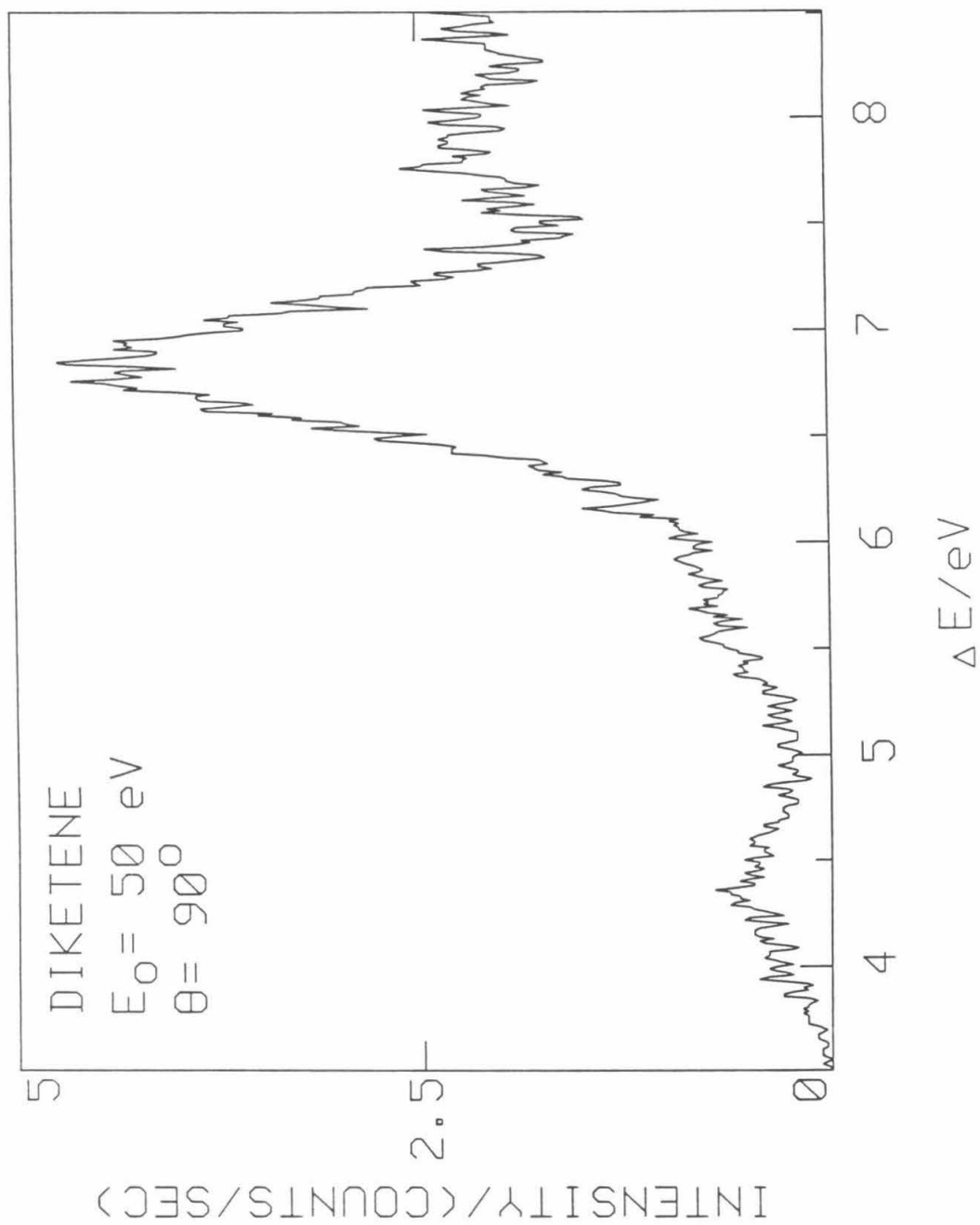


FIGURE 5

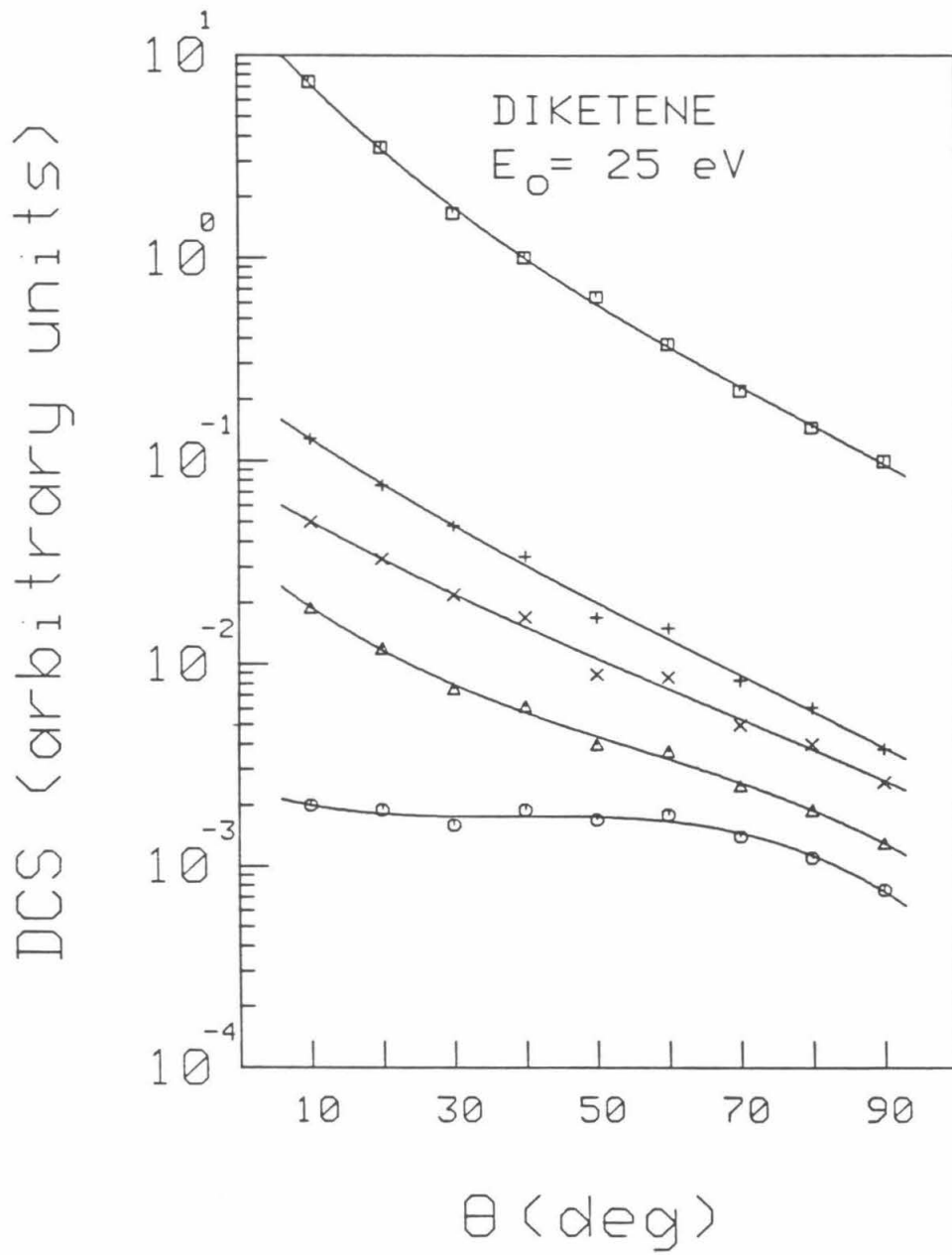
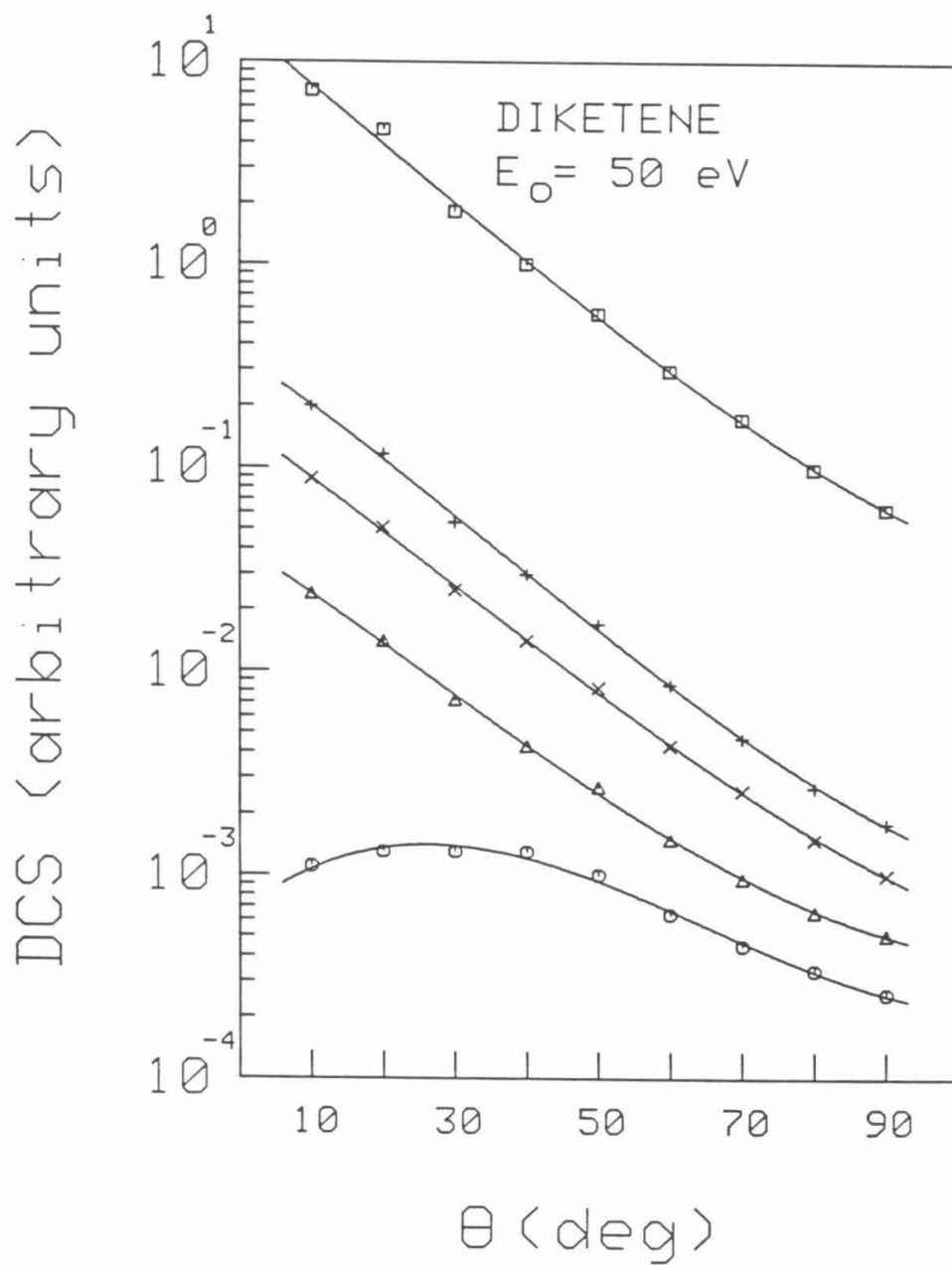


FIGURE 6



CHAPTER 5

Paper 2: *STUDY OF GAS PHASE PRODUCTS FORMED BY FLASH-VACUUM PYROLYSIS OF HALOMETHANES USING ELECTRON ENERGY-LOSS SPECTROSCOPY*

STUDY OF GAS PHASE PRODUCTS FORMED BY FLASH-
VACUUM PYROLYSIS OF HALOMETHANES USING
ELECTRON ENERGY-LOSS SPECTROSCOPY¹

I. M. Xavier Jr.², K. N. Walzl³, M. R. Arnazzi and A. Kuppermann
*Arthur Amos Noyes Laboratory of Chemical Physics⁴,
California Institute of Technology, Pasadena, CA 91125*

(Received)

Abstract

Thermal decomposition of chlorodifluoromethane, chloroform, dichloromethane and chloromethane under flash-vacuum pyrolysis conditions (900-1100°C) was investigated by the technique of electron energy-loss spectroscopy, using an impact energy of 50 eV and a scattering angle of 10°. The pyrolytic reaction follows a hydrogen chloride α -elimination reaction pathway. The difluoromethylene radical was produced from the chlorodifluoromethane pyrolysis at 900°C and identified by its $\tilde{X}^1A_1 \rightarrow \tilde{A}^1B_1$ band at 5.04 eV.

¹ This work was supported in part by the U. S. Department of Energy, Contract No. DE-AM03-76F00767, Project Agreement No. DE-AT03-76ER72004.

² Work performed in partial fulfillment of the requirements for the Ph.D. degree in Chemistry at the California Institute of Technology.

³ Present address: The Pennsylvania State University, Department of Chemistry, University Park, PA 16802.

⁴ Contribution No.

1. Introduction

The thermal decomposition of four halomethane molecules that follow similar pyrolysis pathways provides clues for generation of gas phase halocarbenes. By comparison between the electronic spectra of the pyrolytic precursor molecule at room temperature and at high temperature, one can determine the efficiency of decomposition and identify the possible pyrolytic products.

This report presents an electron energy-loss study of the hydrogen chloride (HCl) α -elimination from halomethanes under flash-vacuum pyrolysis (FVP) conditions.^{1,2} The FVP conditions employed in this study were 1-10 *mTorr* of the gas sample over a quartz pyrolyzer surface at 900-1100°C. Under these conditions, thermal activation takes place primarily by contact with the hot pyrolyzer walls, so that processes observed in this study result mainly from very fast heterogeneous reactions.¹

Electron-impact spectroscopy has been previously used in our laboratory for investigation of the methyl (CH₃) radical and some of its pyrolytic precursors.³ In that work, the number density of CH₃ radicals in the jet at the pyrolysis temperature was estimated to be 10¹³ molecules/cm³ on the basis of the intensity of the 5.73 eV band.

2. Experimental

The spectrometer used in the present experiment has been described previously.⁴ Briefly, electrons are emitted from a tungsten filament and focused into a hemispherical monochromator. The monoenergetic electrons are then focused into the scattering region and, after interaction with the target molecules, enter a hemispherical energy-loss analyzer prior to detection.

The spectrometer resolution (as measured by the full width at half-maximum of the elastically scattered feature) varied between 70 and 100 *meV*. For all reported spectra, the incident electron energy was 50 *eV* and the scattering angle was 10°.

In order to produce thermal decomposition of the halomethanes, an *in situ* pyrolysis technique was employed.³ The pyrolysis takes place within a graphite-coated quartz tube with an inner diameter of 0.060 *in*. The pyrolyzer is heated by tantalum sheathed double stranded tungsten-rhenium alloy wires wound over a 0.35 *in* length of the quartz tube, and temperatures up to 1100°C (as measured by an optical pyrometer) can be reached. Since the pyrolysis is done at low pressures, the residence time in the pyrolyzer is kept in the few milliseconds' range and thermal activation results mainly from collisions with the wall. Because the distance from the end of the pyrolyzer to the scattering center region is short, most of the reactive intermediates should be detected. The background pressures in the scattering chamber are quite low ($< 5 \times 10^{-5}$ Torr), so recombination rates are slow.

The investigation of four halomethanes are reported: chlorodifluoromethane (Aldrich, 99.9%); chloroform (J.T.Baker, 99.5%); dichloromethane (J. T. Baker, 99.7%) and chloromethane (Aldrich, 99.5%). The chloroform and dichloromethane samples were subjected to three liquid-nitrogen, freeze-pump-thaw cycles. Hydrogen chloride (Matheson, 99.0%) was used as reference in the study of the high-temperature spectra.

3. Results and Discussion

Figure 1 shows the electron energy-loss spectrum of the HCl jet. The spectrum is featureless in the region 2.0-6.5 *eV*, which is followed by a broadband continuum with a maximum around 8 *eV*. The four peaks in the region above 9 *eV* consist

mainly of the $C^1\Pi$ and $b^3\Pi$ states, which are Rydberg states corresponding to the $\pi \rightarrow 4s$ transition.⁵ The strongest peak at 9.62 eV is assigned as $C^1\Pi(v' = 0)$, while the two peaks at 9.93 and 10.28 eV are the $C(v' = 1, 2)$ bands, respectively. The small peak at 9.31 eV corresponds to $b^3\Pi(v' = 0)$.⁶

In Figures 2 and 3, we show the energy-loss spectra of chlorodifluoromethane at room temperature and at 900°C. The room temperature spectrum shows a broadband continuum with the maximum around 8.2 eV, followed by two peaks at 9.24 and 10.00 eV, which can be assigned as the Rydberg transitions $Cl \rightarrow 4s$ and $Cl \rightarrow 4p$, respectively. The high-temperature spectrum suggests an extensive decomposition of the precursor molecule and we can observe the familiar $b(v' = 0)$ and $C(v' = 0, 1, 2)$ bands of HCl at the high-energy-loss side. However, there is a new broadband feature starting at 4.2 eV and peaking at 5.04 eV. We attribute this band to the $\tilde{X}^1A_1 \rightarrow \tilde{A}^1B_1$ transition of the difluoromethylene (CF_2) radical. The spectrum of this radical was first observed and identified in the region 3300-2300 Å by Venkateswarlu.⁸ This transition was assigned later by Mathews⁹ as $\tilde{X}^1A_1 \rightarrow \tilde{A}^1B_1$. In our case, the possibility of the combination of two CF_2 can be eliminated by comparison with the electron energy-loss spectrum of tetrafluoroethylene.¹⁰ The CF_2 radical appears to be unreactive with itself and is thermochemically stable ($\Delta H_f^\circ = -49 \pm 3 \text{ kcal/mol}$).¹¹

Figure 4 shows the chloroform spectrum at room temperature. The first band with the maximum at 7.10 eV can be assigned as an $n \rightarrow \sigma^*$ Rydberg transition.¹² The shoulder at 8.31 eV and the peak at 8.72 eV are both believed to stem from the $n \rightarrow 4s$ Rydberg manifold.¹² The higher energy transition at 9.26 eV can be attributed as an $n \rightarrow 4p$ Rydberg. The one dominant feature at still higher energy is a peak at 10.62 eV.

Figure 5 presents the chloroform spectrum at 1000°C, which at high energy loss very much resembles the HCl one, as a result of the efficient thermal decomposition.

Beginning at about 4 eV, we have two broadband continua with peaks roughly at 6.3 and 8.0 eV. The last one probably corresponds to the HCl continuum, while the first one occurs in the same region (5.0-7.0 eV) where tetrachloroethylene shows an intense broad transition.¹⁶ Tetrachloroethylene can be formed by bimolecular processes that usually do not occur under FVP conditions except in the case of radical-radical reactions.² These facts suggest that the first broadband is probably due mainly to the combination of two dichloromethylenes (CCl₂) to give tetrachloroethylene. It is known that the radical CCl₂ has a weak visible absorption band in the region 2.21-2.81 eV¹³ and an ultraviolet absorption band centered at 3.76 eV.¹⁴ The shoulderlike band in the region 4.0-5.0 eV could tentatively be attributed as the ¹A₁ → ¹A₂ band of CCl₂, which *ab initio* and CI calculations predict to be at 4.5 eV.¹⁵ However, there is no conclusive evidence for the presence of thermochemically unstable CCl₂ ($\Delta H_f^\circ = 39 \pm 3 \text{ kcal/mol}$).¹¹

In Figures 6 and 7, the dichloromethane spectra are displayed at room temperature and at 1100°C, respectively. The room temperature spectrum has a shoulder at 7.16 eV that can be assigned as an *n* → σ^* Rydberg transition.¹² The first peak with the maximum at 8.26 eV can be attributed to degenerate *n* → 4*s* Rydberg transitions, while the broadband at 9.12 eV is due to *n* → 4*p* Rydberg transitions.¹² At still higher energy is a sharp peak at 10.30 eV. The high-temperature spectrum suggests that the dichloromethane is only partially decomposed at 1100°C. The strong and sharp peak at 9.6 eV is the C¹Π(*v*' = 0) transition of the HCl. Except for a shoulderlike feature in the region 5.0-6.0 eV that could not be assigned, the rest of the spectrum resembles a broad and noisy version of the room temperature one. No evidence for the presence of the thermochemically unstable CClH ($\Delta H_f^\circ = 71 \pm 5 \text{ kcal/mol}$)¹¹ was found at this temperature.

Figure 8 shows the room temperature spectrum of chloromethane. The shoulder from 6.50 to 7.65 eV can be assigned as an *n* → σ^* Rydberg transition.¹²

The next band centered at 7.91 eV is attributed to an $n \rightarrow 4s$ Rydberg transition.¹² Then, we have an intense feature at 8.91 eV assigned as an $n \rightarrow 4p$ Rydberg transition, followed by a sharp and intense peak at 9.22 eV, which has been tentatively assigned to the $n \rightarrow 3d$ Rydberg transition.¹² Another intense peak is at 10.20 eV and can be considered as the $n \rightarrow 5p$ Rydberg transition.¹²

Finally, Figure 9 presents the spectrum of chromomethane at 1100°C, which is noisy and lacks fine structure of the one at room temperature. There is no HCl feature about 9.6 eV, and we can assume that there was no measurable thermal decomposition at this temperature.

4. Summary

In conclusion, we have used the method of electron energy-loss spectroscopy to investigate the pyrolysis of four halomethanes via HCl α -elimination reaction. At sufficiently high temperature we observed a complete and clean thermal unimolecular decomposition of halomethanes that contain at least one hydrogen and one chlorine atom. The difluoromethylene radical can be easily generated by the chlorodifluoromethane pyrolysis at 900°C. We also assigned the far-ultraviolet bands of the pyrolytic precursor molecules based only on the optical spectra. To our knowledge, no low-energy-loss study of these compounds has been published.^{17,18}

References

1. D. M. Golden, G. N. Spokes, and S. W. Benson, *Angew. Chem. Int. Ed. Engl.*, **12**, 534 (1973).
2. E. Hedaya, *Acc. Chem. Res.*, **2**, 367 (1969).
3. K. N. Walzl, C. F. Koerting, I. M. Xavier Jr., and A. Kuppermann, *J. Chem. Phys.*, **86**, 89 (1987).
4. C. F. Koerting, K. N. Walzl, and A. Kuppermann, *Chem. Phys. Lett.*, **109**, 140 (1984).
5. M. Bettendorff, S. D. Puerimhoff, and R. Buenker, *Chem. Phys.*, **66**, 261 (1982).
6. J. B. Nee, M. Suto, and L.C. Lee, *J. Chem. Phys.*, **85**, 719 (1986).
7. R. Gilbert, P. Sauvageau, and C. Sandorfy, *J. Chem. Phys.*, **60**, 4820 (1974).
8. P. Venkateswarlu, *Phys. Rev.*, **77**, 676 (1959).
9. C. W. Mathews, *Can. J. Phys.*, **45**, 2355 (1967).
10. M. J. Coggiola, W. M. Flicker, O. A. Mosher, and A. Kuppermann, *J. Chem. Phys.*, **65**, 2655 (1976).
11. S. G. Lias, Z. Karpas, and J. F. Liebman, *J. Am. Chem. Soc.*, **107**, 6089 (1985).
12. B. R. Russell, L. O. Edwards, and J. W. Raymond, *J. Am. Chem. Soc.*, **95**, 2129 (1973).
13. D.E. Milligan and M. E. Jacox, *J. Chem. Phys.*, **47**, 703 (1967).
14. T. Ha, H. U. Gremlich, and R. E. Bühler, *Chem. Phys. Lett.*, **65**, 16 (1979).
15. M. T. Nguyen, M. C. Kerins, A. F. Hegarty, and N. J. Fitzpatrick, *Chem. Phys. Lett.*, **117**, 295 (1985).
16. C. F. Koerting, K. N. Walzl, and A. Kuppermann, *J. Chem. Phys.*, in press.
17. A. Kuppermann, W. M. Flicker, and O. A. Mosher, *Chem. Rev.*, **79**, 77 (1979).

18. S. Trajmar, D. F. Register, and A. Chutjian, *Phys. Rep.*, **97**, 219 (1983).

Figure Captions

- Fig. 1 Electron energy-loss spectrum of hydrogen chloride with $E_o = 50 \text{ eV}$ and $\theta = 10^\circ$. All spectra were measured at the same impact energy and scattering angle, using an effusive jet as the target source.
- Fig. 2 Electron energy-loss spectrum at room temperature of chlorodifluoromethane.
- Fig. 3 Electron energy-loss spectrum at 900°C of chlorodifluoromethane.
- Fig. 4 Electron energy-loss spectrum at room temperature of chloroform.
- Fig. 5 Electron energy-loss spectrum at 1000°C of chloroform.
- Fig. 6 Electron energy-loss spectrum at room temperature of dichloromethane.
- Fig. 7 Electron energy-loss spectrum at 1100°C of dichloromethane.
- Fig. 8 Electron energy-loss spectrum at room temperature of chloromethane.
- Fig. 9 Electron energy-loss spectrum at 1100°C of chloromethane.

FIGURE 1

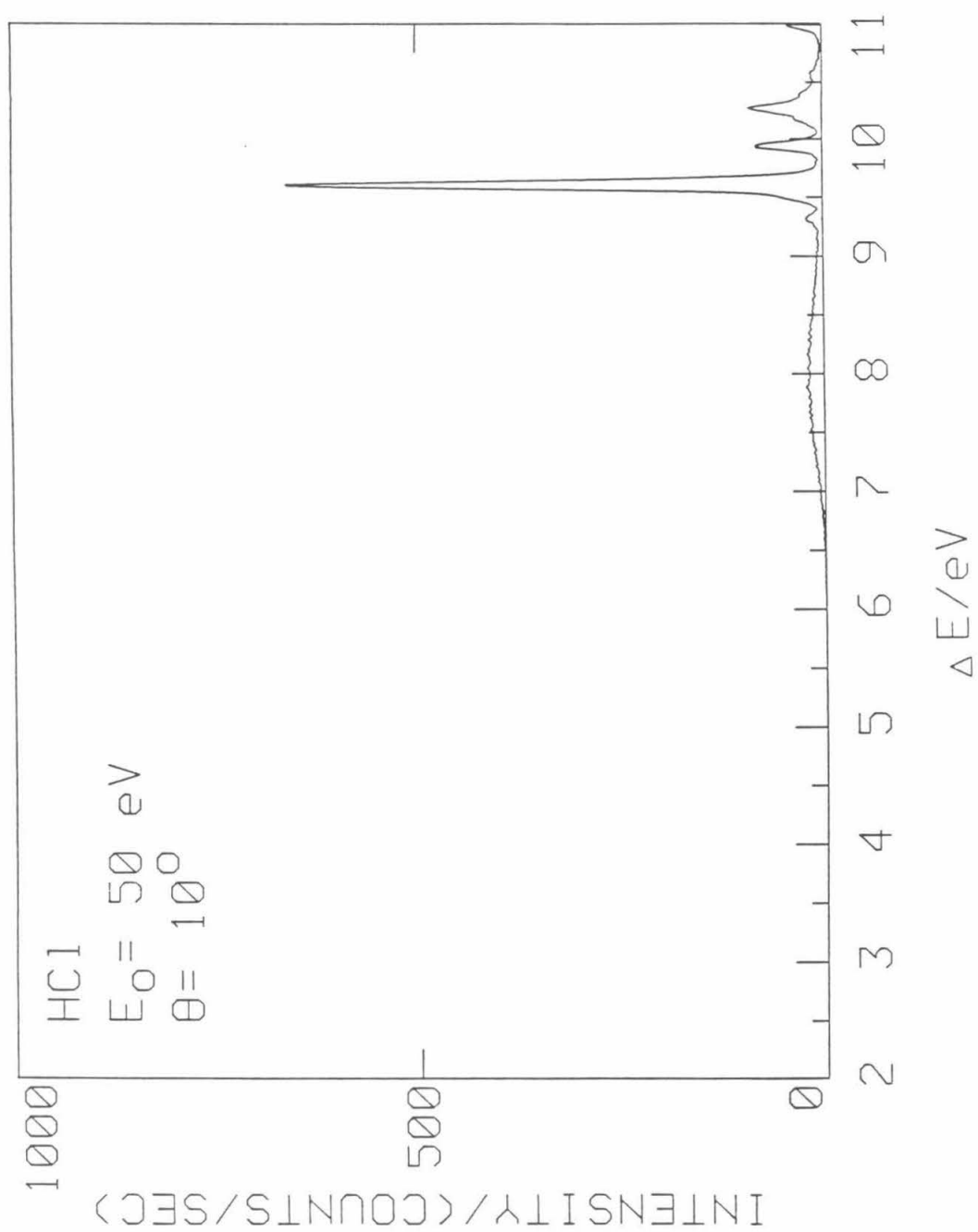


FIGURE 2

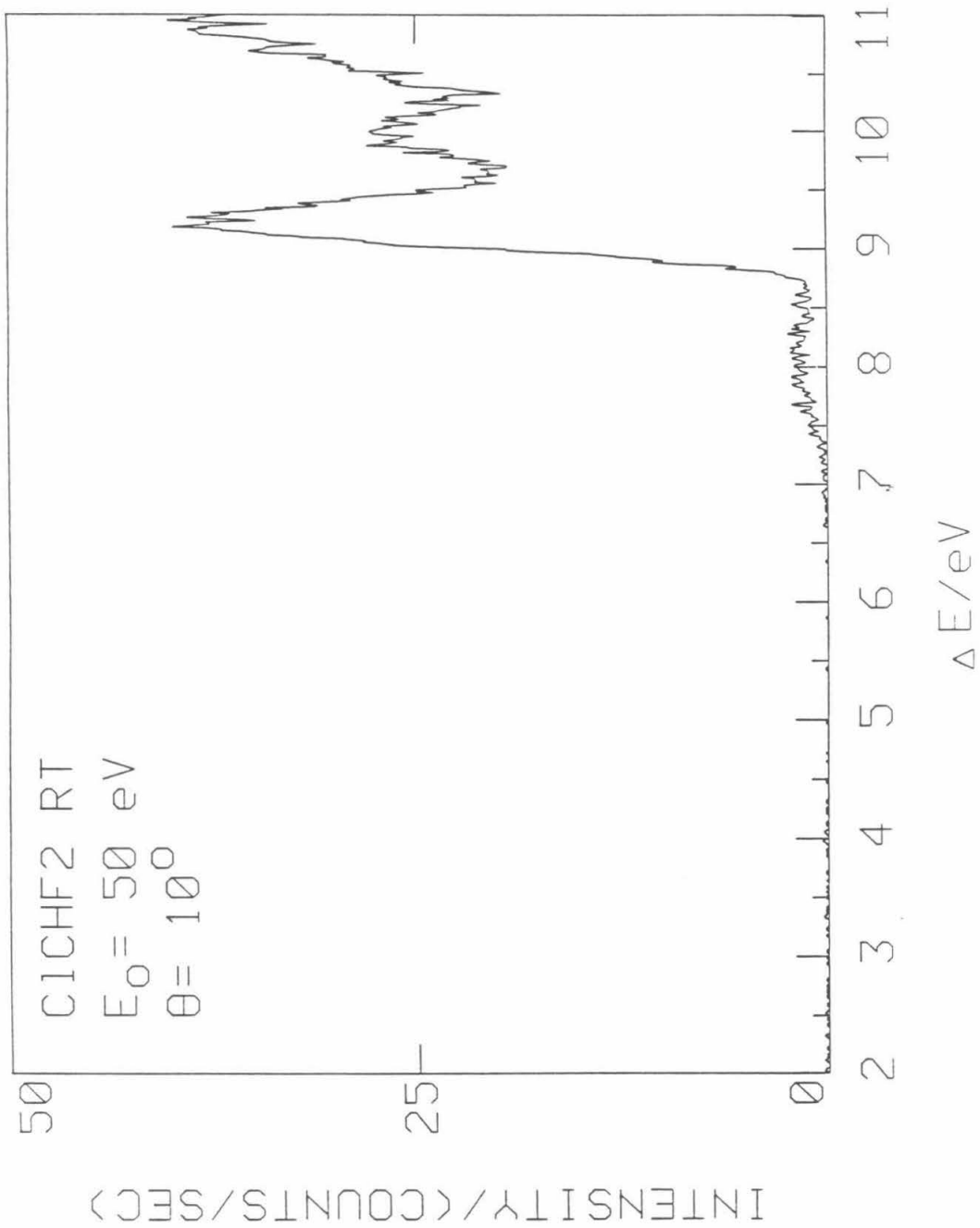


FIGURE 3

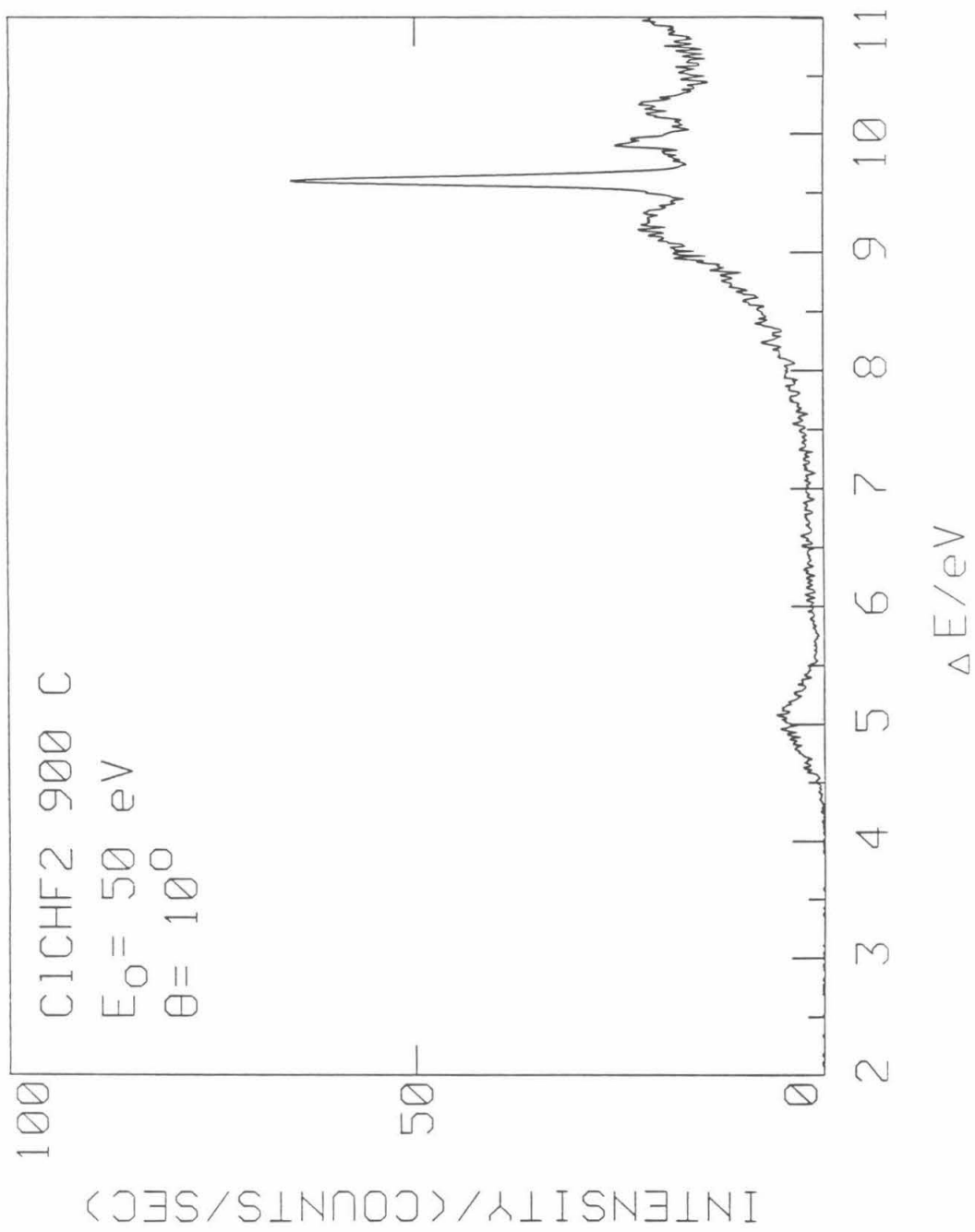


FIGURE 4

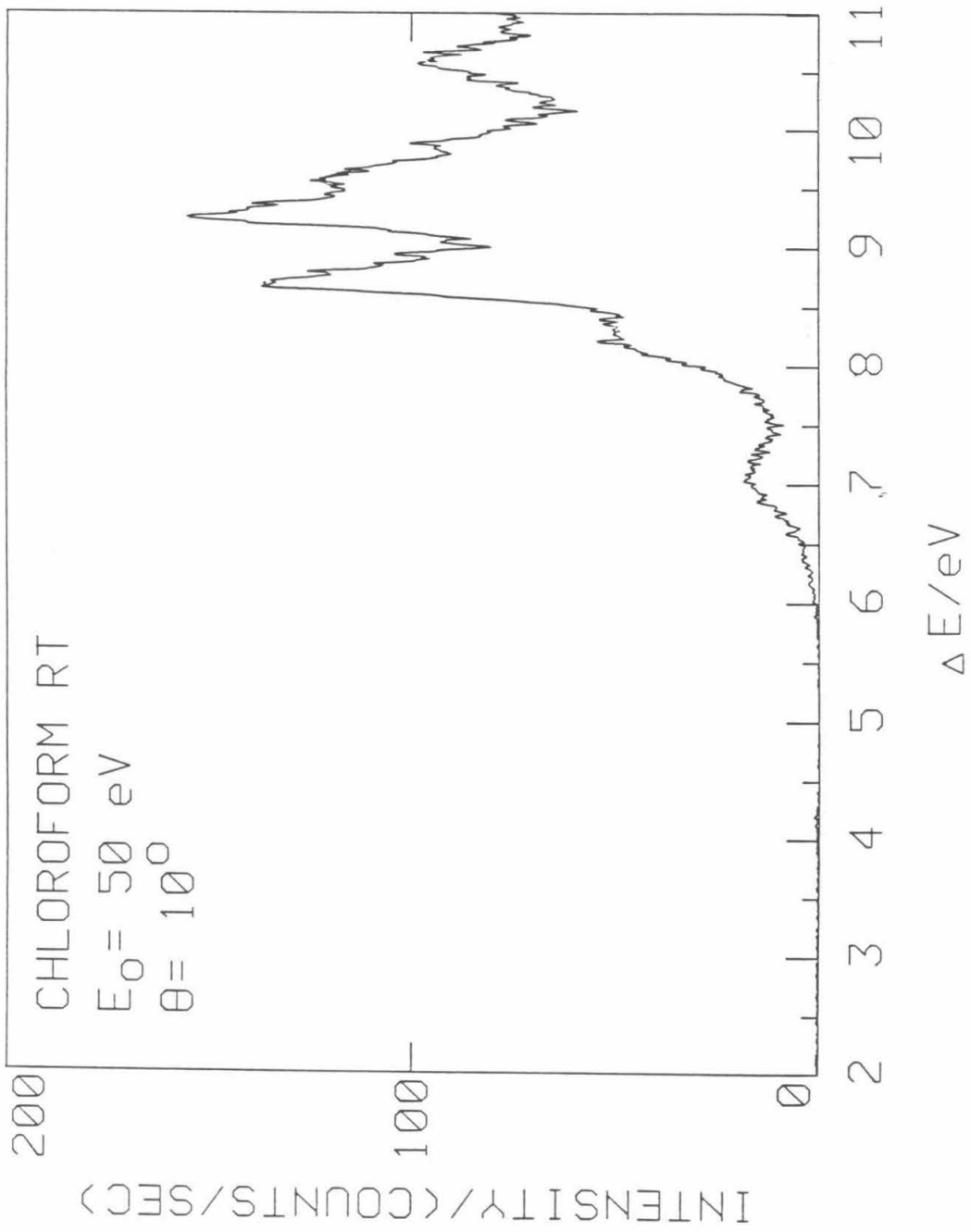


FIGURE 5

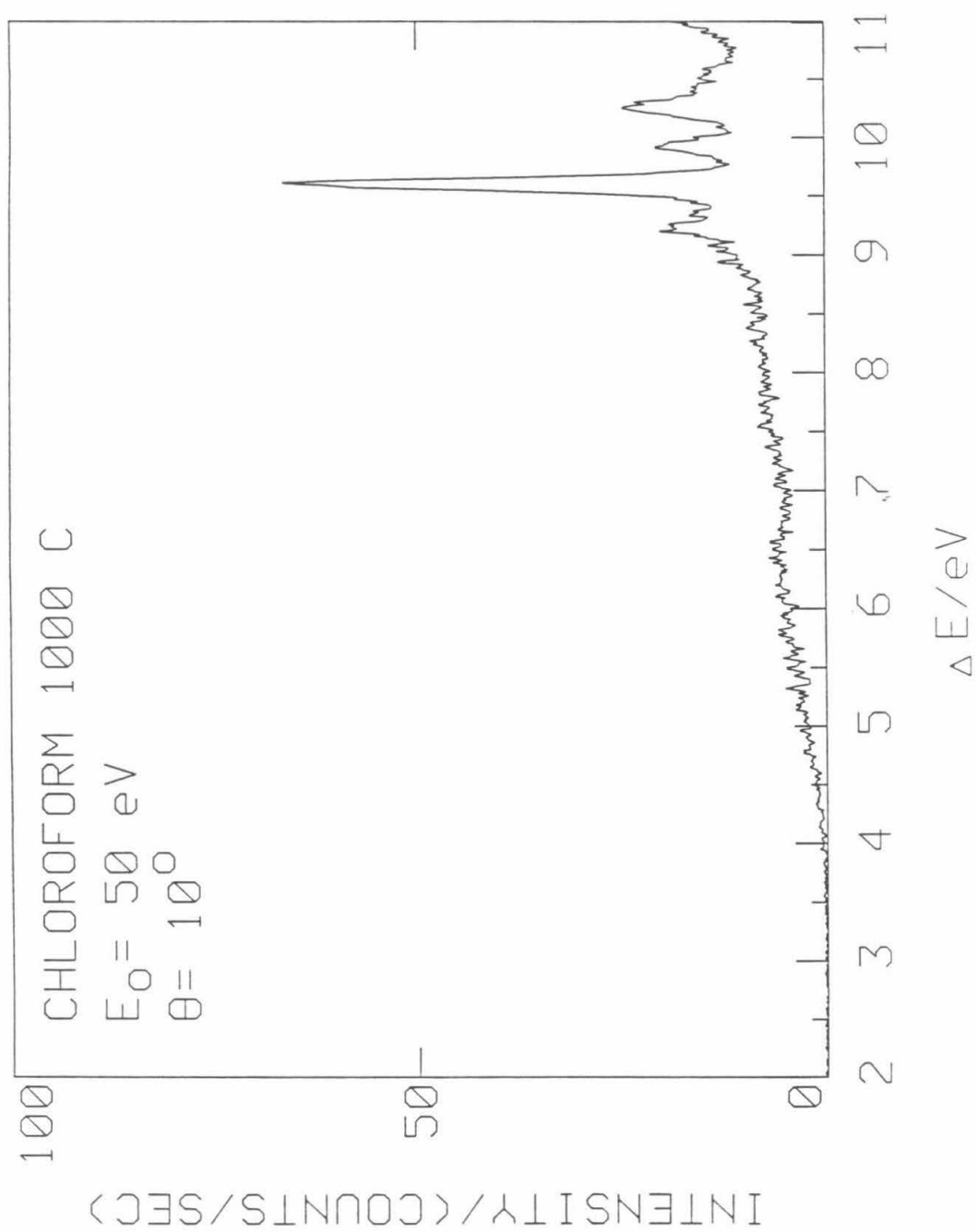


FIGURE 6

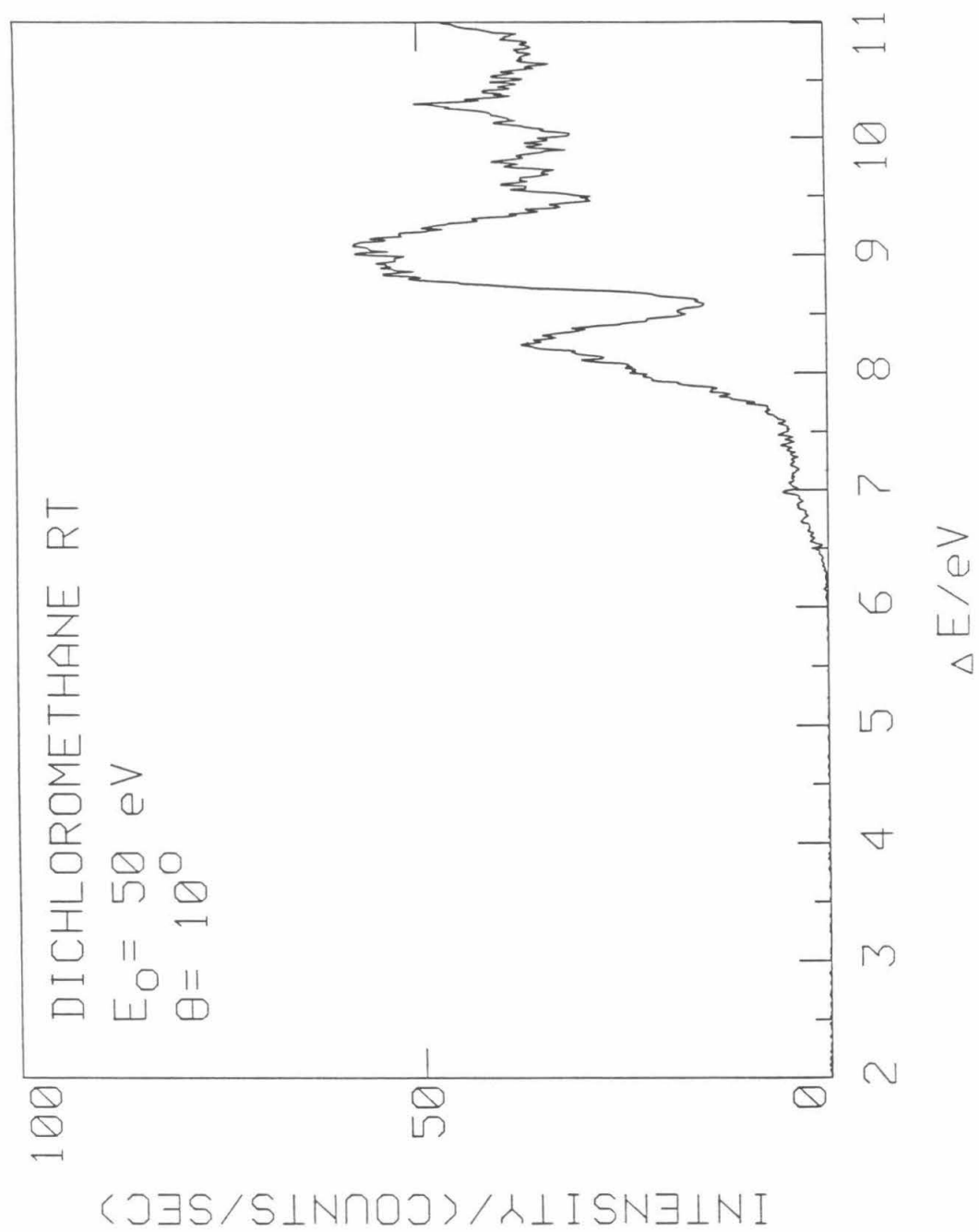


FIGURE 7

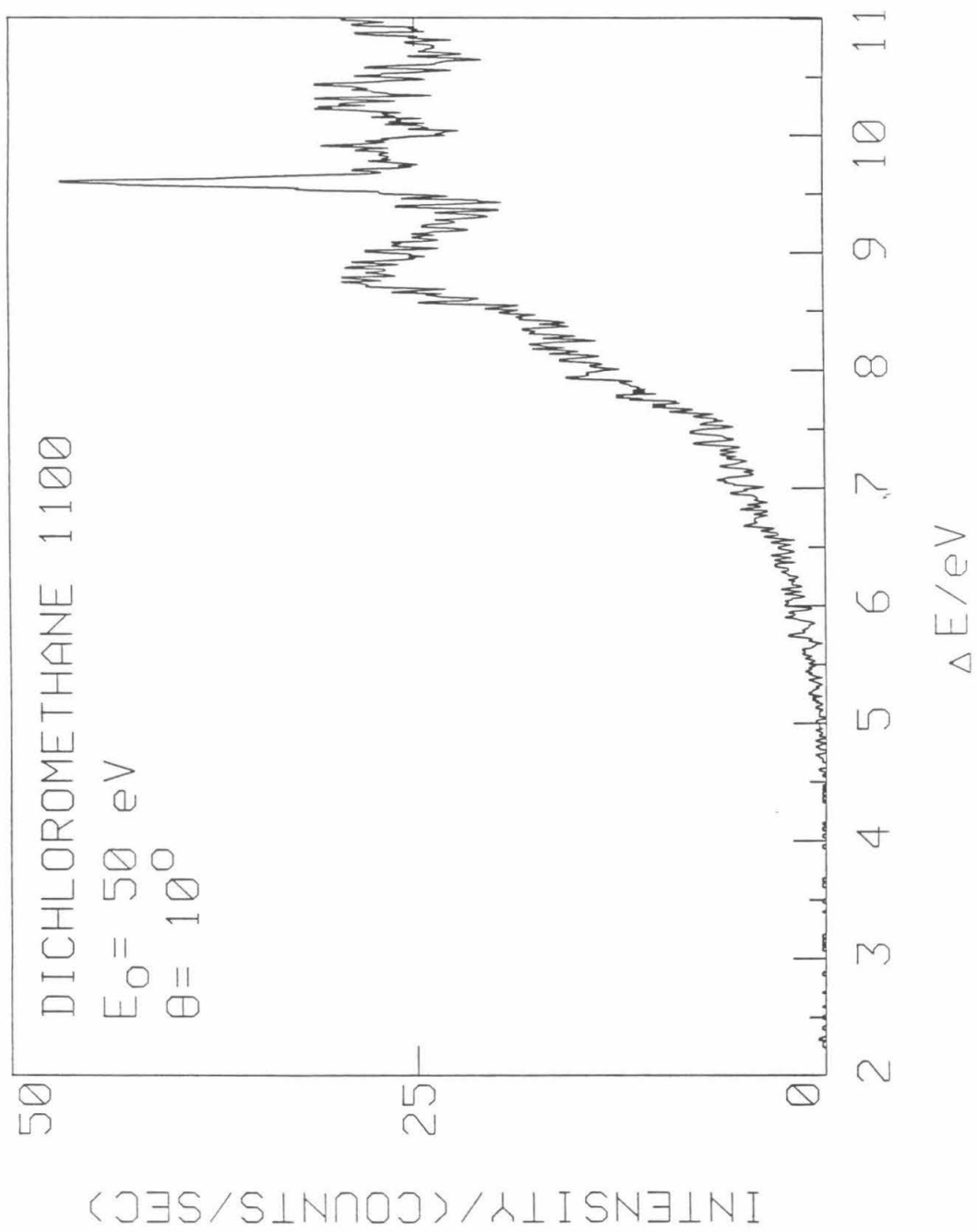


FIGURE 8

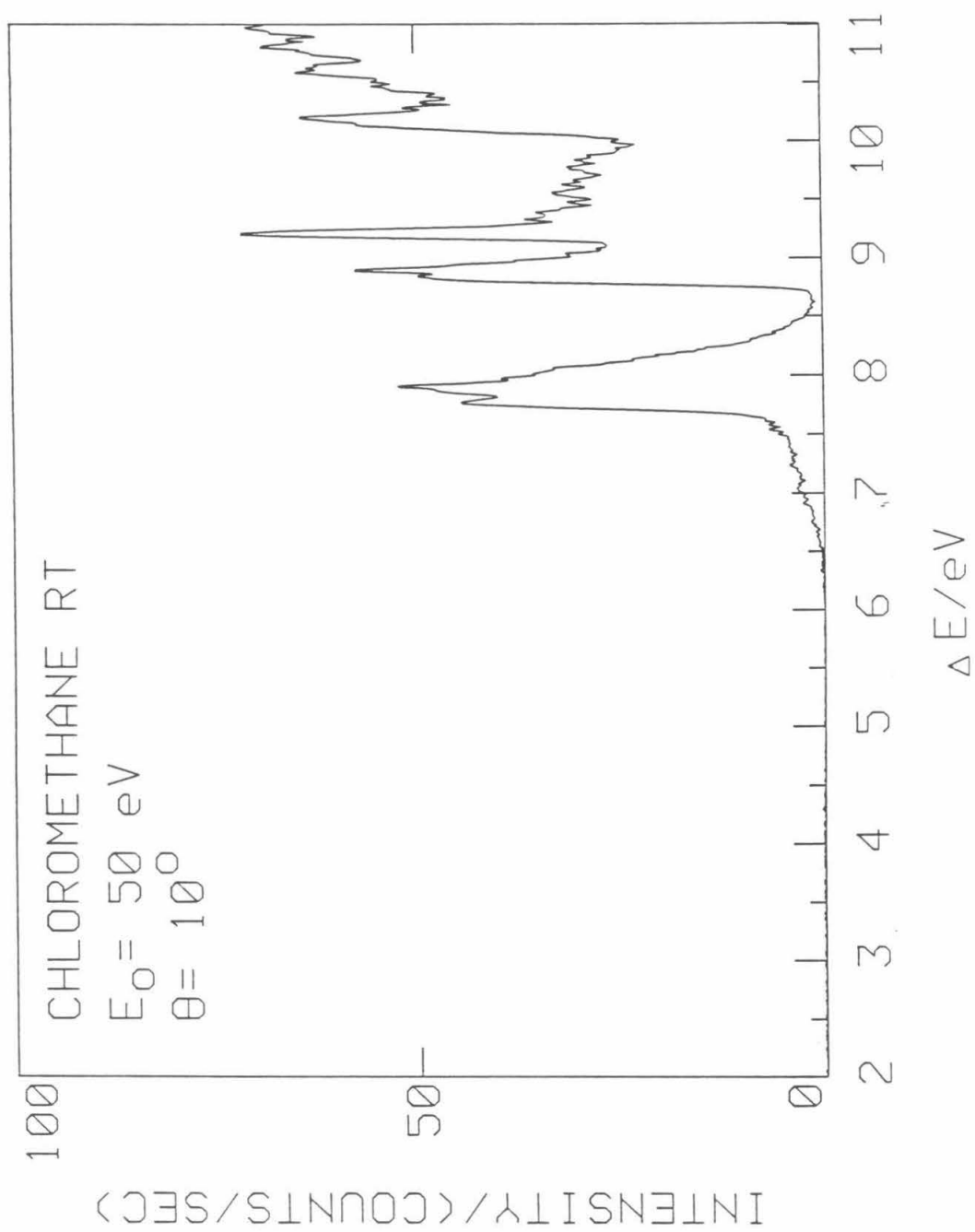
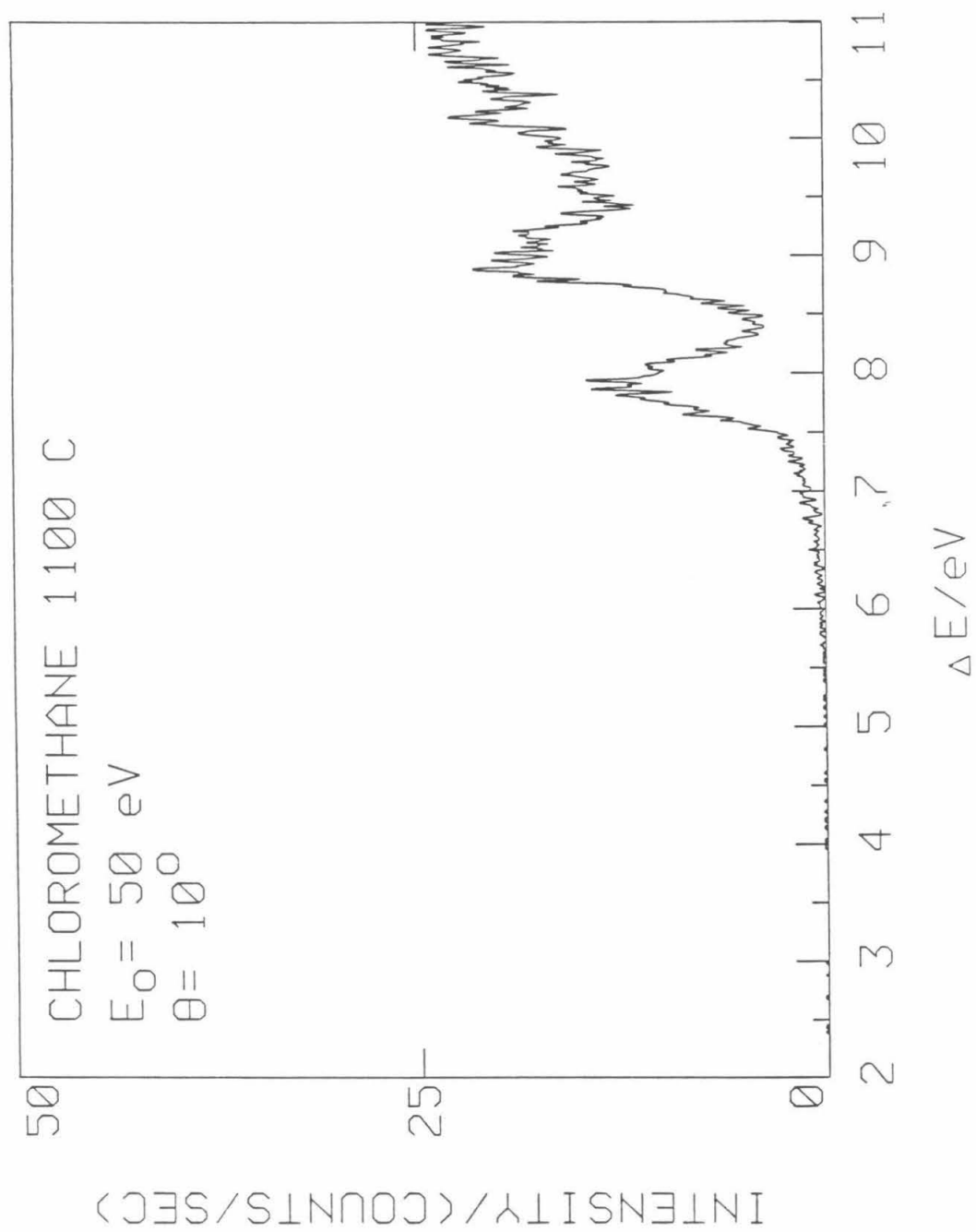


FIGURE 9



CHAPTER 6

EXPLORATORY STUDIES

a) DIKETENE

The far-ultraviolet spectrum of diketene was assigned in Chapter 4. Here we will be concerned with the flash-vacuum pyrolysis of diketene. It is known from the literature¹ that diketene (at pressures around 100 Torr) cleaves cleanly into ketene at 550°C. The pyrolysis of diketene has been shown to be a homogeneous, unimolecular process by demonstrating that the intermolecular secondary deuterium isotope effect is pressure-dependent, decreasing with decreasing pressure.² An activation energy of 50 kcal/mol was obtained for the pyrolysis of diketene in a flow system.²

In our laboratory, we used the method of electron energy-loss spectroscopy to investigate the temperature dependence of the flash-vacuum pyrolysis of diketene. The diketene (Aldrich, 98%) sample was subjected to three liquid-nitrogen, freeze-pump-thaw cycles. The temperature range studied varied from 500° to 1000°C, in steps of 100°C. The temperature was measured by a thermocouple or an optical pyrometer. We observed that under flash-vacuum pressures (1-10 mTorr) a higher temperature, 900°C, was necessary to achieve the complete decomposition of diketene molecule into two ketene molecules.

Figure 1 shows the room temperature spectrum of diketene, while Figure 2 shows the spectrum at 800°C. At this temperature we can observe new features, for example, a shoulder band around 6 eV, but the strongest peak is still the 6.88 eV peak of diketene, and this suggests only partial decomposition. Figures 3 and 4 show the spectra of diketene at 900°C and 1000°C, respectively. At these temperatures, the spectra look completely different from the one at room

temperature. The diketene peak at 6.88 eV seems to be absent and the strongest peak now is at 7.06 eV, the $\pi \rightarrow \pi^*$ transition of ketene, which was studied previously by this group.³ Figure 5 shows a room-temperature spectrum of ketene³ for comparison.

b) TRIFLUOROMETHYL IODIDE

Figure 6 shows the room-temperature spectrum of trifluoromethyl iodide (CF_3I , Aldrich, 98%). There is a weak continuous A band peaking around 4.7 eV that corresponds to $n \rightarrow \sigma^*$ continuum transitions⁴. The peak at 7.26 eV and the strong peak at 7.91 eV correspond to the $\tilde{\text{C}} - \tilde{\text{X}}$ and $\tilde{\text{D}} - \tilde{\text{X}}$ bands, respectively.⁵ The peak at 8.89 eV is the $\tilde{\text{E}} - \tilde{\text{X}}$ band⁵.

Figure 7 presents the spectrum of trifluoromethyl iodide at 1000°C. We can observe the absence of the strong CF_3I peak at 7.91 eV and the appearance of many new sharp peaks. These facts suggest a complete thermal decomposition. Dulgnan *et al.* have reported the thermal decomposition of CF_3I at 1000°C producing trifluoromethyl (CF_3) radical and iodine (I) atom⁶. Before trying to find features that are due to CF_3 radical, let us first identify the features that are due to the iodine molecule (I_2) and atom. The weak peaks at 8.96 and 10.17 eV, as well as the shoulders at 7.12, 7.87, 8.26, and 9.40 eV can be considered as I_2 bands.⁷ The iodine-atom spectrum is a very congested one.⁸ We can assign all the strong peaks and the other features, except perhaps the shoulder at 8.37 eV, as iodine-atom bands. The CF_3 radical has several transitions in the region 7.50 to 8.49 eV.⁹ Its strong peaks are at 7.74, 7.85, 7.95, 8.17, 8.27, and 8.37 eV.^{6,9} Thus, the shoulder at 8.37 eV may possibly be considered as a CF_3 feature.

c) TRICHLOROBROMOMETHANE

Figure 8 shows the room-temperature spectrum of trichlorobromomethane (BrCCl_3). The BrCCl_3 sample (Aldrich, 99%) was subjected to three freeze-pump-thaw cycles. We can observe two broad peaks at 6.72 and 8.16 eV followed by an even broader peak superimposed with three smaller peaks at 9.00, 9.33, and 9.62 eV. No far-ultraviolet spectrum of BrCCl_3 has been reported in the literature.

Figure 9 shows the spectrum of chlorine (Cl_2) molecule at room temperature for comparison with the high-temperature BrCCl_3 spectrum. The Cl_2 shows peaks at 8.12, 9.20, and 9.74 eV. The two last peaks can be assigned as $\pi_g \rightarrow 4p\sigma$ and $\pi_g \rightarrow 4p\pi$ Rydberg transitions,¹⁰ respectively.

Figure 10 shows the BrCCl_3 spectrum at 900°C. Now we have a very congested and noisy spectrum. It was suggested that this thermal decomposition occurs via production of trichloromethyl (CCl_3) radicals and bromine (Br) atoms,¹¹ but in our case the carbon-chlorine bonds were broken, too. The spectrum shows a broad band peaking around 6.3 eV which combined with a shoulder around 9.6 eV and a broad peak around 10.4 eV would suggest the presence of tetrachloroethylene (C_2Cl_4).¹² The sharp features are tentatively attributed to Br, Br_2 , Cl, and Cl_2 . The Br peaks are at 8.12, 8.39, 8.58, 9.45, and 10.20 eV.¹³ The Br_2 feature is at 8.66 eV.¹⁴ The Cl features are at 9.04 and 10.12 eV.¹⁵ Finally, the Cl_2 has a peak at 9.22 eV, which corresponds to the strongest Cl_2 peak in figure 9.

d) HEXACHLOROACETONE

Figure 11 presents the room temperature spectrum of hexachloroacetone ($\text{CCl}_3\text{COCCl}_3$). The $\text{CCl}_3\text{COCCl}_3$ sample (Aldrich, 98%) was subjected to three liquid nitrogen freeze-pump-thaw cycles. In this spectrum, the first feature is a

broadband continuum peaking around 4.2 eV, followed by two broad peaks at 6.31 and 7.62 eV, respectively. An even broader peak with two smaller sharp peaks superimposed occurs at 9.28 and 9.68 eV. The far- ultraviolet spectrum of $\text{CCl}_3\text{COCCl}_3$ has not been reported in the literature.

Figure 12 shows the $\text{CCl}_3\text{COCCl}_3$ spectrum at 900°C . This spectrum suggests partial decomposition with well-defined, new features. Again, a broadband peaking around 6.3 eV in connection with peaks at 9.6 and 10.4 eV is indicative of tetrachloroethylene.¹² A sharp peak at 9.2 eV can be recognized as the strongest Cl_2 peak in Figure 9. Starting about 8 eV and ending just before 9 eV, there is a broad peak with some structural features that can be attributed to the $X^1\Sigma^+ \rightarrow A^1\Pi$ carbon monoxide band with some of its vibrational structure.¹⁶ The shoulderlike feature in the region 4.0-5.0 eV was not identified (see chloroform in page 38 of the Chapter 5).

e) *DICHLOROBROMOMETHANE*

Figure 13 shows the spectrum of dichlorobromomethane (BrCHCl_2) at room temperature. The BrCHCl_2 sample (Aldrich, 98%) was subjected to three liquid-nitrogen, freeze-pump-thaw cycles. The spectrum starts with a broadband continuum shoulder peaking around 5.8 eV, followed by a broad peak at 6.62 eV. A broad shoulder starts at 7 eV, ending at 8.2 eV, and is followed by a broad flat peak that ends at 9 eV. Then we have two broad peaks at 9.28 and 10.45 eV, respectively. The spectrum of BrCHCl_2 in the far-ultraviolet region has not been reported in the literature.

Figure 14 shows the spectrum of hydrogen bromide (HBr , Matheson, 99.8%) at room temperature for comparison with the high-temperature BrCHCl_2 spectrum. The HBr spectrum starts with a broadband continuum peaking around 6.8 eV,

which is attributed to the $4p\sigma \rightarrow \sigma^*$ band.¹⁷ This band is followed by a series of sharp peaks at 8.33, 8.76, 9.08, 9.35, 9.91, 10.08, 10.41, and 10.80 eV, which have been assigned by Nee *et al.*¹⁷ The two first sharp peaks correspond to the Rydberg states of $C^1\Pi$ and $b^3\Pi$ which belong to the ns series with $n = 5$.¹⁷

Figure 15 shows the BrCHCl_2 spectrum at 1000°C . The spectrum looks somewhat noisy and congested. It was suggested that this thermal decomposition occurs via production of a dichloromethyl (CHCl_2) radical and bromine atom,¹⁸ but in our case the carbon-chlorine and carbon-hydrogen bonds were broken, too. Once again, a broadband around 6.3 eV plus two peaks at 9.6 and 10.4 eV is indicative of tetrachloroethylene.¹² There are bromine atom sharp peaks at 8.10, 8.37, 8.56, 9.43, and 10.18 eV.¹³ The Br_2 feature is at 8.64 eV.¹⁴ There are HBr peaks at 8.31, 8.74, 10.40 and 10.80 eV.¹⁷ The strong and sharp peak at 9.62 eV is due mainly to HCl¹⁹ (see Figure 1 in Chapter 5), but has some contribution from the C_2Cl_4 9.6 eV peak. The shoulders in the regions 4.0-5.0 eV (see chloroform in page 38 of the Chapter 5) and 7.0-8.0 eV were not identified.

References

1. S. Andreades and H. D. Carlson, *Org. Synth.*, **45**, 50 (1965).
2. J. S. Chickos and D. E. Sherwood, Jr., *J. Org. Chem.*, **43**, 1146 (1978).
3. R. P. Frueholtz, W. M. Flicker, and A. Kuppermann, *Chem. Phys. Lett.*, **38**, 57 (1976).
4. A. Gedanken, *Chem. Phys. Lett.*, **137**, 462 (1987).
5. G. Herzberg, *Molecular Spectra and Molecular Structure III, Electronic Spectra and Electronic Structure of Polyatomic Molecules*, Van Nostrand, Princeton (1966), p. 532.
6. M. T. Dulgnan, J. W. Hudgens, and J. R. Wyatt, *J. Phys. Chem.*, **86**, 4156 (1982).
7. A. Hiraya, K. Shobatake, R. J. Dovan, and A. Hopkirk, *J. Chem. Phys.*, **88**, 52 (1988).
8. C. C. Kiess and C. H. Corliss, *J. Res. Nat. Bur. Stand. Sect. A*, **63**, 1 (1959).
9. N. Basco and F. G. M. Hathorn, *Chem. Phys. Lett.*, **8**, 291 (1971).
10. L. C. Lee, M. Suto, and K. Y. Tang, *J. Chem. Phys.*, **84**, 5277 (1986).
11. S. W. Benson and H. E. O'Neal, *Kinetic Data on Gas Phase Unimolecular Reactions*, NSRDS-NBS21, Washington (1970), p.500.
12. C. F. Koerting, K. N. Walzl, and A. Kuppermann, *Chem. Phys. Lett.*, **109**, 140 (1984).
13. J. L. Tech, *J. Res. Nat. Bur. Stand. Sect. A*, **67**, 505 (1963).
14. R. J. Donovan and D. Husain, *Trans. Faraday Soc.*, **62**, 2643 (1966).
15. L. J. Radziemski, Jr. and V. Kaufman, *J. Opt. Soc. Am.*, **64**, 366 (1974).
16. S. Trajmar, J. K. Rice, and A. Kuppermann, *Adv. Chem. Phys.*, **18**, 15 (1970).
17. J. B. Nee, M. Suto, and L. C. Lee, *J. Chem. Phys.*, **85**, 4919 (1986).

18. Reference 12, page 499.
19. J. B. Nee, M. Suto, and L.C. Lee, *J. Chem. Phys.*, **85**, 719 (1986).

Figure Captions

- Fig. 1 Electron energy-loss spectrum at room temperature of diketene with $E_o = 50$ eV and $\theta = 10^\circ$. All spectra were measured with an effusive jet as the target source.
- Fig. 2 Electron energy-loss spectrum at 800°C of diketene with $E_o = 100$ eV and $\theta = 15^\circ$.
- Fig. 3 Electron energy-loss spectrum at 900°C of diketene with $E_o = 50$ eV and $\theta = 10^\circ$.
- Fig. 4 Electron energy-loss spectrum at 1000°C of diketene with $E_o = 50$ eV and $\theta = 10^\circ$.
- Fig. 5 Electron energy-loss spectrum at room temperature of ketene with $E_o = 50$ eV and $\theta = 20^\circ$.
- Fig. 6 Electron energy-loss spectrum at room temperature of trifluoromethyl iodide with $E_o = 50$ eV and $\theta = 10^\circ$.
- Fig. 7 Electron energy-loss spectrum at 1000°C of trifluoromethyl iodide with $E_o = 50$ eV and $\theta = 10^\circ$.
- Fig. 8 Electron energy-loss spectrum at room temperature of bromotrichloromethane with $E_o = 50$ eV and $\theta = 10^\circ$.
- Fig. 9 Electron energy-loss spectrum at room temperature of chlorine with $E_o = 50$ eV and $\theta = 10^\circ$.
- Fig. 10 Electron energy-loss spectrum at 900°C of bromotrichloromethane with $E_o = 50$ eV and $\theta = 10^\circ$.
- Fig. 11 Electron energy-loss spectrum at room temperature of hexachloroacetone with $E_o = 50$ eV and $\theta = 10^\circ$.
- Fig. 12 Electron energy-loss spectrum at 900°C of hexachloroacetone with $E_o = 50$ eV and $\theta = 10^\circ$.

Fig.13 Electron energy-loss spectrum at room temperature of bromodichloromethane with $E_o = 50 \text{ eV}$ and $\theta = 10^\circ$.

Fig. 14 Electron energy-loss spectrum at room temperature of hydrogen bromide with $E_o = 50 \text{ eV}$ and $\theta = 10^\circ$.

Fig.15 Electron energy-loss spectrum at 1000°C of bromodichloromethane with $E_o = 50 \text{ eV}$ and $\theta = 10^\circ$.

FIGURE 1

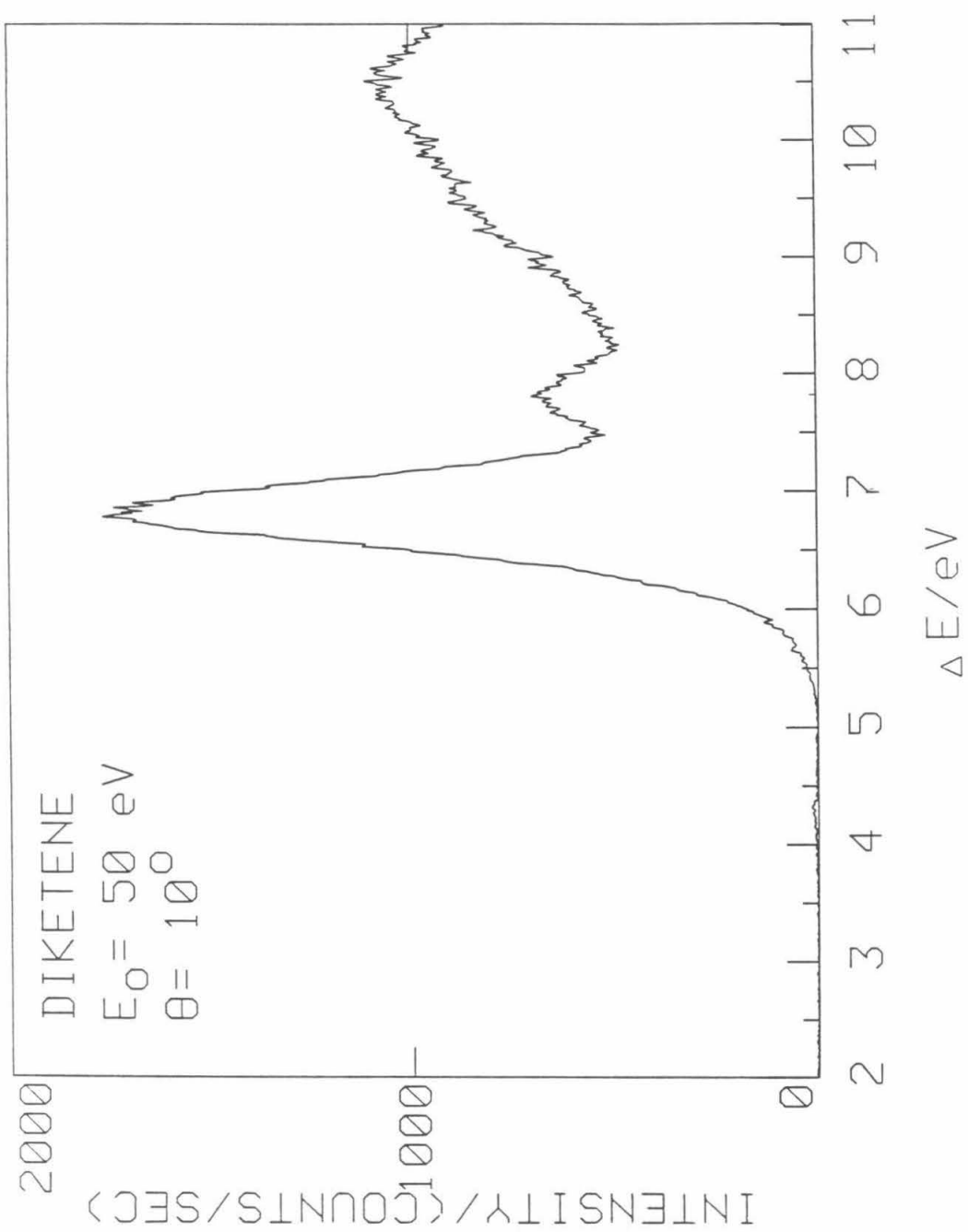


FIGURE 2

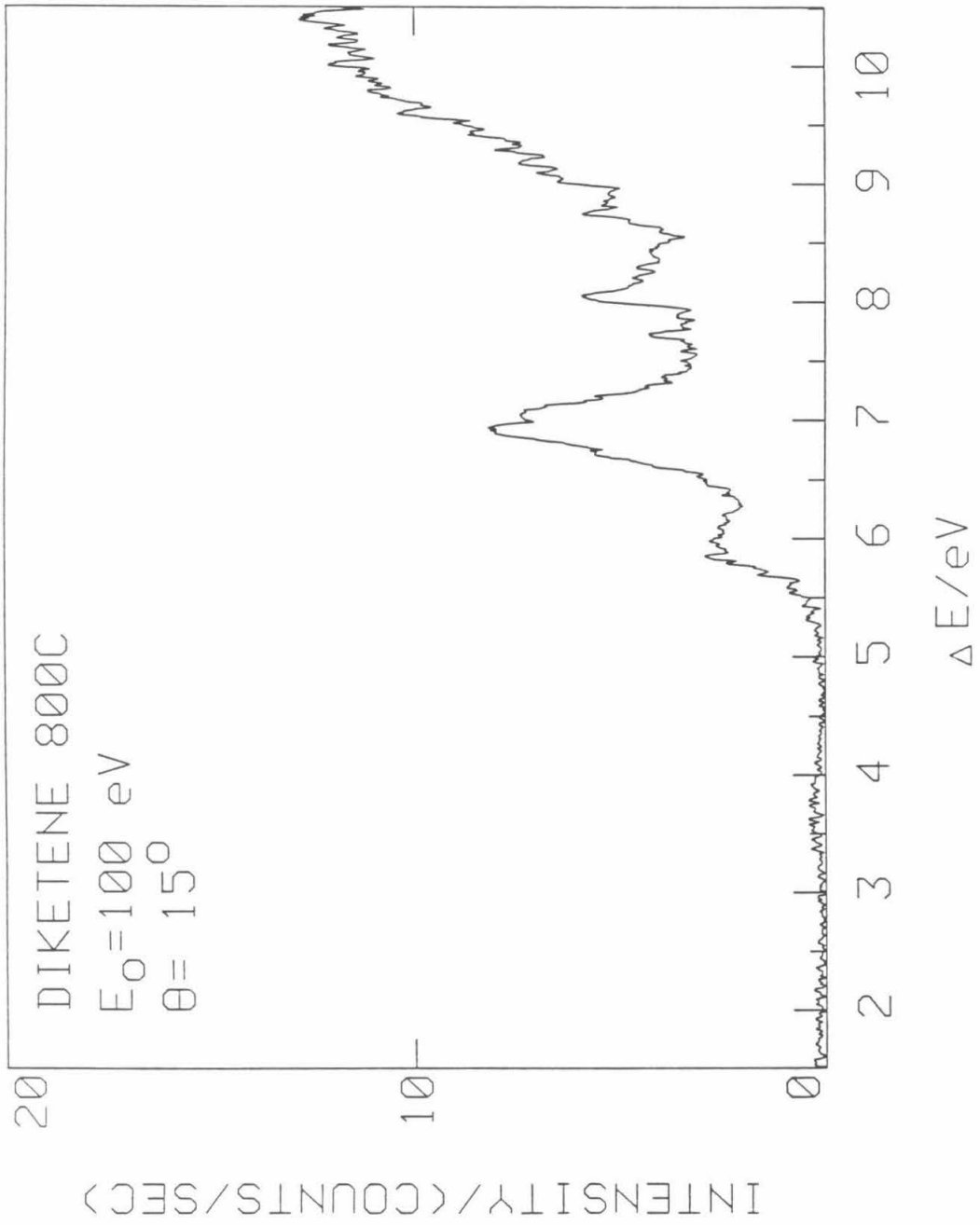


FIGURE 3

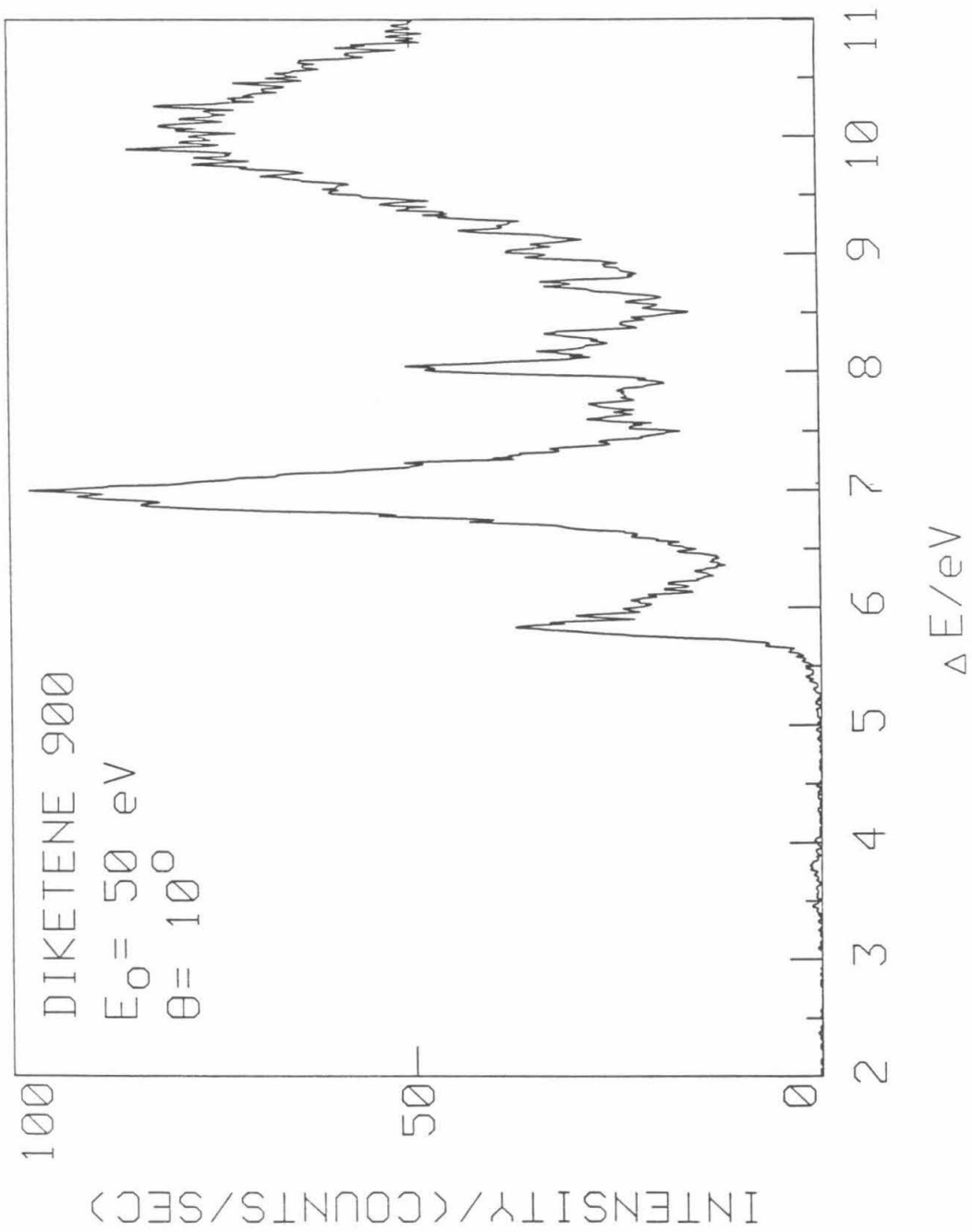


FIGURE 4

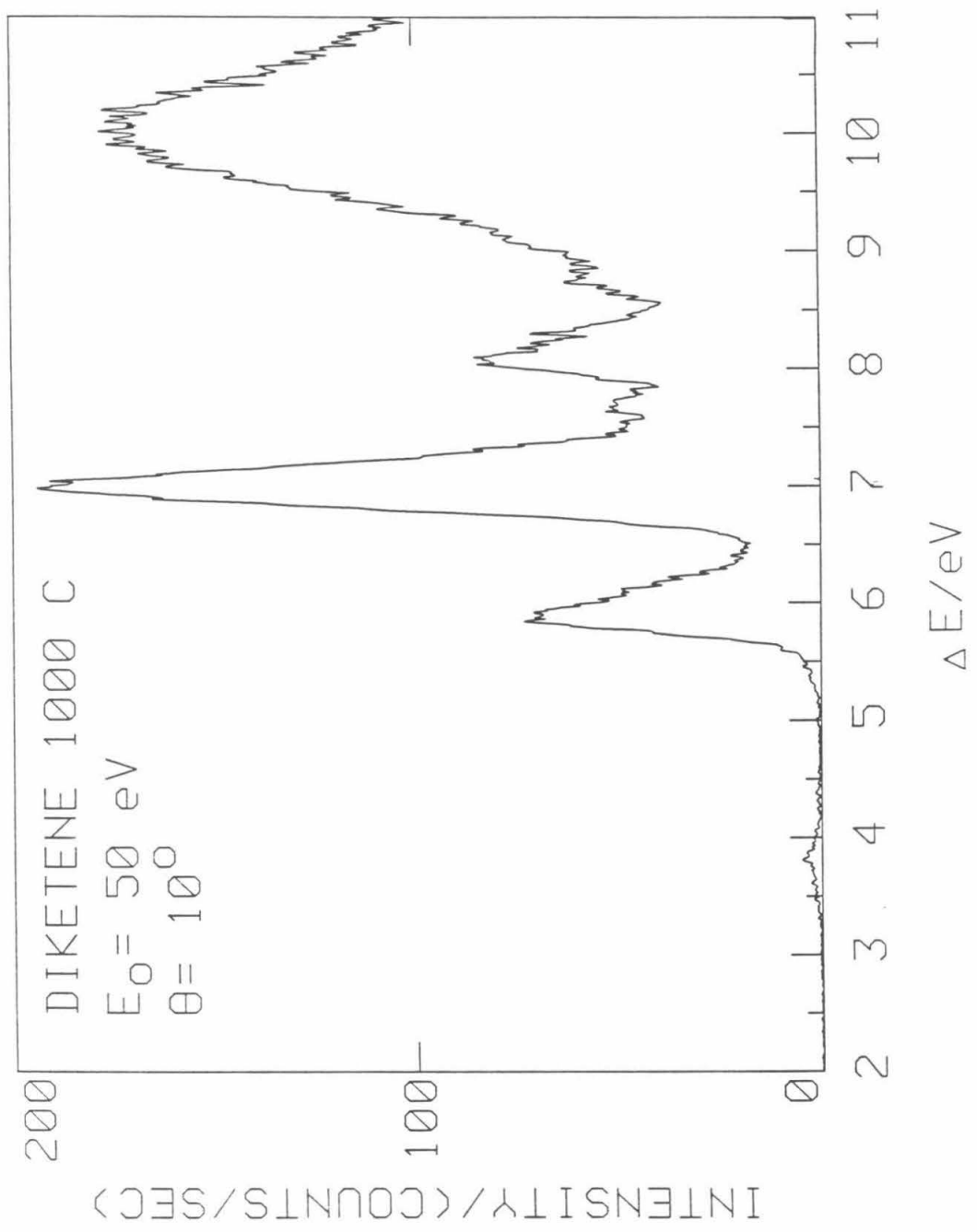


FIGURE 5

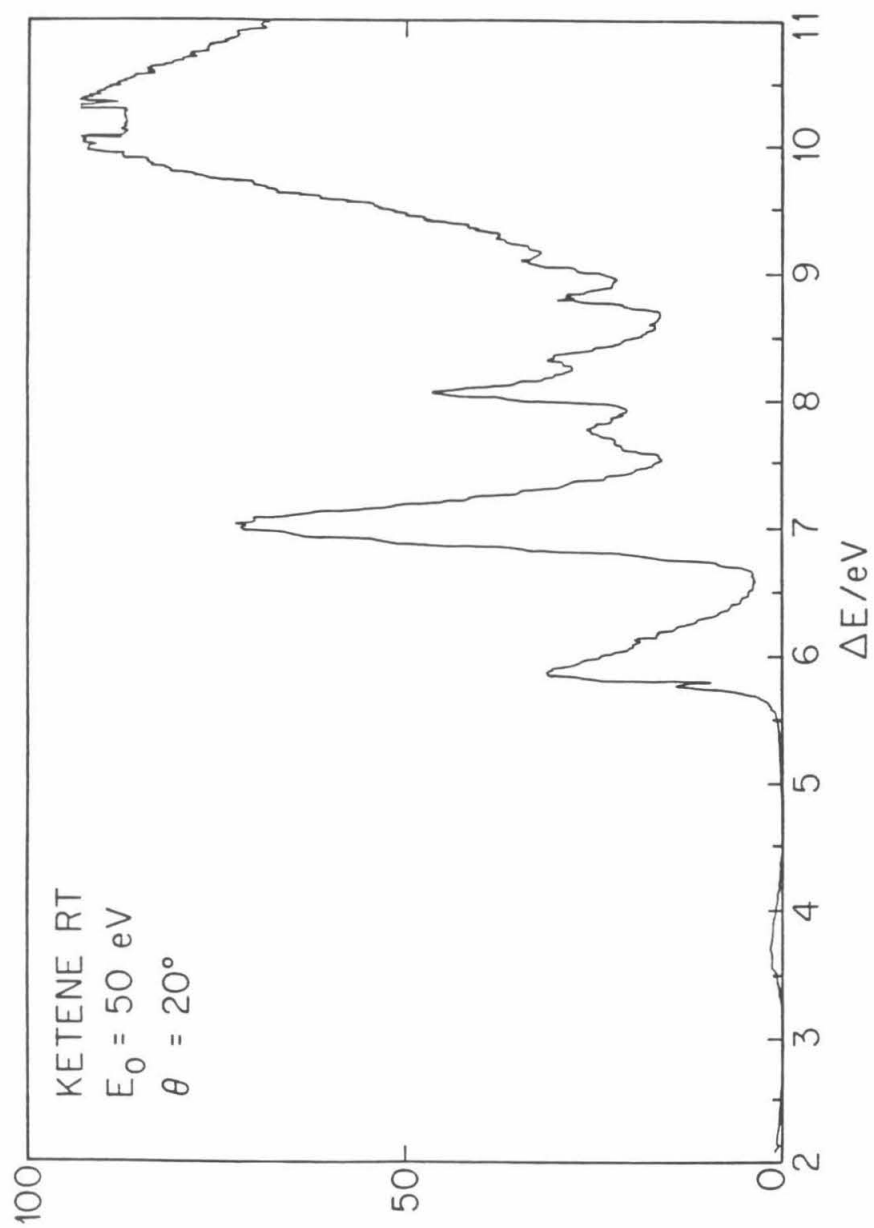


FIGURE 6

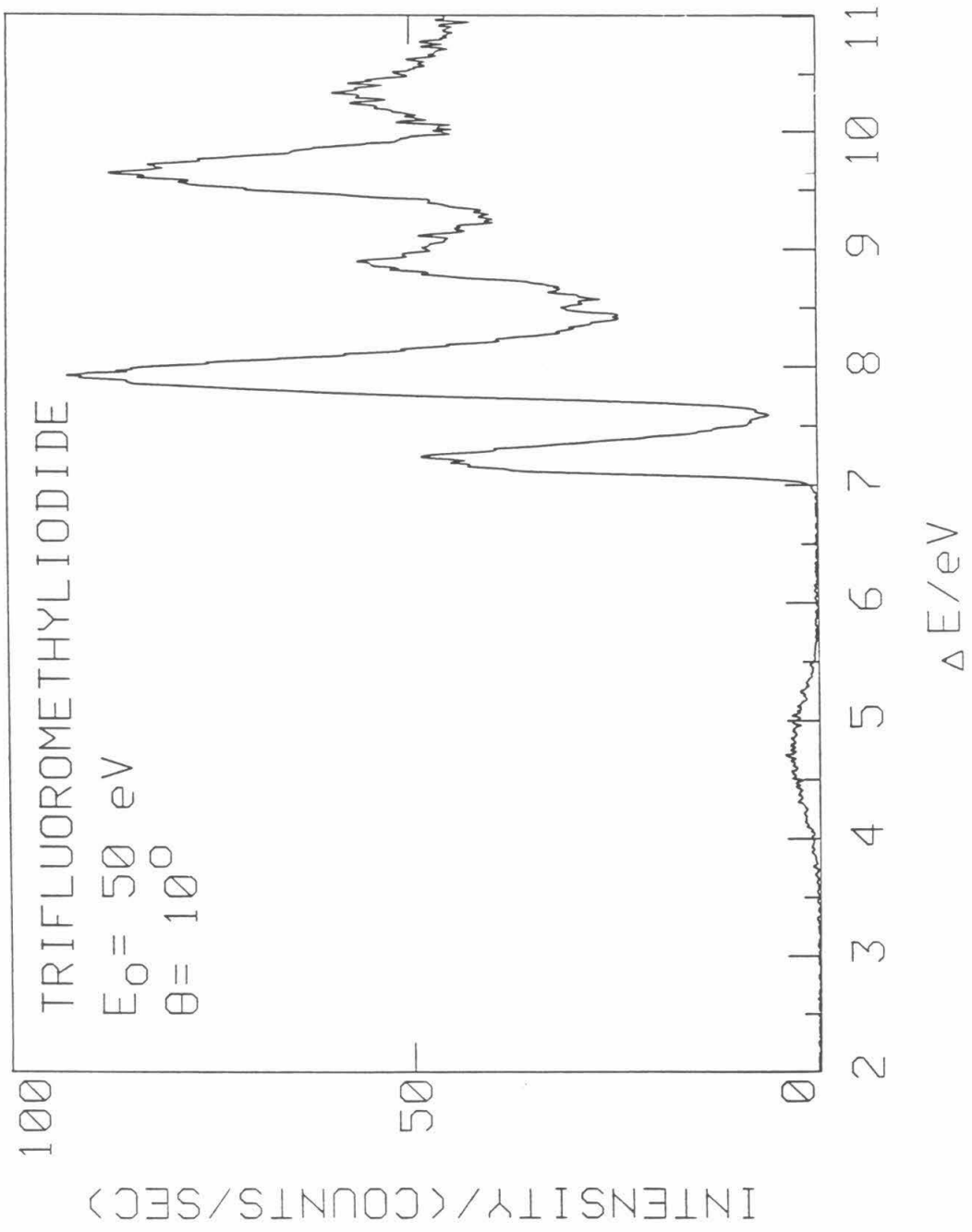


FIGURE 7

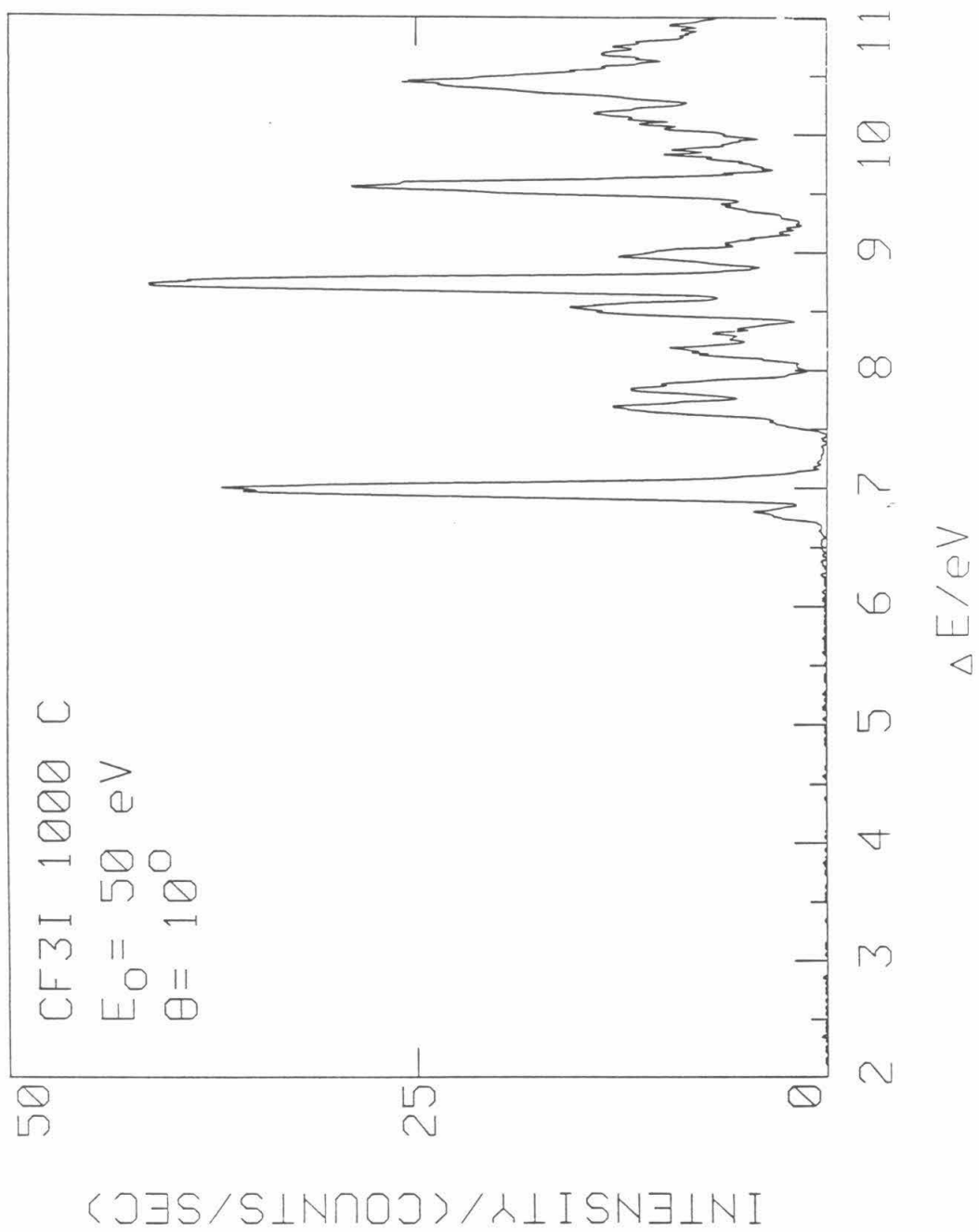


FIGURE 8

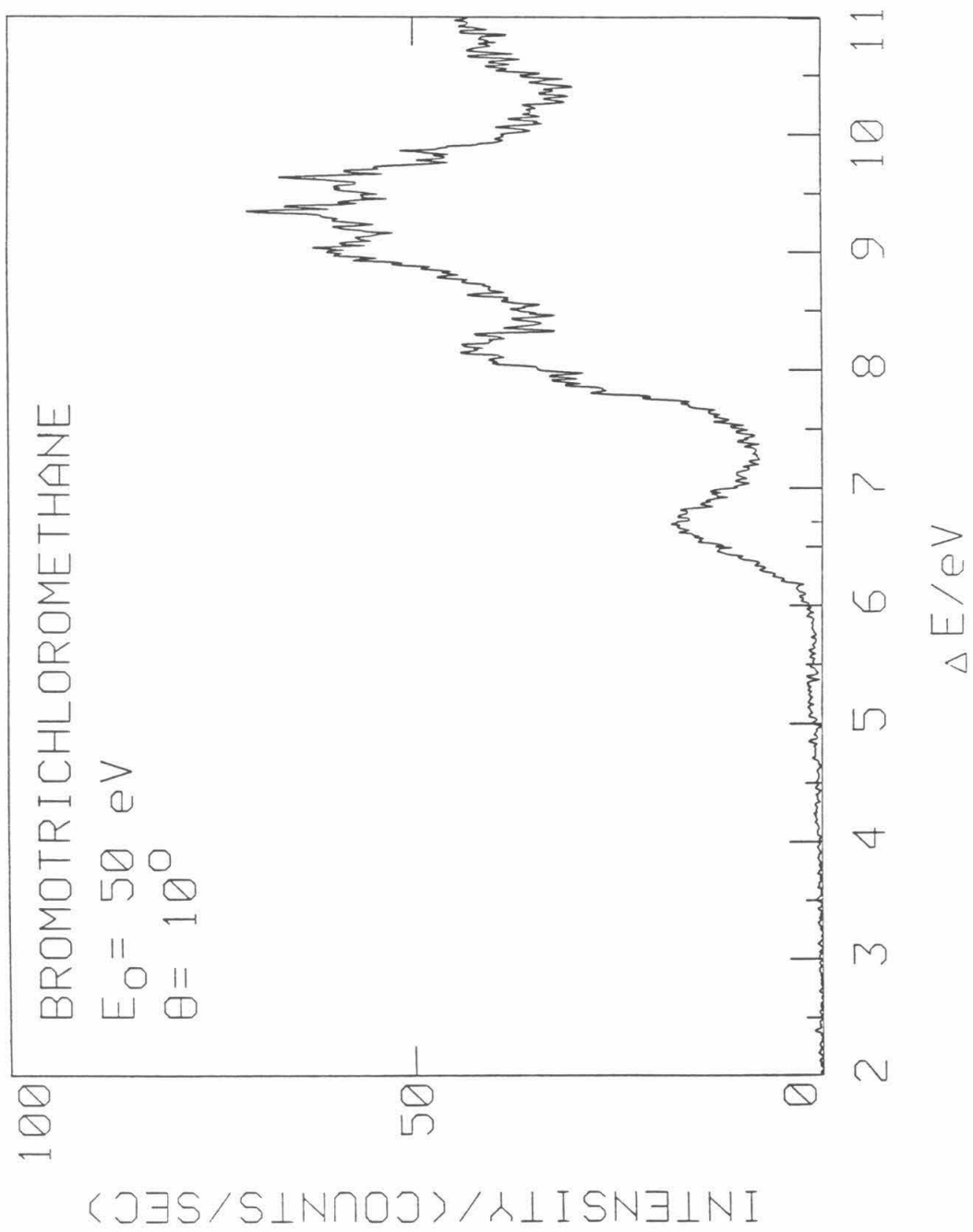


FIGURE 9

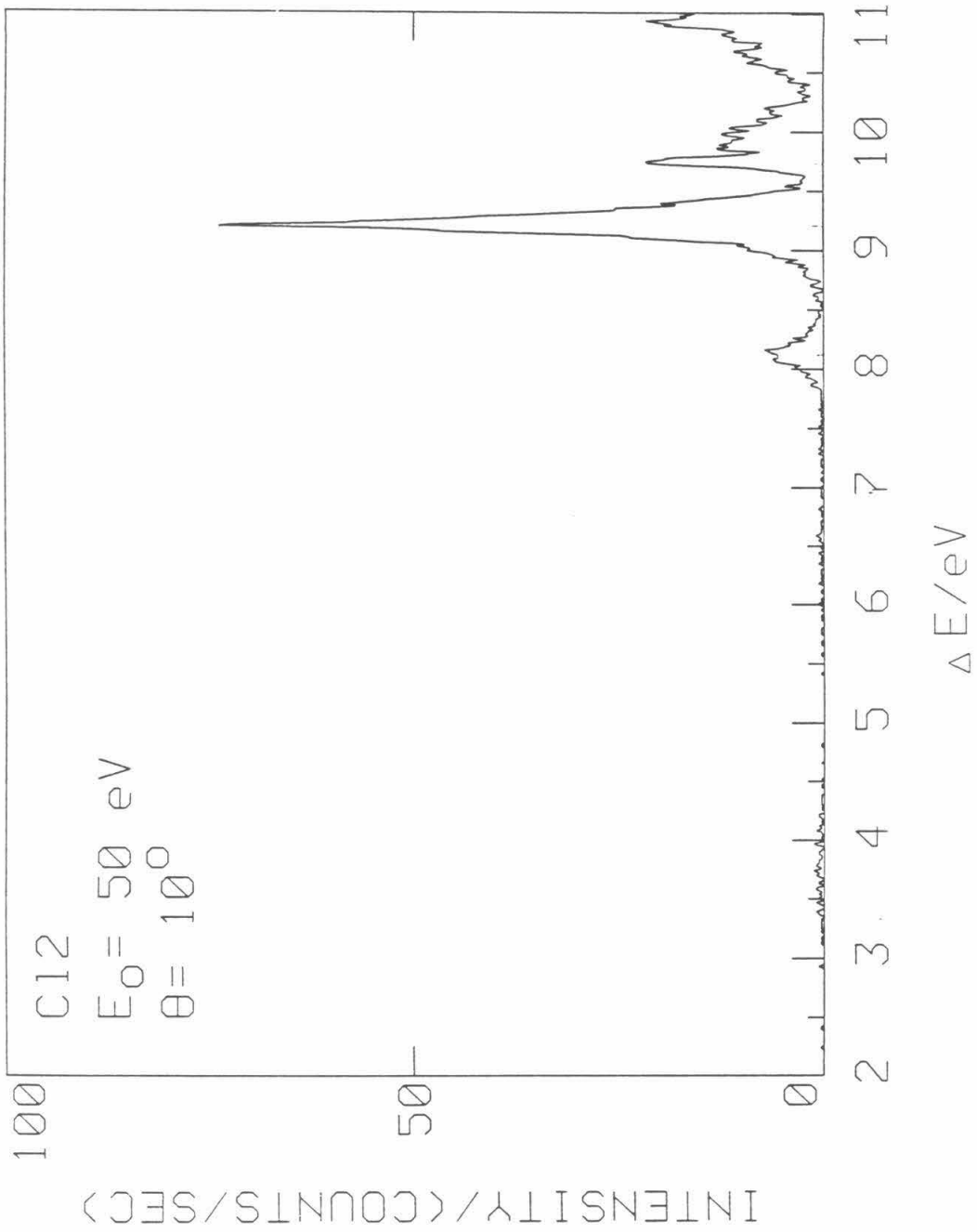


FIGURE 10

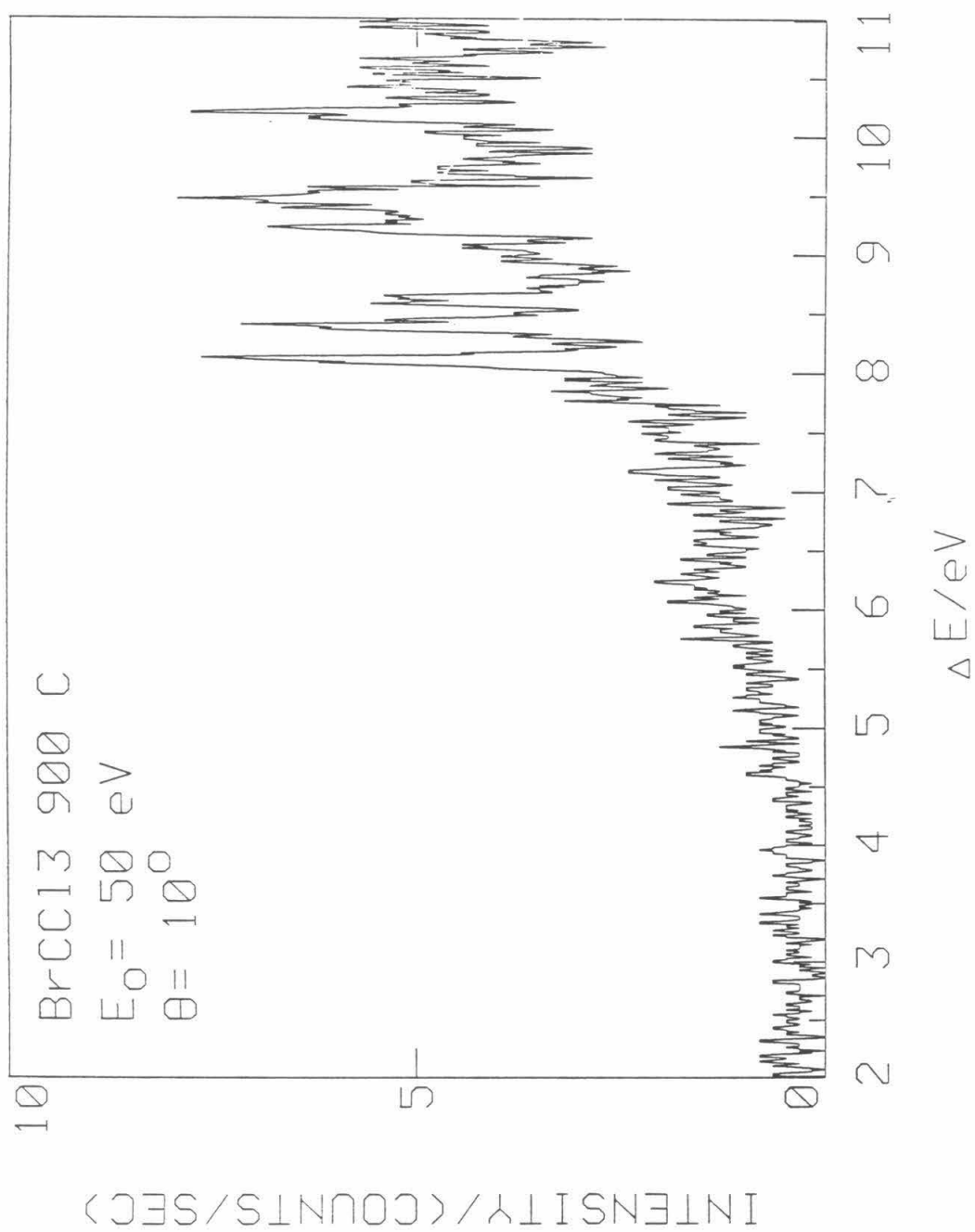


FIGURE 11

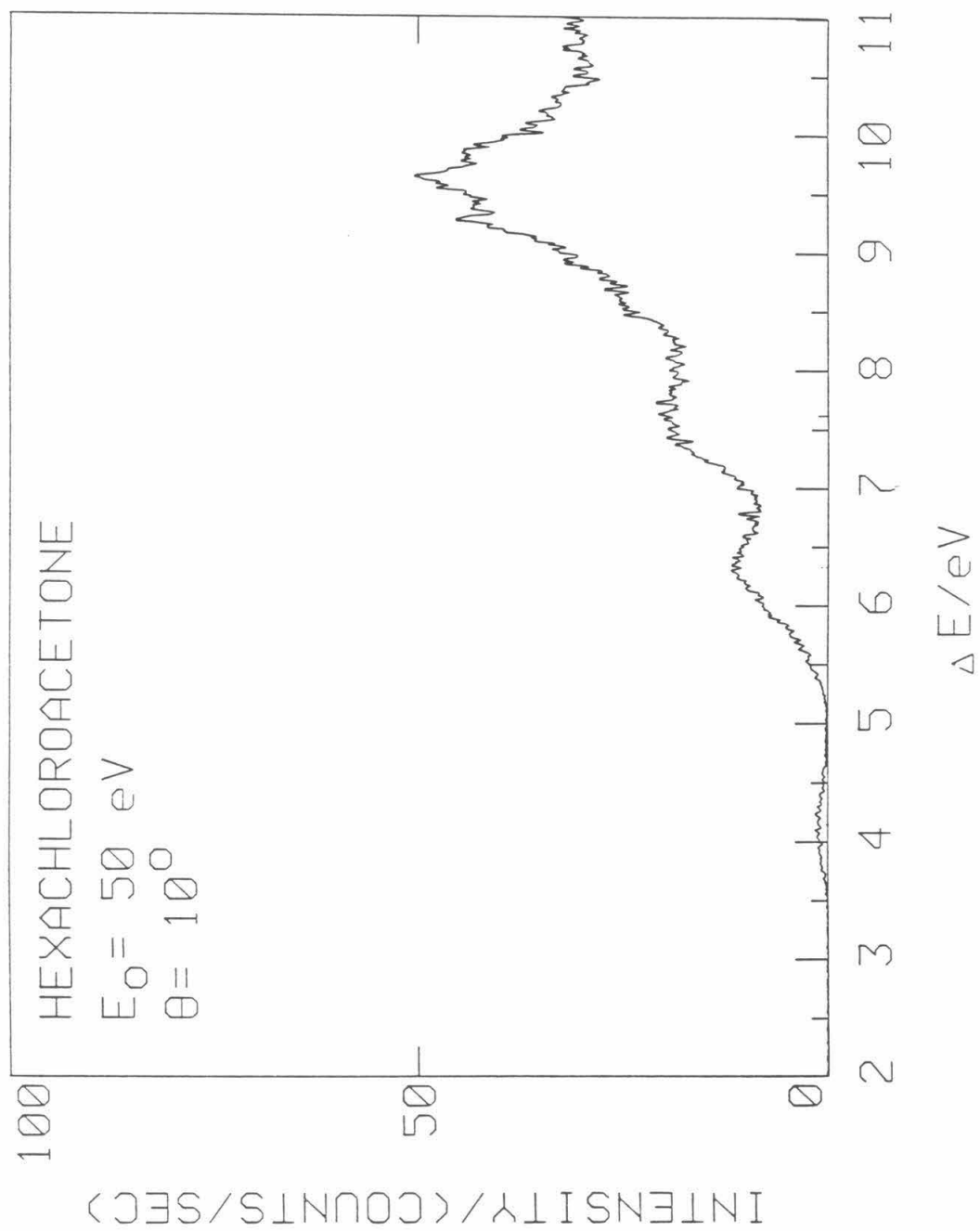


FIGURE 12

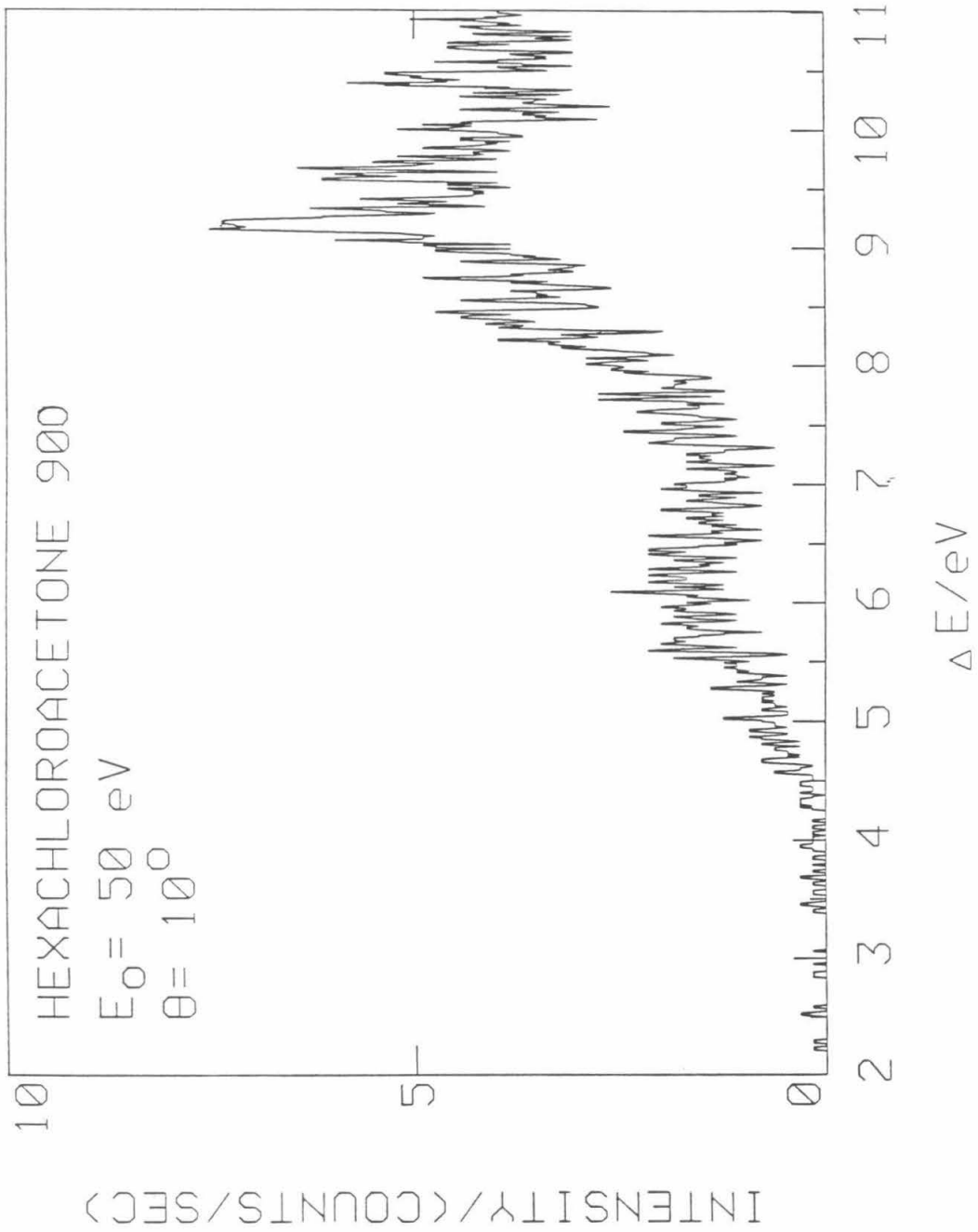


FIGURE 13

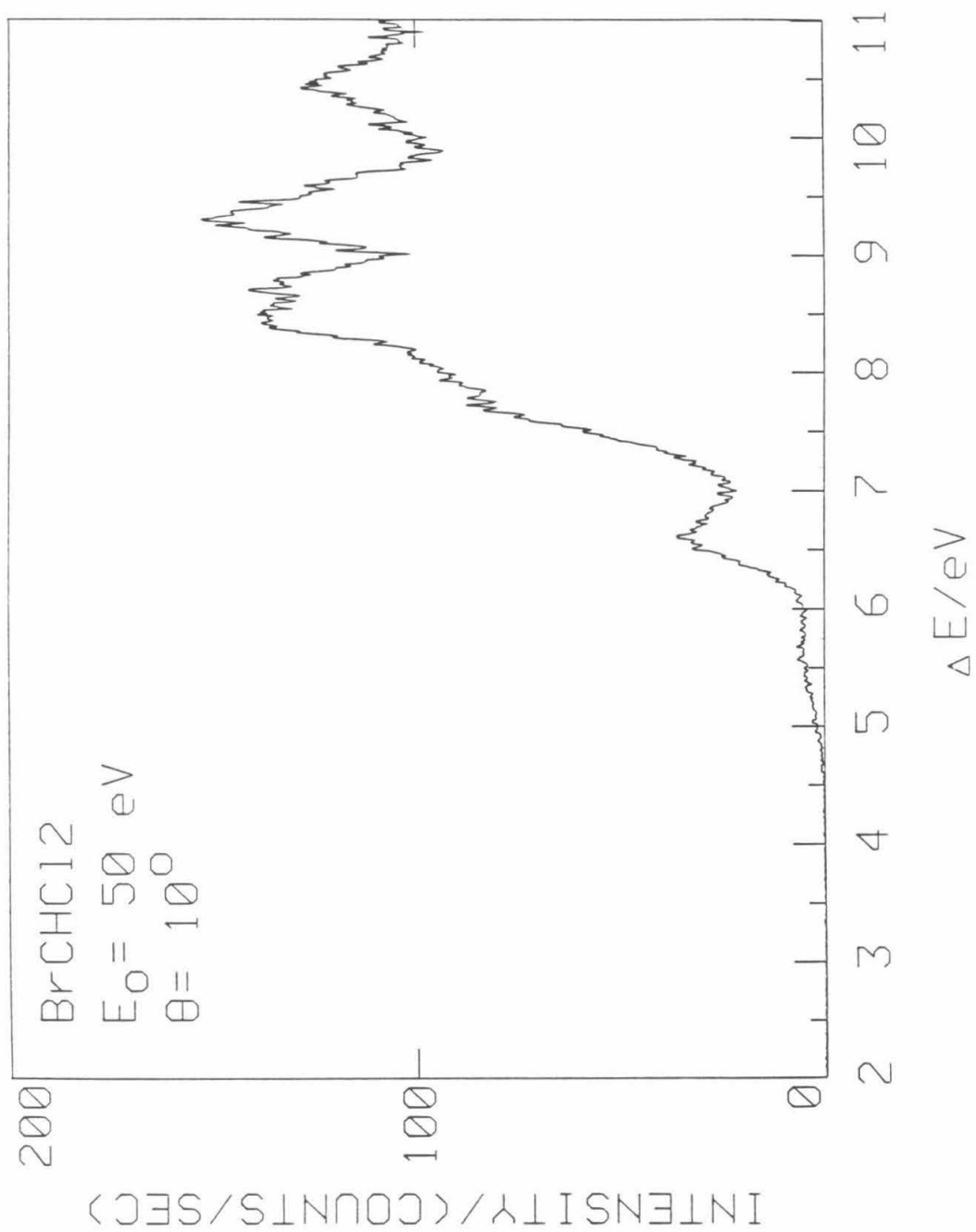


FIGURE 14

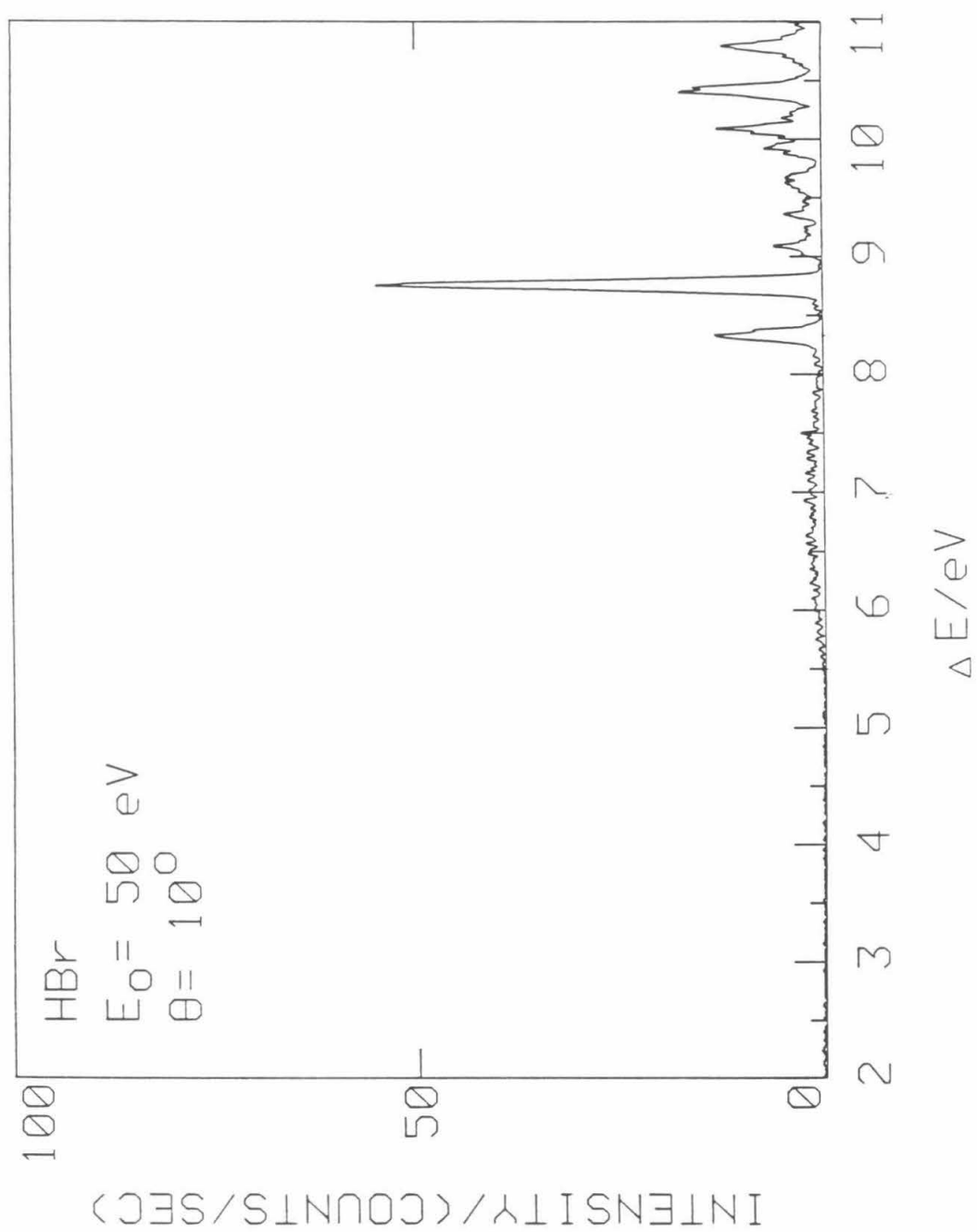
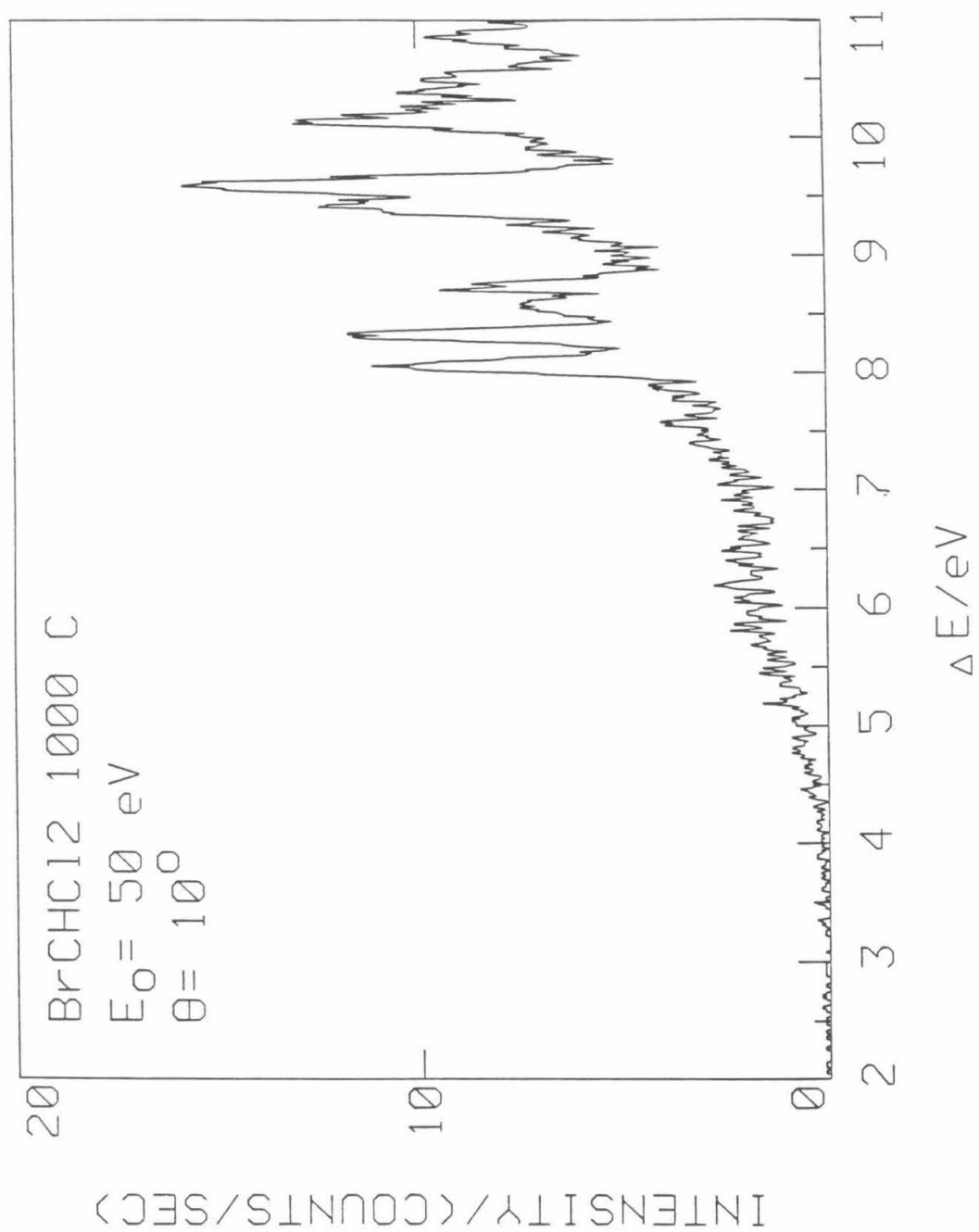


FIGURE 15



APPENDIX 1

Paper 3: *AN ELECTRON-IMPACT SPECTROSCOPY INVESTIGATION
OF CH₃ AND SOME OF ITS PYROLYTIC PRECURSORS*

(Published at *J. Chem. Phys.*, **86**, 89 (1987).)

An Electron-Impact Spectroscopy Investigation of CH_3
and Some of Its Pyrolytic Precursors^a

K. N. Walzl^b, C. F. Koerting^c, I. M. Xavier, Jr.^d, and A. Kuppermann

Arthur Amos Noyes Laboratory of Chemical Physics,^e

California Institute of Technology, Pasadena, CA 91125

(Received 14 August 1986; accepted 3 September 1986)

Abstract

The electronic spectrum of the methyl radical CH_3 was investigated by the technique of variable-angle, electron energy-loss spectroscopy. By means of pyrolytic decomposition, three possible sources of this radical were tried (tetramethyl tin, ethyl nitrite, and di-*t*-butyl-peroxide). The spectra of these precursors were obtained. Using di-*t*-butyl-peroxide, relative differential cross sections for the lowest-allowed A_2'' 3s Rydberg transition in CH_3 (5.73 eV) were determined at incident energies of 50 eV and 25 eV. The behavior of the differential cross section for this band is analogous to that of a spin-allowed transition in a closed shell system and, as expected, in the vicinity of this band no transition of a spin-forbidden nature is detected.

^a This work was supported in part by the U. S. Department of Energy, Contract No. DE-AM03-76F00767, Project Agreement No. DE-AT03-76ER72004.

^b Work performed in partial fulfillment of the requirements for the Ph.D degree in Chemistry at the California Institute of Technology.

^c Present address: E. I. Dupont de Nemours and Co., Inc., Wilmington, DE 19818.

^d On leave from Departamento de Quimica Fundamental; Universidade Federal de Pernambuco; 50000, Recife, Pernambuco; Brazil.

^e Contribution No. 7456

1. INTRODUCTION

Free radicals play a major role in upper atmospheric chemistry, interstellar chemistry, and combustion chemistry. Many have low-lying electronic states energetically accessible under combustion conditions. In order to fully understand these processes it is necessary to understand the nature of the electronic states involved.

The methyl radical is one of the most important of the polyatomic free radicals and, being one of the simplest hydrocarbons, is a useful model system for molecular orbital theory. It has been extensively studied by Herzberg via optical techniques¹. CH₃ is planar with D_{3h} symmetry and has the ground-state electron configuration

$$(1a_1)^2(2a_1)^2(2e')^4(2a_2'')^1.$$

The ground state is of ²A₂'' symmetry, the unpaired electron lying in a p_z orbital of a₂'' symmetry. The lowest observed transition is the ²A₁' ← ²A₂'' 3s Rydberg excitation at 5.73 eV. The forbidden excitation to the lowest ²E' valence state has not been observed; however, calculations by Lengsfeld *et al.*² and McDiarmid³ place it about 1.5 eV above the lowest 3s Rydberg state. The transitions to the 3p Rydberg states are also dipole, symmetry-forbidden in D_{3h} symmetry, but Hudgens *et al.*⁴ have found them to be at 7.42 eV by a resonantly enhanced, multiphoton ionization technique. The excitation energy of the 3d state is 8.27 eV¹, and the first ionization potential (IP) is at 9.85 eV.^{1b}

A useful technique for probing the nature of electronic transitions is the method of variable-angle, electron energy-loss spectroscopy. When an electron scatters from and excites an atom or molecule, two mechanisms of electronic excitation are possible. The first is the long-range Coulomb excitation and is caused by the electric field produced when an electron passes the target. The differential cross section (DCS) for a transition excited in this manner exhibits a maximum at

the scattering angle $\theta = 0^\circ$ (no change in direction) and decreases by approximately two orders of magnitude as θ increases from 0° to 90° ^{5,6}. The second mechanism of electronic excitation involves the physical exchange of the incident electron with a target electron. The incident electron may exchange with a target electron of either the same or opposite spin; the former exchange process may or may not result in target excitation, while the latter results in excitation to a spin-forbidden state. Transitions excited primarily by this mechanism possess a nearly uniform DCS as a function of scattering angle because of the loss of directional information carried by the incident electron^{5,6}.

With the above considerations in mind, a variable-angle, electron energy-loss spectroscopy study was undertaken of the polyatomic, free-radical CH_3 . It was hoped that this investigation would yield information about possible low-lying, spin-forbidden transitions. Previous electron spectroscopy of free radicals had been limited to stable species that were triatomic or smaller; for example, the electron spectroscopy and differential cross sections have been determined for doublet-doublet allowed and doublet-quartet forbidden transitions in NO_2 by Rianda *et al.*⁷. The present paper reports the first electron-impact spectroscopy investigation of a transient, polyatomic free radical.

2. EXPERIMENTAL

The spectrometer used in the present experiments has been described previously⁸. Briefly, electrons are emitted from a tungsten filament and focused into a hemispherical monochromator. The monoenergetic electrons are then focused into the scattering region and, after interaction with the target molecules, enter a hemispherical analyzer prior to detection.

In order to generate the methyl radicals for the study, an *in situ* pyrolysis technique was employed^{8b}. A quartz tube of 0.060 inch ID with an outer layer of

stainless steel sheathed heater wire (Figure 1) produces an effusive jet of molecules. Pyrolysis temperatures of up to 800°C, as measured by a thermocouple placed on the tube's outer surface, were used in these experiments.

Three sources of methyl radicals were investigated. The first was tetramethyl tin (Aldrich, 99%), known to be a reliable source of methyl radicals⁹. Taylor and Milazzo¹⁰ found a 30% conversion of tetramethyl tin at ≈600°C, with 20% of the organic products existing as CH₃. Using our inlet, temperatures of ≈ 800°C were required to achieve appreciable decomposition. Unfortunately, after five hours of continuous operation, the quartz capillary became obstructed with metallic tin.

A second source of methyl radicals that was tried was ethyl nitrite. It is known that ethyl nitrite thermally decomposes by the reaction¹¹



The gaseous ethyl nitrite was synthesized by mixing ethanol (U. S. Industrial Chemicals Co., anhydrous) and isoamyl nitrite (Aldrich, 97%) in a 2:1 ratio by volume; an ester alcoholysis takes place, producing isoamyl alcohol and continuously bubbling ethyl nitrite¹². A pyrolysis temperature of 450°C was used for the decomposition.

The third source of methyl radicals used was di-*t*-butyl-peroxide (Columbia Organic Chemicals Co., Inc.). It has been shown^{13,14} that the decomposition of di-*t*-butyl-peroxide (TBP) proceeds according to the following scheme:



Since this was the precursor that was used for nearly all of the investigation, an optimization of the temperature needed for methyl production was carried out. The ratio of the methyl peak intensity at 5.73 eV to the acetone peak intensity at 6.36 eV versus temperature was examined at an incident-electron energy $E_0 = 50$ eV and scattering angle $\theta = 10^\circ$ (Figure 2). The ratio was found to possess a

maximum at $300 \pm 50^\circ\text{C}$, and this temperature was used in all subsequent studies. The number density of methyl radicals in the jet at this temperature was estimated to be 10^{13} molecules/cm³, on the basis of the intensity of that 5.73 eV band.

3. RESULTS AND DISCUSSION

In Figure 3 are shown two electron-impact spectra taken at $E_0 = 100$ eV and $\theta = 0^\circ$ between 4.5 and 9.5 eV energy loss. Figure 3a is the spectrum of tetramethyl tin obtained using the pyrolysis source at room temperature. It consists of two broad features with an onset at 5.7 eV and maxima at 6.71, 8.24, and 8.57 eV. Only two previous spectra for this compound have been reported. The first describes merely a continuum with an onset at 5.6 eV rising up to 6.2 eV.¹⁵ The second shows a maximum at 6.7 eV and ends at 7.1 eV.¹⁶ Ours is the first reported UV spectrum of this compound extending to the first IP, located at about 9.7 eV.¹⁷ Intense 3s Rydberg transitions are known to occur in molecules with T_d symmetry, if the originating orbital is of t_2 type.¹⁸ In this case, the 6.71 eV and 8.24 eV features can be fit to the first two members of a Rydberg series with a quantum defect of 0.84 and and IP = 9.62 eV. Figure 3b shows the same spectral region of the compound with the source heated to 800°C . Immediately apparent are the sharp transitions located at 5.70, 8.30, and 8.98 eV. The 5.70 eV transition is assigned to the methyl A_2'' 3s Rydberg excitation. The 8.30 eV and 8.98 eV transitions are assigned to the 3d and 4d Rydberg excitations, respectively. Also of interest is the shoulder extending from 4.90 to 5.75 eV not present in the room-temperature spectrum. It is possible that this shoulder is due to incompletely dissociated tetramethyl tin.

As stated previously, operation of the source with tetramethyl tin was limited to about five hours. In addition, the lowest allowed methyl transition strongly overlapped with the lowest band of the compound, making DCS measurements more difficult. A second precursor investigated was ethyl nitrite. It was expected

that there could be much overlap of the methyl bands with the spectral features arising from the additional products NO and formaldehyde, and this was indeed found to be the case. Figure 4a shows the spectrum of ethyl nitrite without heating. It consists of several broad, structureless features. Previous studies^{19,20} have examined only the lowest band in the region between 3.10 and 4.09 eV^{14,19}, not shown in Figure 4a. Peaks are observed at 5.69, 6.70, 7.76, 8.24, 8.94, 9.44, and 9.76 eV. In analogy with results for methyl nitrite²¹, the transition at 5.69 eV is assigned as $\pi \rightarrow \pi^*$ from an OCH_2CH_3 -localized orbital to a NO-localized orbital. The remaining bands are probably attributable to Rydberg transitions. Figure 4b shows the spectrum of the pyrolyzed ethyl nitrite; the spectrum is highly congested. No feature can be definitively attributed to a known methyl radical feature; every peak in the spectrum can be assigned to either NO²² or formaldehyde^{23,24}. One interesting observation is that the intensities of two $\gamma(\text{A } ^2\Sigma^+ \leftarrow \text{X } ^2\Pi)$ features at 5.92 eV and 6.27 eV are much larger with respect to the nearby $\beta(\text{B } ^2\Pi \leftarrow \text{X } ^2\Pi)$ peaks (at 5.47, 5.75, 6.04, and 6.33 eV) than previously reported.^{25,26} In fact, under conditions of similar incident electron energy and scattering angle, the height of the transition at 6.27 eV is only about 10% of the height of the 6.34 eV transition.^{25,26}

The precursor molecule that was finally used to generate methyl radicals was TBP. Figure 5a shows a spectrum of TBP between 4.25 and 7.75 eV energy-loss at $E_0 = 50$ eV and $\theta = 10^\circ$ at room temperature. It consists of a rising continuum with very little structure visible (the sharp feature at 6.67 eV is due to a Hg contamination). In Figure 5b is shown TBP at a pyrolysis temperature of 400°C (results obtained prior to temperature optimization). The spectrum is drastically different and, as expected, most of the features are due to the pyrolysis product acetone with the exceptions being the sharp peak at 5.74 eV and the broad feature between 5.8 and 6.3 eV. The peak at 5.74 eV is again attributed to the methyl 3s Rydberg transition.

To help confirm the nature of the methyl transition, an angular study was conducted. Figure 6a again shows the spectrum of TBP at $E_0 = 50$ eV and $\theta = 10^\circ$ between 5.6 and 6.4 eV energy loss and at the optimum temperature of 300°C . In contrast, the spectrum of TBP under the same conditions except at $\theta = 60^\circ$ is shown in Figure 6b. It is apparent that no drastic changes occur, although the ratio of the methyl 3s Rydberg transition to the acetone singlet–singlet A_1 3s transition at 6.36 eV goes from approximately 1:2 to 1:3. Increasing the angle further to 90° produces a change in this ratio back to about 1:2; however, because of the increase in the relative intensity of the intervening region of the spectrum, the methyl peak is obscured. Most of the increase in the relative intensity between 5.8 and 6.3 eV is due to the presence of the singlet–triplet $\pi \rightarrow \pi^*$ band of acetone. As previously discussed, the intensity of such spin-forbidden bands are constant with angle, while the intensity of fully allowed bands decreases with angle, hence the relative increase in the acetone singlet–triplet $\pi \rightarrow \pi^*$ band.

The DCS curves plotted in Figure 7 illustrate the integrated intensity changes for these bands. The elastic peak and the acetone $n \rightarrow 3s$ peak exhibit an intensity decrease of about two orders of magnitude as should fully allowed bands. The methyl A_2'' 3s Rydberg band seems to be exhibiting this behavior also, but the curve begins to become more constant, starting at $\theta = 60^\circ$. This is the angle where the spin-forbidden $\pi \rightarrow \pi^*$ band of acetone begins manifesting itself more strongly and, if this effect is subtracted out using the known angular behavior of this acetone band²⁴ and the acetone 3s Rydberg transition as a scaling feature, the DCS curve behaves more like a fully allowed band. At $E_0 = 50$ eV, there seems to be little contribution from a spin-forbidden transition in methyl in the region of the A_2'' 3s Rydberg band.

For CH_3 , one would probably expect no low-lying, spin-forbidden bands to be in evidence. All transitions from the highest-occupied a_2'' orbital are spin-

allowed because the electron is unpaired. Likewise, only a spin-allowed version of the predicted lowest valence transition is possible. This contrasts with allowed Rydberg transitions converging to the second IP, which would have spin-forbidden counterparts. A calculation by Millie and Berthier²⁷ places the second IP approximately 5 eV higher than the first IP. Thus, a spin-allowed excitation from the $2e'$ orbital to the $3s$ orbital would lie at about 10.5 eV and the spin-forbidden excitation at about 9.5 eV, allowing a singlet-triplet splitting of 1 eV (as Brongersma and Oosterhoff²⁸ found for the $3s$ Rydberg transition from a corresponding orbital in methane).

Another angular study was performed with the incident energy lowered to $E_0 = 25$ eV (Figure 8). In this case the behavior is not as marked; however, the general trend, suggesting that there is no spin-forbidden contribution to the methyl spectrum in the vicinity of the A''_2 $3s$ Rydberg band, is confirmed.

4. SUMMARY

The spectra of three pyrolytic sources of methyl radicals (tetramethyl tin, ethyl nitrite, di-*t*-butyl-peroxide) were investigated by variable-angle, electron energy-loss spectroscopy, both at room temperature and at elevated temperatures. Of the three precursors, di-*t*-butyl-peroxide was found to be the most useful for radical generation. The spectrum of the decomposition co-product acetone has only moderate overlap with that of methyl and also is fairly well understood, so that its effect can be removed. Regarding the $3s$ Rydberg excitation in CH_3 , it has been found to possess a DCS in accord with its fully allowed nature.

5. ACKNOWLEDGMENTS

One of the authors (IMX) acknowledges a graduate fellowship from CAPES and UFPE (Brazil).

REFERENCES

1. (a) G. Herzberg, *Proc. R. Soc. London Ser. A* **262**, 291 (1961); (b) G. Herzberg, *Electronic Spectra of Polyatomic Molecules* v3. (Van Nostrand, Princeton, 1966), pp. 347, 513-15.
2. B. H. Lengsfeld III, P. E. Siegbahn, and B. Liu, *J. Chem. Phys.* **81**, 710 (1984).
3. R. McDiarmid, *Theor. Chim. Acta* **20**, 282 (1971).
4. J. W. Hudgens, T. G. DiGiuseppe, and M. C. Lin, *J. Chem. Phys.* **79**, 571 (1983).
5. A. Kuppermann, J. K. Rice, and S. Trajmar, *J. Phys. Chem.* **72**, 3894 (1968).
6. S. Trajmar, J. K. Rice, and A. Kuppermann, *Adv. Chem. Phys.* **18**, 15 (1970).
7. R. Rianda, R. P. Frueholz, and A. Kuppermann, *J. Chem. Phys.* **79**, 5914 (1983).
8. (a) C. F. Koerting, K. N. Walzl, and A. Kuppermann, *Chem. Phys. Lett.* **109**, 140 (1984); (b) C. F. Koerting, Ph.D. Thesis, California Institute of Technology, Pasadena, CA (1985).
9. I. S. Zaslonko and V. N. Smirnov, *Kinet. i Katal.* **20**, 575 (1979).
10. J. E. Taylor and T. S. Milazzo, *J. Phys. Chem.* **82**, 847 (1978).
11. F. A. Houle and J. L. Beauchamp, *J. Amer. Chem. Soc.* **101**, 4067 (1979).
12. G. Caldwell and J. Bartmess, *Org. Mass Spect.* **17**, 456 (1982).
13. J. Raley, R. F. Rust, and W. E. Vaughan, *J. Amer. Chem. Soc.* **70**, 88 (1948).
14. L. Batt and S. W. Benson, *J. Chem. Phys.* **36**, 895 (1962).
15. H. W. Thompson and J. W. Linnett, *Proc. R. Soc. London Ser. A* **156**, 108 (1936).

16. P. P. Shorygin, V. A. Petukhov, O. M. Nefedov, S. P. Kolesnikov, and V. I. Shiryaev, *Theoret. Exp. Chem.* **2**, 146 (1966).
17. S. Evans, J. C. Green, P. J. Joachim, A. F. Orchard, D. W. Turner, and J. P. Maier, *J. Chem. Soc. Farad. Trans. 2* **68**, 905 (1972).
18. M. Robin, *Higher Excited States of Polyatomic Molecules* v1. (Academic Press, New York (1974)), pp. 137–38.
19. H. W. Thompson and C. W. Purkis, *Trans. Farad. Soc.* **32**, 674 (1936).
20. J. W. Goodeve, *Trans. Farad. Soc.* **30**, 504 (1934).
21. M. Tanaka, *Bull. Chem. Soc. Japan* **39**, 766 (1966).
22. R. P. Frueholz, R. Rianda, and A. Kuppermann, *J. Chem. Phys.* **68**, 775 (1978).
23. S. Taylor, D. Wilden, and J. Comer, *Chem. Phys.* **70**, 291 (1982).
24. K. N. Walzl, C. F. Koerting, and A. Kuppermann, submitted for publication.
25. E. N. Lassettre, A. Skerbele, M. A. Dillon, and K. J. Ross, *J. Chem. Phys.* **48**, 5066 (1968).
26. R. Rianda, Ph. D. Thesis, California Institute of Technology, Pasadena, CA (1981).
27. P. Millie and G. Berthier, *Int. Jour. Quant. Chem.* **2S**, 67 (1968).
28. H. H. Brongersma and L. J. Oosterhoff, *Chem. Phys. Lett.* **3**, 437 (1969).

FIGURE CAPTIONS

Figure 1. Schematic diagram showing the free-radical beam source. GI: gas inlet, H: heater, QT: quartz tube, SL: swagelock fitting, TS: tantalum shield.

Figure 2. Graph of the ratio of integrated intensity for the methyl 3s Rydberg transition at 5.73 eV to the acetone, 3s Rydberg transition at 6.36 eV as a function of temperature. $E_0 = 50$ eV, $\theta = 10^\circ$.

Figure 3. Energy-loss spectrum of tetramethyl tin with a) pyrolysis source off, b) pyrolysis source on $T = 800^\circ\text{C}$. For both spectra $E_0 = 100$ eV, $\theta = 0^\circ$. Incident-electron current = 5 nAmp, estimated sample pressure = 1 mtorr.

Figure 4. Energy-loss spectrum of ethyl nitrite with a) pyrolysis source off, b) pyrolysis source on, $T = 450^\circ\text{C}$. For both spectra $E_0 = 50$ eV, $\theta = 10^\circ$. Incident-electron current = 10 nAmp, estimated sample pressure = 1 mtorr.

Figure 5. Energy-loss spectrum of TBP with a) pyrolysis source off, b) pyrolysis on, $T = 400^\circ\text{C}$. For both spectra $E_0 = 50$ eV, $\theta = 10^\circ$. Conditions same as Figure 4.

Figure 6. Energy-loss spectrum of TBP at a pyrolysis temperature of 300°C and $E_0 = 50$ eV: a) $\theta = 10^\circ$, b) $\theta = 60^\circ$, c) $\theta = 90^\circ$. Conditions same as Figure 4. Vertical lines indicate magnitude of error in spectral intensity.

Figure 7. DCS plot of pyrolyzed TBP $E_0 = 50$ eV. Elastic scattering (EP) $\times 0.1$: + , acetone 3s Rydberg $\times 100$: \bigcirc , methyl 3s Rydberg $\times 100$: \square , methyl 3s Rydberg (corrected by subtracting contribution of acetone spin-forbidden band) $\times 100$: \triangle . Arbitrary units are the same for all curves, which are multiplied by scaling factor before plotting.

Figure 8. DCS plot of pyrolyzed TBP $E_0 = 25$ eV. EP $\times 0.1$: + , acetone 3s Rydberg $\times 100$: \bigcirc , methyl 3s Rydberg $\times 1000$: \square , corrected methyl 3s Rydberg $\times 1000$: \triangle .

FIGURE 1.

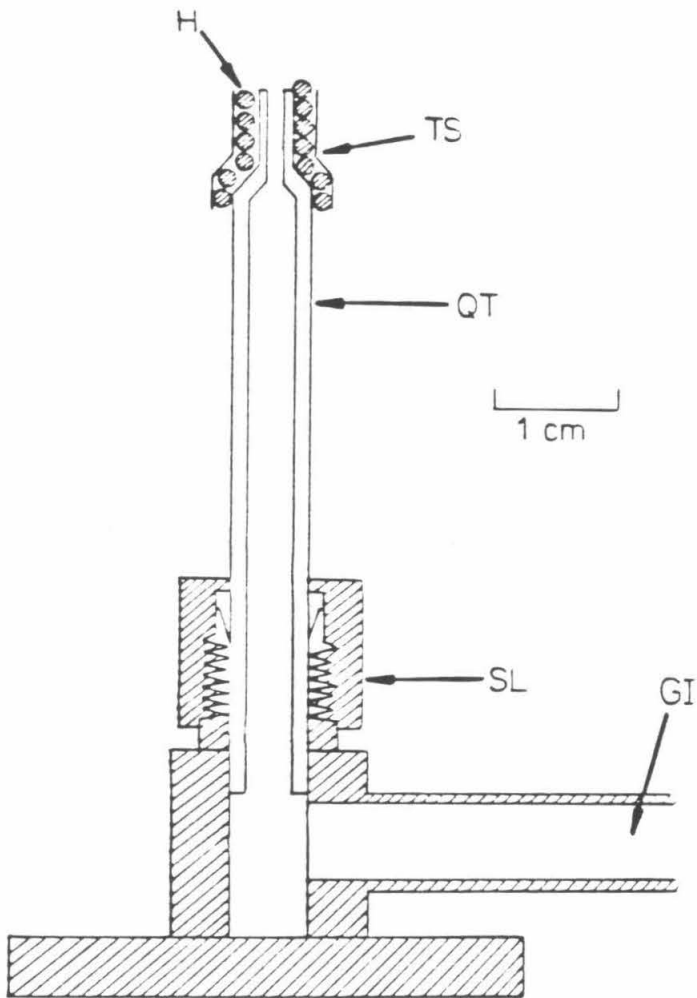


FIGURE 2.

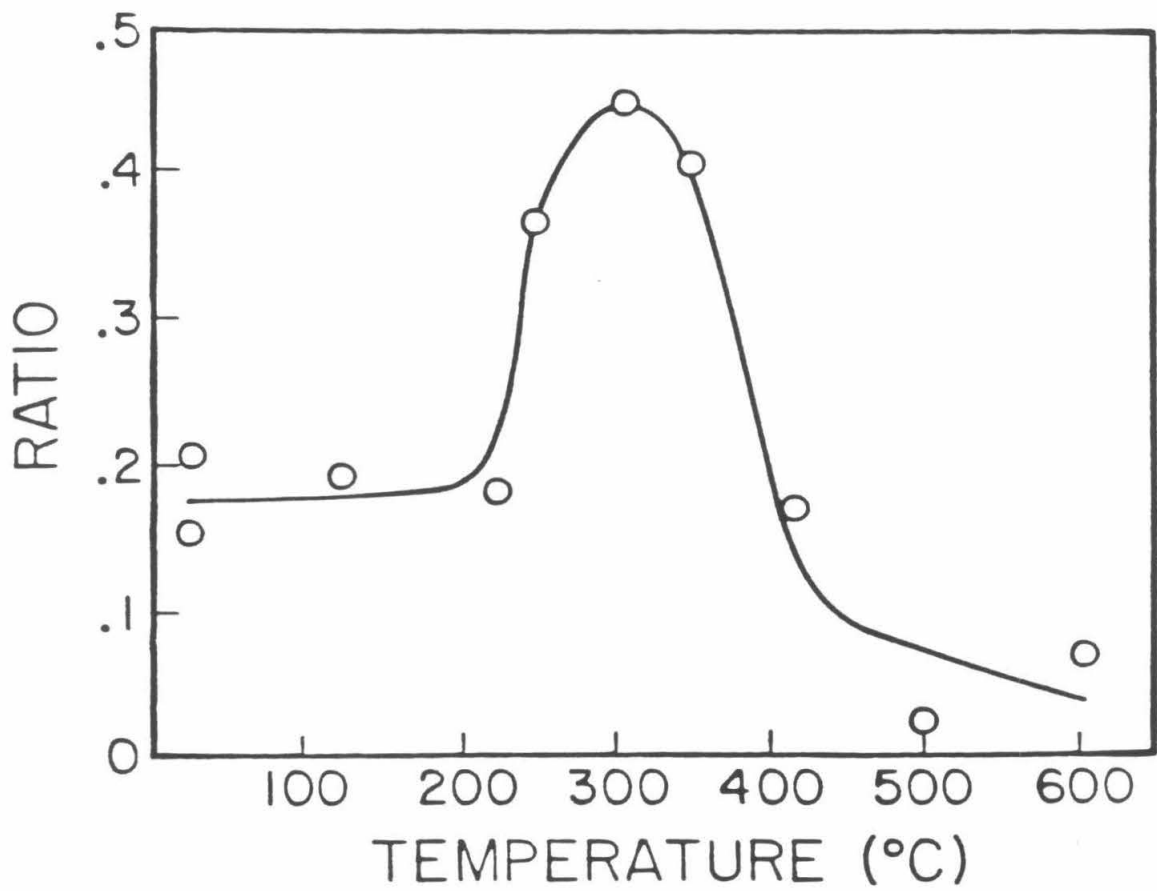


FIGURE 3.

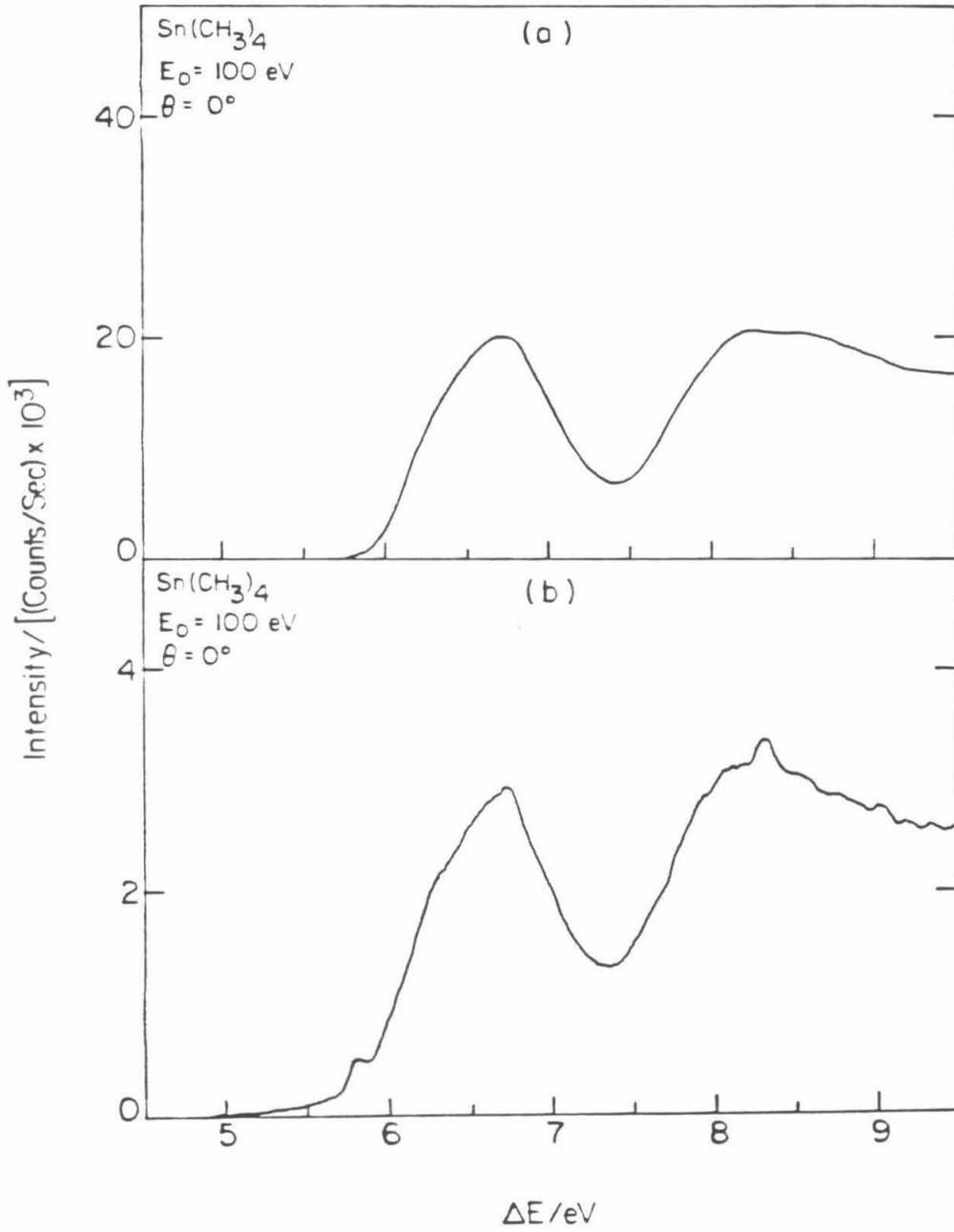


FIGURE 4.

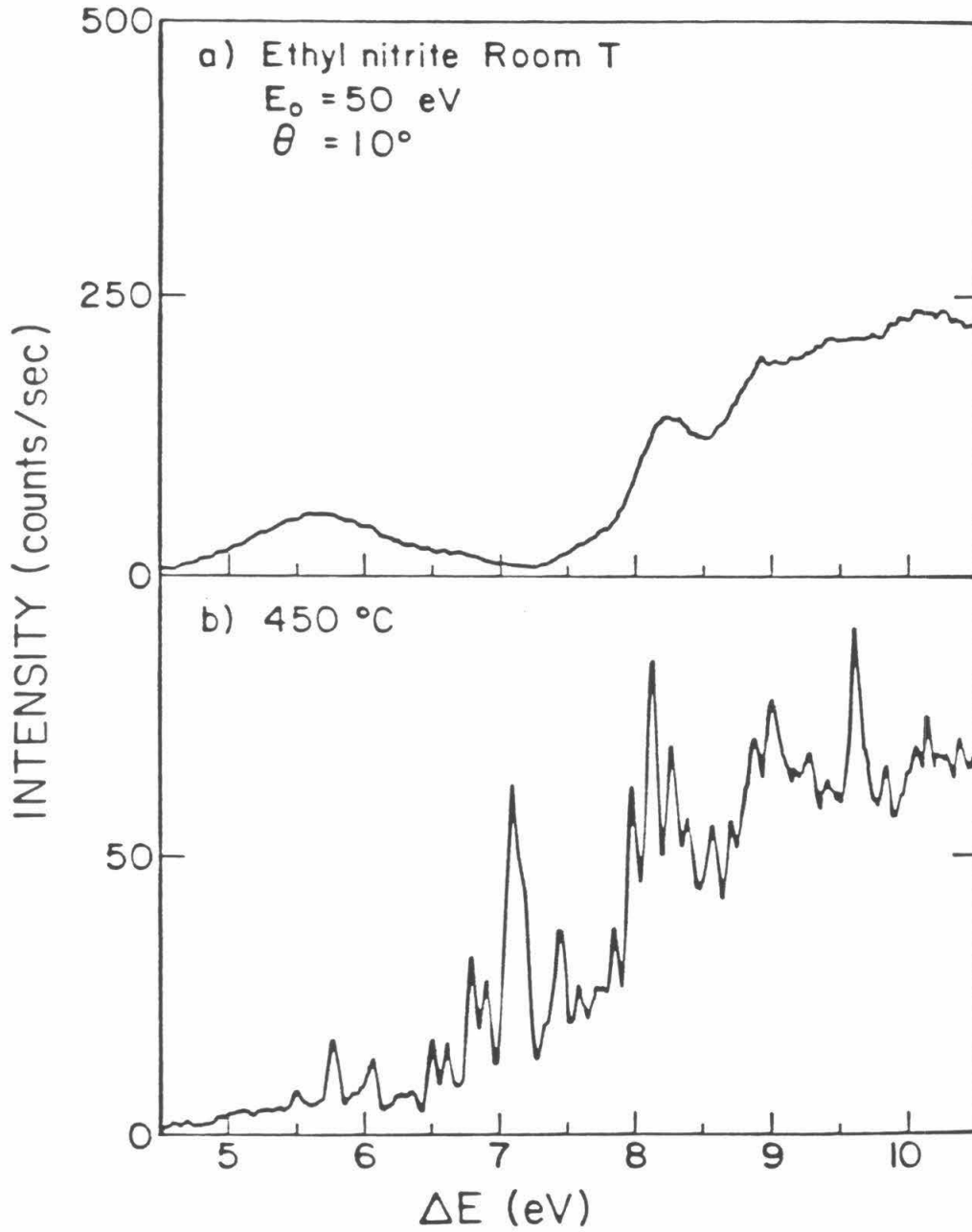


FIGURE 5.

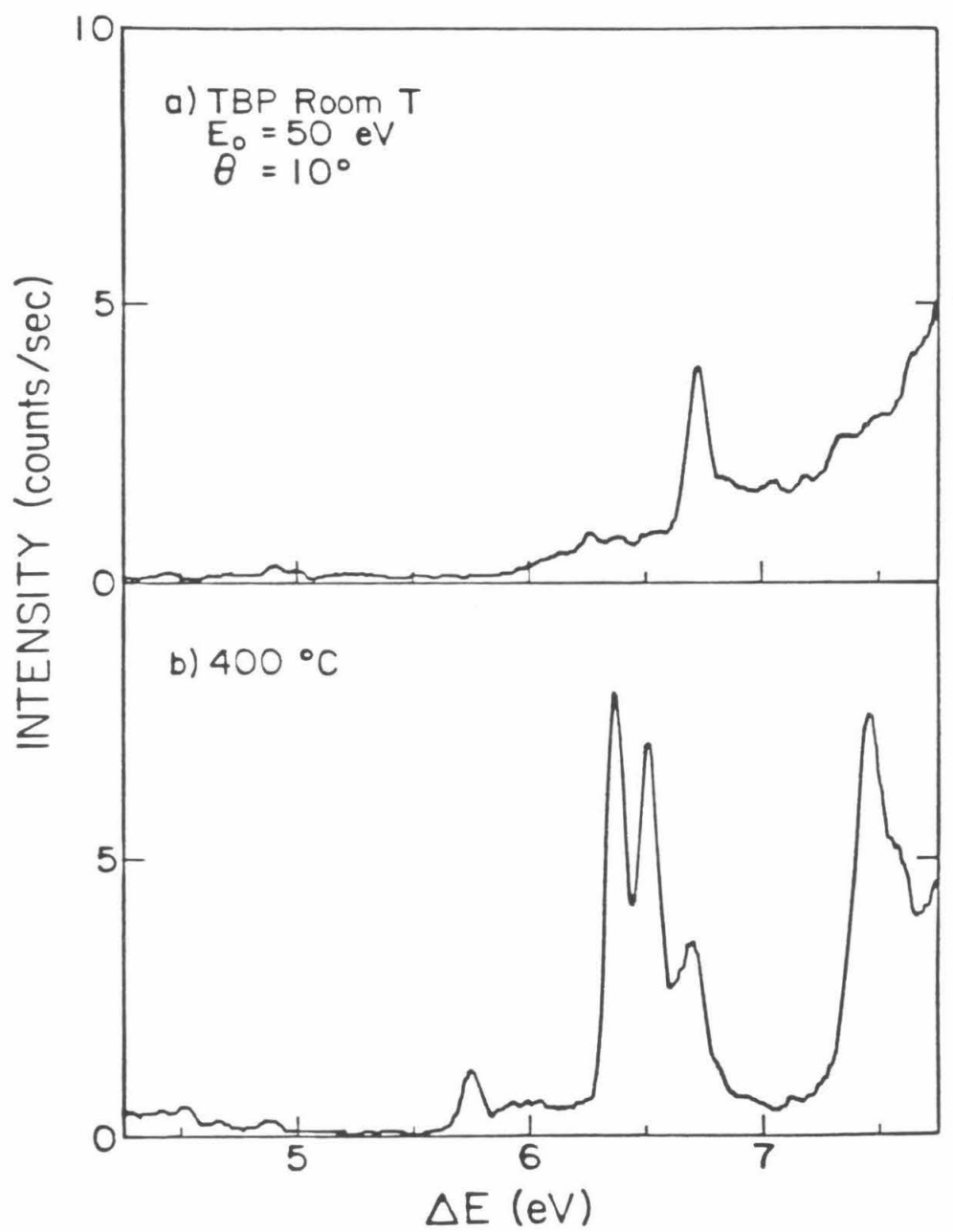


FIGURE 6.

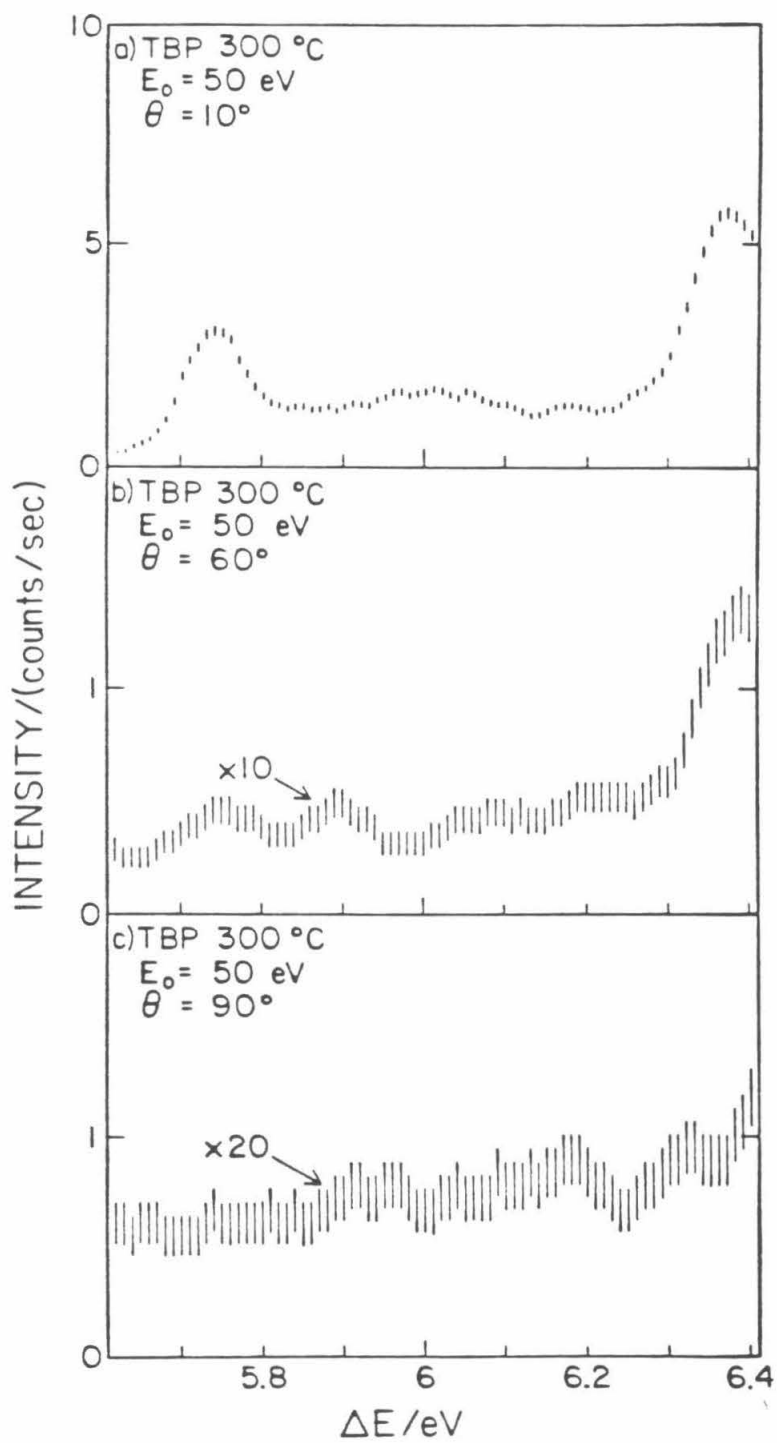


FIGURE 7.

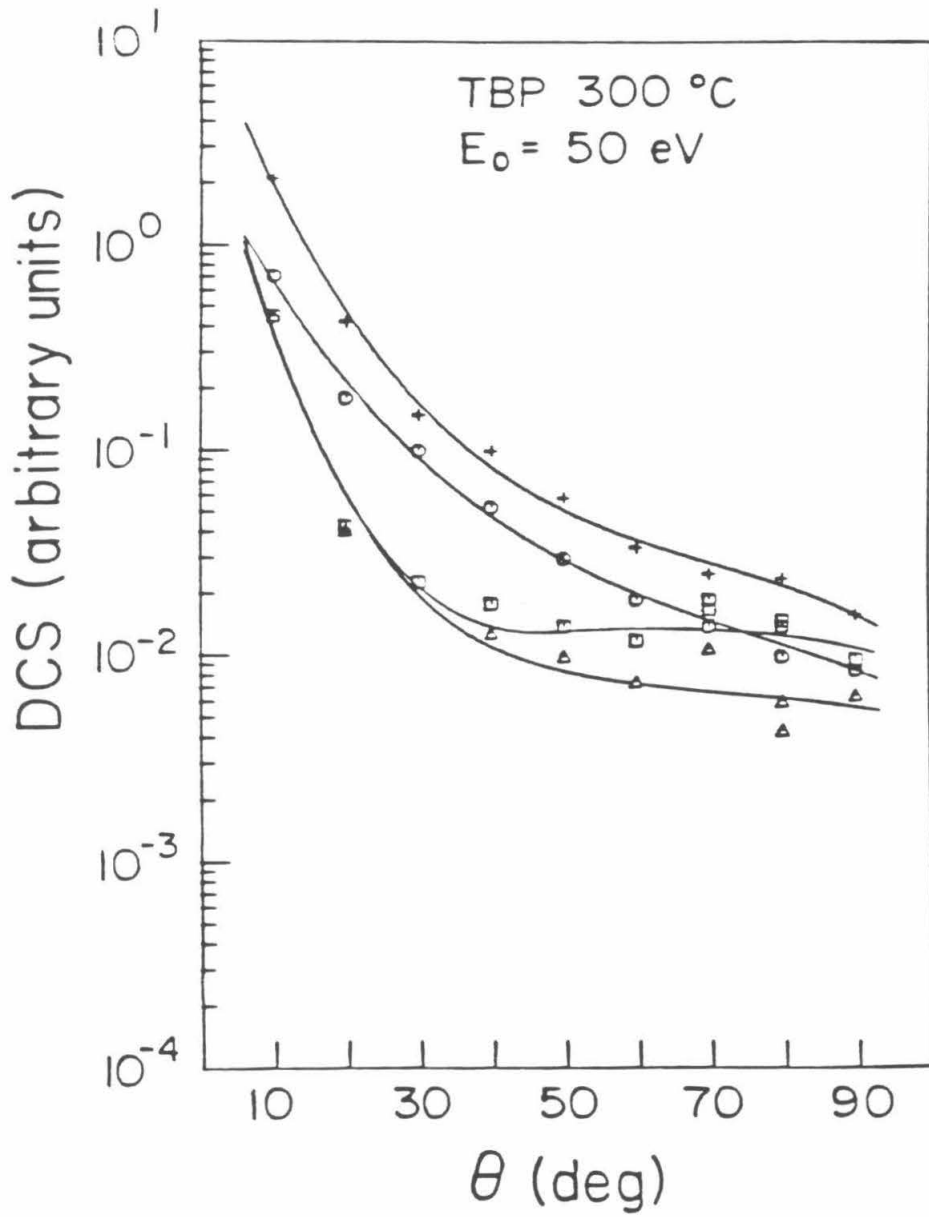
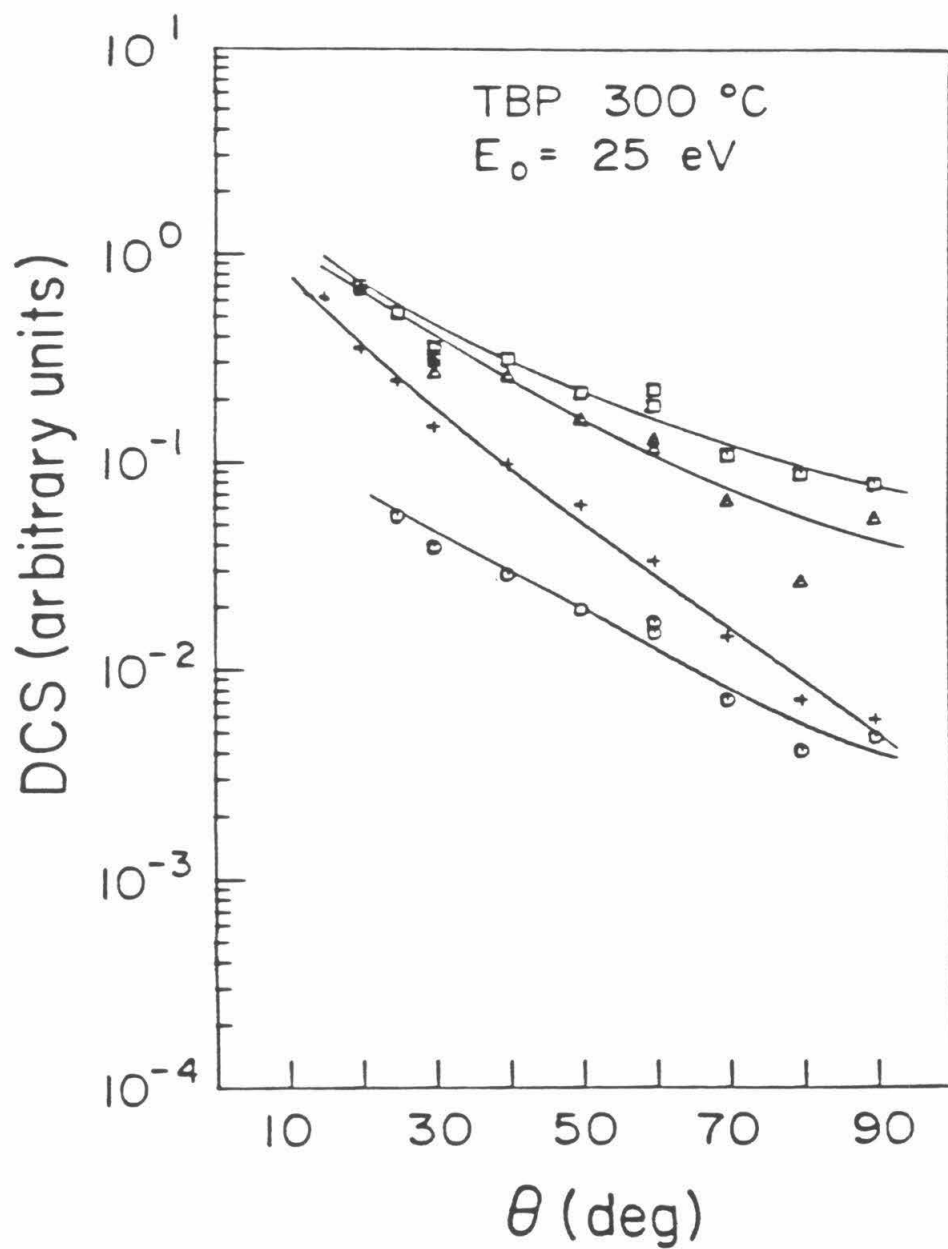


FIGURE 8.



APPENDIX 2

Paper 4: *ELECTRON-IMPACT SPECTROSCOPY OF VARIOUS
DIKETONE COMPOUNDS*

(Published at *J. Chem. Phys.*, **86**, 6701 (1987).)

**Electron-Impact Spectroscopy of Various
Diketone Compounds^a**

K. N. Walzl,^b I. M. Xavier, Jr.,^c and A. Kuppermann
Arthur Amos Noyes Laboratory of Chemical Physics,^d
California Institute of Technology, Pasadena, CA 91125

(Received 10 December 1986; accepted 15 January 1987)

Abstract

The spectra of the diketone compounds biacetyl, acetylacetone, acetonylacetone, 1,2-cyclohexanedione, and 1,4-cyclohexanedione have been investigated by the technique of low-energy, variable-angle, electron energy-loss spectroscopy. With this method, low-lying, spin-forbidden transitions have been observed. The energy difference between the lowest spin-allowed and spin-forbidden $n \rightarrow \pi^*$ excitations in the acyclic diketones is found to be 0.35 eV, on average, which is nearly the same as that of comparable acyclic monoketone compounds; in 1,2-cyclohexanedione, however, this energy difference is 0.84 eV, more than twice as large. This discrepancy in the magnitude of the $n \rightarrow \pi^*$ singlet-triplet splittings may be attributed to differing amounts of overlap between the initial and final orbitals.

^a This work was supported in part by the U. S. Department of Energy, Contract No. DE-AM03-76F00767, Project Agreement No. DE-AT03-76ER72004.

^b Work performed in partial fulfillment of the requirements for the Ph.D. degree in Chemistry at the California Institute of Technology.

^c On leave from Departamento de Quimica Fundamental; Universidade Federal de Pernambuco; 50000, Recife, Pernambuco; Brazil.

^d Contribution No. 7516.

1. INTRODUCTION

Because of their importance in photochemistry and photophysics, diketones have been studied extensively by both spectroscopic¹⁻⁵ and theoretical⁶⁻⁹ methods. Compounds with two carbonyl groups provide useful structures for the study of intramolecular energy transfer, found to be a relevant process in both singlet and triplet excited states¹⁰ and interactions involving remote carbonyl groups.¹¹ Work has been performed, primarily photoelectron spectroscopy,¹² in order to identify the mechanism by which carbonyl groups interact with each other. Even though the "through-space" interaction is expected to be small between two carbonyl groups in the same molecule,^{8,13} the "through-bond" interaction leads to molecular orbitals with clearly split energies.¹⁴

In order to more fully understand the nature of the interaction between the carbonyl groups in diketone compounds, it is helpful to have a complete picture of the low-lying electronic states, both allowed and forbidden. With the exception of biacetyl, the low-lying triplet states have not been definitively detected in most larger diketones. In biacetyl the two lowest, singlet-triplet transitions have been observed in fluorescence² and by opto-acoustic spectroscopy.¹ Electron-impact spectroscopy is a useful technique for observing and identifying forbidden, especially spin-forbidden, transitions in spectra. It is known that a spin-forbidden band exhibits a relatively constant intensity with scattering angle while a spin-allowed band is strongly forward-peaked, falling by two orders of magnitude between the scattering angles 10° to 90°.¹⁵ The combination of these effects results in a relative intensity increase of a spin-forbidden band with increased scattering angle. Another advantage of the electron-impact method is that spectral features in the far ultraviolet are easily examined. The compounds biacetyl, acetylacetone, acetonylacetone, 1,2-cyclohexanedione, and 1,4-cyclohexanedione were chosen for study as representative samples of such compounds.

2. EXPERIMENTAL

The electron spectrometer and the methods of data accumulation and analysis have been described previously.¹⁶ Briefly, an electron beam is energy-selected by a hemispherical, electrostatic energy analyzer (and the associated focusing lenses) and scattered from target vapor in a collision cell. In this work the incident beam current was between 0.5–10 nA and was typically 3 nA. Sample pressures were estimated to be between 1–10 mtorr. Electron energy-losses were determined at angles between 0° – 90° by means of a second electrostatic energy analyzer and detector.

The spectrometer resolution (as measured by the full width at half-maximum of the elastically scattered feature) varied between 50 meV and 125 meV for all reported spectra and was typically 85 meV. Peak locations determined from the spectra have an estimated uncertainty of ± 0.07 eV, and Franck-Condon limits are estimated to be within ± 0.15 eV.

Liquid samples of biacetyl (Matheson, Coleman and Bell 97+%), acetylacetone (J. T. Baker 99.7%), acetonylacetone (Aldrich 97%) and 1,2-cyclohexanedione (Aldrich 98%) were subjected to three freeze-pump-thaw cycles and used without further purification. 1,4-Cyclohexanedione (Aldrich 98%), a room temperature solid, was warmed to approximately 50° C during scanning to provide sufficient vapor pressure.

3. RESULTS

BIACETYL (2,3-BUTANEDIONE)

The biacetyl molecule is of C_{2h} symmetry with the two highest occupied molecular orbitals being largely nonbonding and confined to the oxygen atoms. The degeneracy of the two oxygen nonbonding orbitals, n_1 and n_2 is lifted by the interaction of these two orbitals. The levels arising from the symmetry-adapted linear combinations of these orbitals are designated n_+ and n_- , where $n_{\pm} = 1/\sqrt{2} (n_1 \pm n_2)$, with symmetries a_g and b_u , respectively. The energy difference is 1.9 eV, with I.P. (n_+ , a_g) = 9.55 eV and I.P. (n_- , b_u) = 11.45 eV.¹⁷ For two carbonyl groups bonded directly together the difference in energy between the n_+ and n_- orbitals is found to be relatively independent of torsional angle,¹⁷ implying that the through-bond interaction dominates the through-space interaction even for biacetyl. The next two lower occupied π orbitals have ionization potentials IP(b_g) = 13.20 eV and IP(a_u) = 14.73 eV.¹⁸ The two lowest unoccupied molecular orbitals are π^* in nature with $\pi^*(b_g)$ higher than $\pi^*(a_u)$.

Fig. 1 shows the low energy-loss region of the biacetyl spectrum between 2.0 eV and 7.0 eV at $E_0 = 25$ eV and $\theta = 10^\circ$ and 90° . In the 10° spectrum (Fig. 1a), one observes two low energy-loss features and a shoulder on the edge of a very intense band at about 7.0 eV. The lowest is the $\tilde{A}^1A_u \leftarrow \tilde{X}^1A_g$ transition with a measured onset at 2.67 eV, maximum at 2.91 eV, and extending to 3.45 eV.¹⁹ Lying between 3.82 eV and 5.28 eV with a maximum at 4.49 eV is a transition that *ab initio* SCF and CI results indicate should be designated $\tilde{B}^1B_g \leftarrow \tilde{X}^1A_g$.⁶ The broadness of this band may be due to the presence of an enolic $\pi \rightarrow \pi^*$ excitation.²⁰ The sharp peak at 6.24 eV is the first 3s member of an *s* Rydberg series converging to the lowest ionization potential, I.P. = 9.53 eV. As the scattering angle is increased, three spin-forbidden features become apparent (Fig. 1b).²¹ The lowest, overlapping greatly

with the $\tilde{A}^1A_u \leftarrow \tilde{X}^1A_g$ band, has an onset at 2.28 eV and a maximum at 2.54 eV. It is attributed to a combination of the $\tilde{a}^3B_u \leftarrow \tilde{X}^1A_g$ spin-forbidden excitation,¹ previously seen in fluorescence experiments,² and a $^3A_u \leftarrow ^1A_g$ excitation,¹⁹ the latter being the dominant contributor. A second spin-forbidden band is seen in the region between 5 eV to 6 eV with a maximum at 5.47 eV. Calculations place several $\pi \rightarrow \pi^*$ spin-forbidden transitions in this region,^{6,22} particularly a $^3B_u \leftarrow ^1A_g$ excitation predicted to be at 5.56 eV.²² A last feature is observed at 5.80 eV and seems to be identifiable as the spin-forbidden counterpart of the 3s Rydberg excitation because of its relative sharpness.

The spectral region extending from 5 eV to 10 eV (just beyond the lowest I.P.) is shown in Fig. 2a under the optical conditions $E_0 = 100$ eV and $\theta = 3^\circ$. All the transitions observed appear to be Rydberg in nature, and indeed, members of three series can be distinguished. Peaks at 6.24, 8.05, and 8.70 eV can be fit as the first three members of an *s* Rydberg series with a quantum defect $\delta = 0.97$. The *s* members are now much weaker than in the 25 eV spectra because the $n_g \rightarrow 3s$ transition is parity-forbidden by dipole selection rules. The first two members of a *p* series at 7.21 eV and 8.42 eV are fit with $\delta = 0.58$, and a feature at 7.72 eV is assigned to a *3d* excitation. Transitions at 6.28 eV and 7.20 eV have been observed previously by Ells.³

ACETYLACETONE (2,4-PENTANEDIONE)

As a room temperature vapor, acetylacetone consists of two structural isomers. One has the expected diketo molecular structure; however, acetylacetone exists predominantly as an enol.^{23,24} In the diketo form the two highest occupied molecular orbitals have a mostly oxygen, nonbonding character and are labeled n_- (I.P. = 9.60 eV) and n_+ (I.P. = 10.15 eV).²³ The highest occupied molecular orbitals in the enol compound are of the π type (I.P. = 9.00 eV) and the nonbonding

type (I.P. = 9.60 eV).²⁵

In Fig. 3 are shown spectra of acetylacetone between 3.0 eV and 6.0 eV energy loss at $E_0 = 25$ eV and $\theta = 10^\circ$ and 90° . At 10° (Fig. 3a) one sees a very strong band between 4.10 eV and 5.73 eV with a maximum at 4.70 eV. It is identified with the lowest spin-allowed $\pi \rightarrow \pi^*$ transition in the enol molecule.²⁴ One also observes a weak band with an onset at 3.83 eV and a maximum at 4.04 eV because of the first spin-allowed $n \rightarrow \pi^*$ band in the acetylacetone diketo form.^{7,24,26} An increase in scattering angle (Fig. 3b) reveals the presence of a spin-forbidden transition beginning at 3.15 eV with a maximum at 3.57 eV and overlapping with the diketo $n \rightarrow \pi^*$ singlet-singlet (S-S) band. This feature can either be attributed to a $\pi \rightarrow \pi^*$ singlet-triplet (S-T) excitation in the acetylacetone enol or possibly a $n \rightarrow \pi^*$ (S-T) excitation in the acetylacetone keto form. An additional spin-forbidden excitation is evident at 5.52 eV and is assigned as a singlet-triplet $3s$ Rydberg excitation in the enol.

The 3.5 eV to 8.5 eV energy-loss region of the spectrum measured at $E_0 = 100$ eV and $\theta = 10^\circ$ is shown in Fig. 2b. All the structure above 5.5 eV can be explained as being due to Rydberg transitions converging to the first I.P. of the enol. Indeed, peaks at 5.84 eV and 7.50 eV are the first two members of an s series with $\delta = 0.93$, peaks at 6.52 eV and 7.75 eV are the first members of a p series with $\delta = 0.66$, and peaks at 7.32 eV and 8.10 eV are the first members of a d series with $\delta = 0.15$. This fact disagrees with the assignment of Nakanishi *et al.*²⁷ who observed transitions at 7.4 eV and 8.08 eV and assigned, with the aid of a CNDO-CI calculation, the former as a valence $\pi \rightarrow \pi^*$ excitation and the latter as a valence $\sigma \rightarrow \sigma^*$ excitation.

ACETONYLACETONE (2,5-HEXANEDIONE)

The similarity between the ultraviolet absorption of 1,4-diketones and their

corresponding monoketones is striking, suggesting that the two carbonyl groups in the diketones can be considered isolated in the ground and first excited states.¹⁰ In fact, Schippers and Dekkers,¹³ using a simple electrostatic model,²⁸ calculated that the splitting of the $n \rightarrow \pi^*$ levels should be only 50 cm^{-1} . This calculation results in an underestimate of the splitting, however, because it neglects any through-bond interaction. Indeed, Dougherty *et al.*¹², using photoelectron spectroscopy, found that for the (limited) group of 1,4-diketones investigated, the mean splitting of the nonbonding orbitals was 0.3 eV. This splitting is still relatively small, explaining why Schippers and Dekkers¹¹ found that the spectra of certain rigid, cyclic 1,4-diketones appeared very similar to those of the complementary monoketones.

The region of the acetonylacetone spectrum between 2.5 eV and 6.5 eV is displayed in Fig. 4. At $E_0 = 25 \text{ eV}$ and $\theta = 10^\circ$ (Fig. 4a), one observes two broadbands and the onset of a third. The lowest, between 3.97 eV and 5.15 eV with a maximum at 4.40 eV, can be assigned with confidence as the spin-allowed $n \rightarrow \pi^*$ excitation. The second band onsets at 5.34 eV and possesses a maximum at 5.85 eV. Since the splitting between n, π^* states is expected to be very small, an assignment for this band is the lowest $\pi \rightarrow \pi^*$ (S-S) excitation. This transition is not observed in the smaller monoketones but is expected to be at a relatively high energy-loss (possibly as high as 9.0 eV) superimposed by Rydberg bands.²⁹ The large peak beginning about 6.2 eV is the $n \rightarrow 3s$ Rydberg excitation (*vide infra*). Increasing the scattering angle (Fig. 4b) produces two changes. The first is an apparent change in the onset and maximum of the spin-allowed $n \rightarrow \pi^*$ transition to 3.55 eV and 4.16 eV, respectively. As previously discussed, this change is due to the presence of a relatively enhanced, spin-forbidden, $n \rightarrow \pi^*$ transition. The second spectral change is the relative increase in intensity in the region between 5.15 eV to 5.34 eV, also caused by a singlet-triplet contribution. A definitive band maximum is not obtained from the spectra.

The Rydberg portion of the acetonylacetone spectrum is included in Fig. 2c, which was measured under the optical conditions $E_0 = 100$ eV and $\theta = 10^\circ$ and spans the energy-losses between 3.5 eV and 8.5 eV. In addition to those already mentioned, peaks are observed at 6.62, 7.49, and 8.17 eV. Assuming that the transition at 6.62 eV corresponds to the $n \rightarrow 3s$ excitation, the transition at 7.49 eV to the $n \rightarrow 3p$ excitation, and the transition at 8.17 eV to the $n \rightarrow 3d$ excitation, the best fit to the previously measured diketone (and ketone^{29,30}) quantum defects is found using an ionization potential I.P. = 9.95 eV. Specifically, for this I.P. one calculates $\delta (n \rightarrow 3s) = 0.98$, $\delta (n \rightarrow 3p) = 0.65$, and $\delta (n \rightarrow 3d) = 0.24$. An additional peak was observed at 8.84 eV and is possibly due to an overlapping combination of higher Rydberg transitions.

1,2-CYCLOHEXANEDIONE

Even though 1,2-cyclohexanedione is exclusively in the ketonic form in the solid state,³¹ it exists to a large extent in the enolic form in solution.³² Calculations indicate that it may be primarily enolic in the gas phase as well.³³ Fig. 5 shows spectra in the energy-loss region between 2.5 eV and 6.0 eV at $E_0 = 50$ eV, $\theta = 10^\circ$ and $E_0 = 25$ eV, $\theta = 50^\circ$. The similarity between the spectrum of acetylacetone and 1,2-cyclohexanedione in this energy-loss region is striking. At $E_0 = 50$ eV and $\theta = 10^\circ$ (Fig. 5a), one sees an intense band between 4.34 eV and 5.70 eV with a maximum at 4.84 eV. As with acetylacetone, this band is assigned to the lowest, spin-allowed $\pi \rightarrow \pi^*$ enol transition. The weak band with an onset at 3.69 eV and maximum at 4.02 eV is due to the lowest, spin-allowed $n \rightarrow \pi^*$ transition of the ketonic form. Even though the orientation of the carbonyl groups is different from that in biacetyl, one expects nearly the same energy difference (1.9 eV) between the n_+ and n_- orbitals because of the dominance of the through-bond interaction.¹⁷ Thus, the second lowest, spin-allowed $n \rightarrow \pi^*$ transition should be at approximately

5.9 eV and should be obscured by enol Rydberg bands. An increase in scattering angle and a decrease in incident electron energy (Fig. 5b) reveal the presence of a spin-forbidden band beginning at 2.70 eV with a maximum at 3.18 eV assigned as the lowest $n \rightarrow \pi^*$ (S-T) excitation of the ketonic form. The DCS curves for these valence transitions confirm their spin-allowed or spin-forbidden nature.

The higher energy-loss region between 4 eV and 10 eV, at $E_0 = 100$ eV and $\theta = 10^\circ$, is shown in Fig. 2d. Only three distinct Rydberg bands are evident, located at 6.10, 6.92, and 7.48 eV. An ionization potential I.P. = 9.40 eV is determined if one assumes the three bands to be due to transitions to the 3s, 3p, and 3d orbitals and also assumes quantum defects $\delta = 0.97, 0.66, \text{ and } 0.34$, respectively.

1,4-CYCLOHEXANEDIONE

1,4-Cyclohexanedione has D_2 symmetry (a "twist" configuration³⁴) with coaxial carbonyl groups. Through-space interactions provide a minimum contribution; thus, the splitting of the two highest occupied, nonbonding orbitals is relatively small (0.2 eV) when compared to that in other 1,4-diketones,^{12,17} with the measured ionization potentials being I.P. (n_-) = 9.65 eV and I.P. (n_+) = 9.85 eV.¹² Fig. 6 shows the 3.0 eV to 6.5 eV energy-loss region of the 1,4-cyclohexanedione spectrum at $E_0 = 50$ eV, $\theta = 5^\circ$ and $E_0 = 25$ eV, $\theta = 35^\circ$. The low intensity of the spectra arises from the relatively low sample pressure achieved for this compound at the scattering center (estimated to be ~ 2 mtorr). Under optical conditions (Fig. 6a) one observes a band with an onset at 3.73 eV and a maximum at 4.68 eV. This is due to the $n \rightarrow \pi^*$, ${}^1A \leftarrow {}^1A$ dipole, symmetry-forbidden transition and has been seen previously in solution (maximum = 4.34 eV)³⁵ and in low-temperature, single crystals (onset = 3.89 eV, maximum = 4.40 eV).³⁶ The onset of a broadband, which appears to be superimposed by a 3s Rydberg transition, is observed

at 5.66 eV and may be due to the $\pi \rightarrow \pi^*$, ${}^1B_1 \leftarrow {}^1A$ excitation. When the incident energy is lowered and the scattering angle increased (Fig. 6b), the $n \rightarrow \pi^*$, ${}^3A \leftarrow {}^1A$ transition becomes evident, onsetting at 3.20 eV and maximizing at 4.13 eV. The presence of another spin-forbidden band with maximum at 5.78 eV is indicated. Contributions to the intensity may come from either the $\pi \rightarrow \pi^*$, the ${}^3B_1 \leftarrow {}^1A$ excitation or the $n \rightarrow 3s$ (S-T) Rydberg excitation.

The 1,4-cyclohexanedione spectrum under optical conditions (Fig. 6a) is extended to 10 eV energy-loss in Fig. 2e. Additional peaks are observed at 6.58, 7.36, and 7.95 eV. (The peak at 6.67 eV is due to an Hg impurity in the vacuum system.) Using an I.P. = 9.75 eV, the mean of I.P. (n_-) and I.P. (n_+),¹² assignments and quantum defects of $n \rightarrow 3s$ ($\delta = 0.93$) at 6.58 eV, $n \rightarrow 3p$ ($\delta = 0.61$) at 7.36 eV, and $n \rightarrow 3d$ ($\delta = 0.25$) at 7.95 eV are determined.

4. DISCUSSION AND CONCLUSIONS

As one might expect from previous results,¹⁰ the energies of the lowest $n \rightarrow \pi^*$ excitations for the acyclic diketones, as the distance between carbonyl groups increases, approach those of acetone. The lowest spin-allowed and spin-forbidden $n \rightarrow \pi^*$ excitations are 2.91 eV and 2.54 eV for biacetyl, 4.04 eV and 3.57 eV for acetylacetone, 4.40 eV and 4.16 eV for acetylacetone, and 4.38 eV and 4.18 eV for acetone.^{29,37} The values for these transitions in 1,4-cyclohexanedione are also comparable to those for acetone, the lowest singlet-singlet and singlet-triplet $n \rightarrow \pi^*$ excitations being 4.68 eV and 4.13 eV, respectively. This trend appears to hold also for the lowest spin-forbidden $\pi \rightarrow \pi^*$ excitation, at least as regards the band onsets (the most reproducible measure of the band positions); the onset is 5.15 eV for both acetylacetone and acetone.

The mean value for the singlet-triplet splitting of the n, π^* state in the acyclic diketones examined in this paper is 0.35 eV, a splitting comparable to the mean

value of 0.30 eV for the small monocarbonyls formaldehyde, acetaldehyde, and acetone.^{29,38,39} A remarkable contrast is provided by 1,2-cyclohexanedione, in which the singlet-triplet splitting for the n,π^* state is 0.84 eV. The singlet-triplet energy difference for a given electron orbital configuration results from the stronger correlation of electron motions in the triplet state than in the singlet state; i.e., the Pauli principle acts as a force minimizing electron-electron repulsion in the triplet state.⁴⁰ A simple qualitative analysis⁴¹ reveals that the magnitude of the singlet-triplet energy splitting is proportional to the overlap integral of the initial and final orbitals. For a single carbonyl group oriented along the z-axis, the highest occupied nonbonding orbital is represented by an oxygen p_y orbital, and there is minimum overlap with the π and π^* orbitals, for which the yz-plane is a nodal plane. This small n,π^* overlap also applies to the case of biacetyl. The highest occupied n orbital and the lowest unoccupied π^* orbital are linear combinations of the corresponding isolated orbitals; however, since the carbonyl groups are oriented in a trans arrangement, the linear combinations of n and π^* orbitals overlap to the same small extent as in the monocarbonyls.

In 1,2-cyclohexanedione, a different orientation may exist because of the constraint imposed by the ring. Unlike the carbonyl groups in biacetyl, which lie in a plane, the two carbonyl groups in 1,2-cyclohexanedione can be twisted away from coplanarity. The overlap of the highest occupied n orbital (a linear combination of individual carbonyl nonbonding orbitals) with the lowest unoccupied π^* orbital (a linear combination of individual carbonyl π^* orbitals) would now be larger, hence, a larger n,π^* singlet-triplet splitting. Whether the effect of the increased orbital overlap is enough to account for an increase of the n,π^* singlet-triplet splitting by a factor larger than two or whether additional factors are at play is uncertain.

In summary, the low-energy, variable-angle, electron energy-loss spectroscopy of five diketone compounds with varying carbonyl separations and orientations

has been investigated. The increase in the number of bands compared to the monocarbonyls is in accord with the splitting caused by the through-bond interaction of like orbitals. Low-lying, spin-forbidden excitations have been observed and in the case of 1,2-cyclohexanedione, a very large singlet-triplet splitting arises from an increased overlap of initial and final orbitals.

5. ACKNOWLEDGMENTS

One of the authors (IMX) wishes to acknowledge a graduate fellowship from CAPES and UFPE (Brazil).

References

1. K. Kaya, W. R. Harshbarger, and M. Robin, *J. Chem. Phys.* **60**, 4231 (1974).
2. G. M. Almy, H. Q. Fuller, and G. D. Kinzer, *J. Chem. Phys.* **8**, 37 (1940).
3. V. R. Ells, *J. Am. Chem. Soc.* **60**, 1864 (1938).
4. J. W. Sidman and D. S. McClure, *J. Am. Chem. Soc.* **77**, 6461 (1955).
5. G. Porter and M. W. Windsor, *Proc. R. Soc. A* **245**, 238 (1958).
6. T. -K. Ha, *Chem. Phys. Lett.* **57**, 64 (1978).
7. G. S. Hammond, W. G. Borduin, and G. A. Guter, *J. Am. Chem. Soc.* **81**, 4682 (1959).
8. D. J. Pasto, D. M. Chipman, and J. J. Worman, *J. Phys. Chem.* **86**, 3981 (1982).
9. R. Hoffmann *Acc. Chem. Res.* **4**, 1 (1971).
10. E. A. Lissi, M. V. Encinas, F. Castañeda, and F. A. Olea, *J. Phys. Chem.* **84**, 251 (1980).
11. P. H. Schippers and H. P. Dekkers, *J. Am. Chem. Soc.* **105**, 145 (1983).
12. D. Dougherty, P. Brint, and S. P. McGlynn, *J. Am. Chem. Soc.* **100**, 5597 (1978).
13. P. H. Schippers and H. P. Dekkers, *J. Chem. Soc. P2* **1982**, 1429 (1982).
14. R. Hoffmann, E. Heilbronner, and R. Gleiter, *J. Am. Chem. Soc.* **92**, 706 (1970).
15. S. Trajmar, J. K. Rice, and A. Kuppermann, *Adv. Chem. Phys.* **18**, 15 (1970).
16. C. F. Koerting, Ph. D. Thesis, California Institute of Technology, Pasadena CA 1985, and references therein.
17. D. O. Cowan, R. Gleiter, J. Hashmall, E. Heilbronner, and V. Hornung, *Angew. Chem. Internat. Ed.* **10**, 401 (1971).

18. S. P. McGlynn and J. L. Meeks, *J. Electron Spectroscopy* **6**, 269 (1975).
19. G. Herzberg, *Electronic Spectra of Polyatomic Molecules* (Van Nostrand Reinhold Co., New York (1966)), p. 667.
20. D. Ben-Amotz and I. Y. Chan, *J. Phys. Chem.* **86**, 2428 (1982).
21. The relative differential cross section (DCS) for the elastic peak and inelastic features were obtained by a method described in the references O. A. Mosher, W. M. Flicker, and A. Kuppermann, *J. Chem. Phys.* **59**, 6502 (1973) and O. A. Mosher, M. S. Foster, W. M. Flicker, A. Kuppermann, and J. L. Beauchamp, *J. Chem. Phys.* **62**, 3424 (1975). In the case of severely overlapping bands, dividing points for calculating DCS's were chosen at a midpoint between the maxima. Because of the great deal of band overlap, all the 25 eV DCS curves exhibited some spin-forbidden behavior, while the 50 eV curves exhibited distinct allowed or forbidden behavior.
22. J. M. LeClercq, C. Mijoule, and P. Yvan, *J. Chem. Phys.* **64**, 1464 (1976).
23. J. Powling and H. J. Bernstein, *J. Am. Chem. Soc.* **73**, 4553 (1951).
24. H. Nakanishi, H. Morita, and S. Nagakura, *Bull. Chem. Soc. Jpn.* **50**, 2255 (1977).
25. A. Schweig, H. Vermeer, and U. Weidner, *Chem. Phys. Lett.* **26**, 229 (1974).
26. R. S. Rasmussen, D. D. Tunnidiff, and R. R. Brattain, *J. Am. Chem. Soc.* **71**, 1068 (1949).
27. H. Nakanishi, H. Morita, and S. Nagakura, *Bull. Chem. Soc. Jpn.* **51**, 1723 (1978).
28. F. London, *J. Phys. Chem.* **46**, 305 (1942).
29. K. N. Walzl, C. F. Koerting, and A. Kuppermann, to be submitted.
30. D. C. Moule and A. D. Walsh, *Chem. Rev.* **75**, 67 (1975).
31. C. Duval and J. Lecomte, *Compt. Rend.* **254**, 36 (1962).

32. G. Schwarzenbach and C. Wittwer, *Helv. Chim. Acta* **30**, 663 (1947).
33. W. E. Noack, *Theo. Chem. Acta* **53**, 101 (1979).
34. P. Dowd, T. Dyke, and W. Klemperer, *J. Am. Chem. Soc.* **92**, 6327 (1970).
35. K. Ozeki, M. Inagaki, and J. Tanaka, *Bull. Chem. Soc. Jpn.* **42**, 3076 (1969).
36. K. Ozeki and J. Tanaka, *Bull. Chem. Soc. Jpn.* **42**, 3390 (1969).
37. W. M. St. John, R. C. Estler, and J. P. Doering, *J. Chem. Phys.* **61**, 763 (1974).
38. S. Taylor, D. Wilden, and J. Comer, *Chem. Phys.* **70**, 291 (1982).
39. W. M. St. John, R. C. Estler, and J. P. Doering, *J. Chem. Phys.* **61**, 763 (1974).
40. N. J. Turro, *Modern Molecular Photochemistry* (The Benjamin/Cummings Publishing Co., Menlo Park (1978)), pp. 28–32.
41. S. P. McGlynn, F. J. Smith, and G. Cilento, *Photochem. Photobio.* **3**, 269 (1964).

Figure Captions

1. 2,3-Butanedione (biacetyl) energy-loss spectra at an incident-electron energy $E_0 = 25$ eV and scattering angles: a) $\theta = 10^\circ$ and b) $\theta = 90^\circ$. Incident-electron current = 2 nA. Spectra are multiplied by any indicated expansion factors before plotting.

2. a) 2,3-Butanedione (biacetyl) energy-loss spectrum between 5.0 eV and 10.0 eV at $E_0 = 100$ eV and $\theta = 3^\circ$. The peak at 6.67 eV is due to an Hg contamination in the vacuum system. b) 2,4-Pentanedione (acetylacetone) energy-loss spectrum between 3.5 eV and 8.5 eV at $E_0 = 100$ eV and $\theta = 10^\circ$. c) 2,5-Hexanedione (acetonylacetone) energy-loss spectrum between 3.5 eV and 8.5 eV at $E_0 = 100$ eV and $\theta = 10^\circ$. d) 1,2-Cyclohexanedione energy-loss spectrum between 4.0 eV and 10.0 eV at $E_0 = 100$ eV and $\theta = 10^\circ$. e) 1,4-Cyclohexanedione energy-loss spectrum between 3.0 eV and 10.0 eV at $E_0 = 50$ eV and $\theta = 5^\circ$.

3. 2,4-Pentanedione (acetylacetone) energy-loss spectra at an incident energy $E_0 = 25$ eV and scattering angles: a) $\theta = 10^\circ$ and b) $\theta = 90^\circ$. Incident electron current = 2 nA.

4. 2,5-Hexanedione (acetonylacetone) energy-loss spectra at an incident energy $E_0 = 25$ eV and scattering angles: a) $\theta = 10^\circ$ and b) $\theta = 90^\circ$. Incident electron current = 4 nA.

5. 1,2-Cyclohexanedione energy-loss spectra at: a) $E_0 = 50$ eV and $\theta = 10^\circ$ and b) $E_0 = 25$ eV and $\theta = 50^\circ$. Incident electron current = 0.5 nA.

6. 1,4-Cyclohexanedione energy-loss spectra at: a) $E_0 = 50$ eV, $\theta = 5^\circ$ and b) $E_0 = 25$ eV, $\theta = 35^\circ$. Incident electron current = 5 nA.

FIGURE 1.

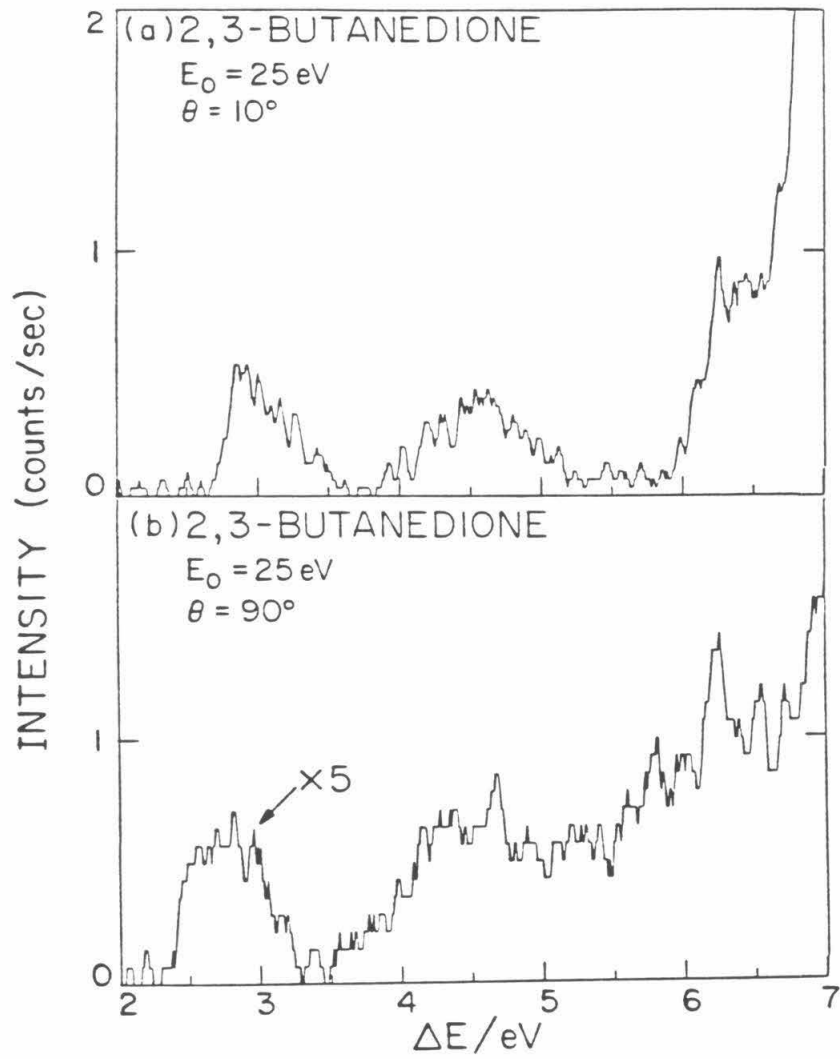


FIGURE 2.

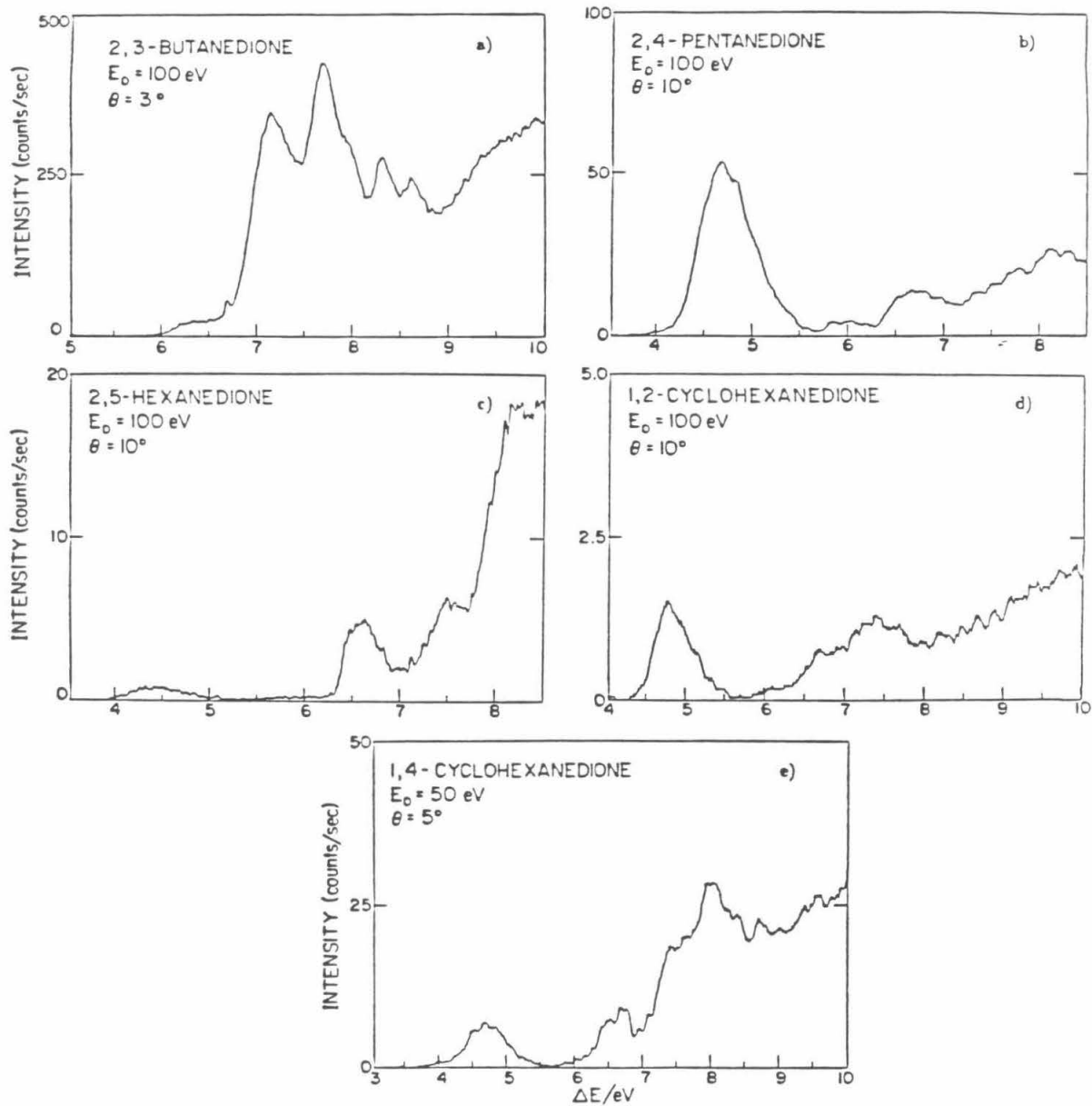


FIGURE 3.

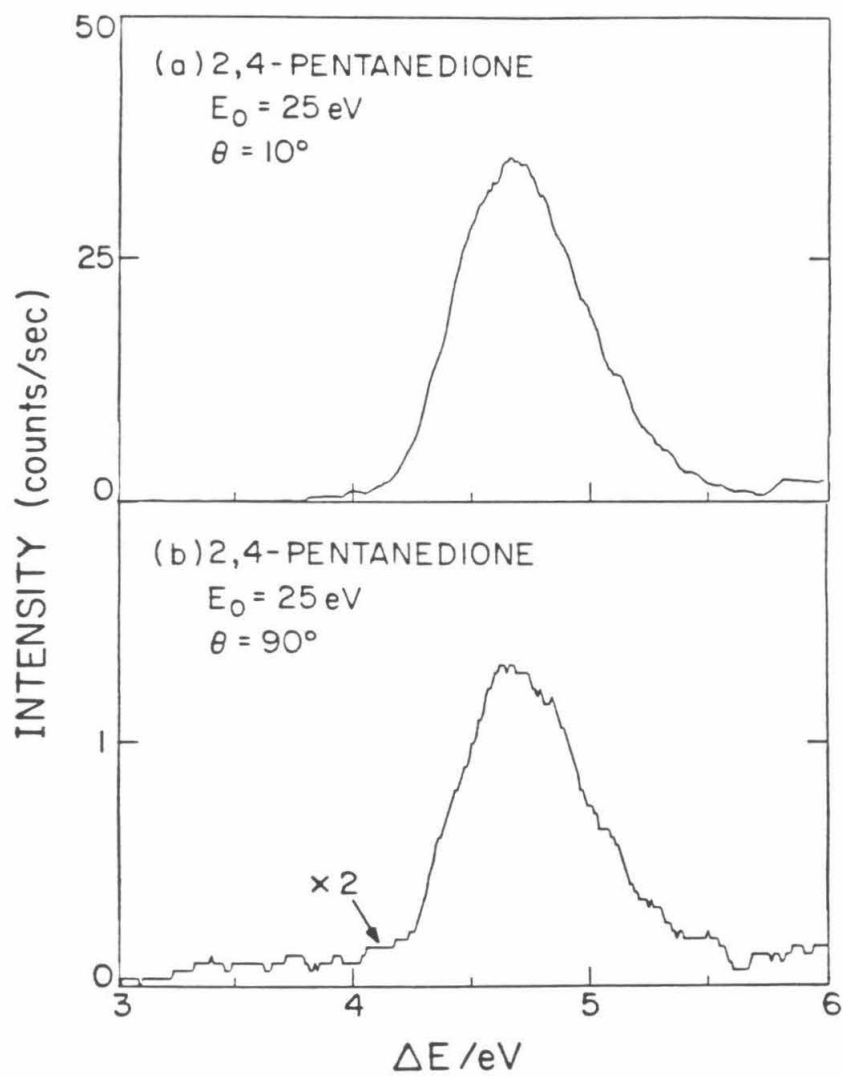


FIGURE 4.

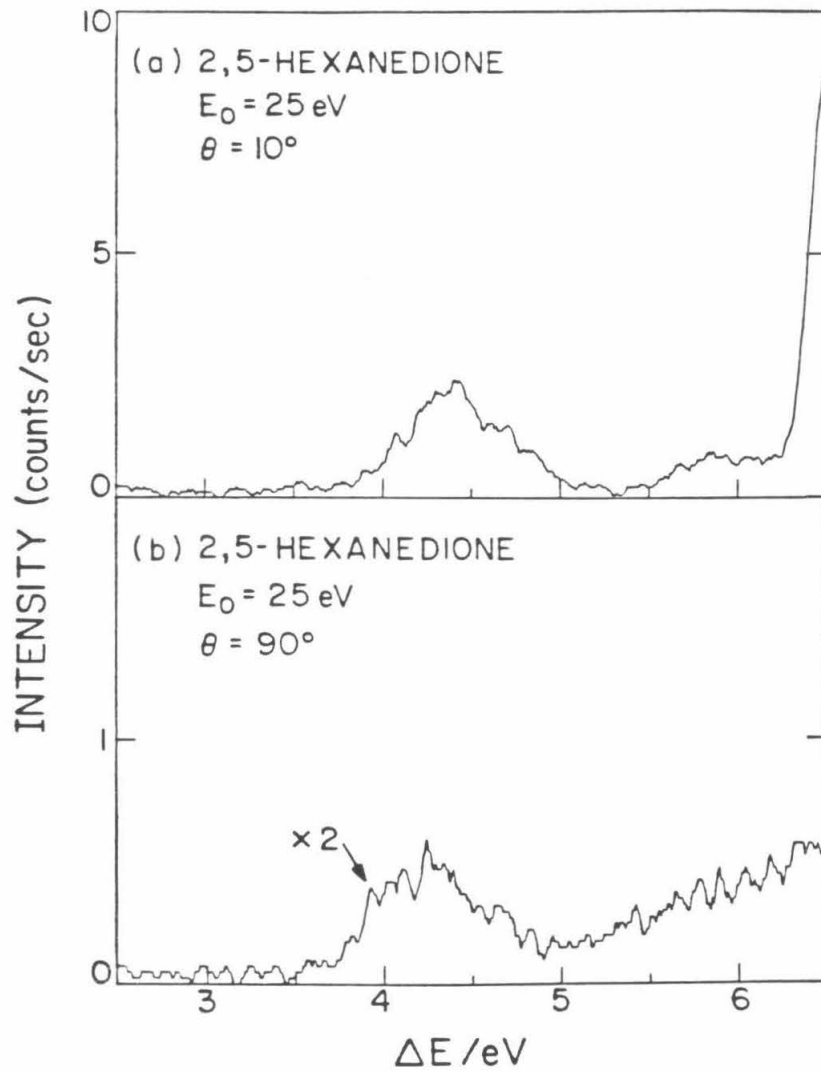


FIGURE 5.

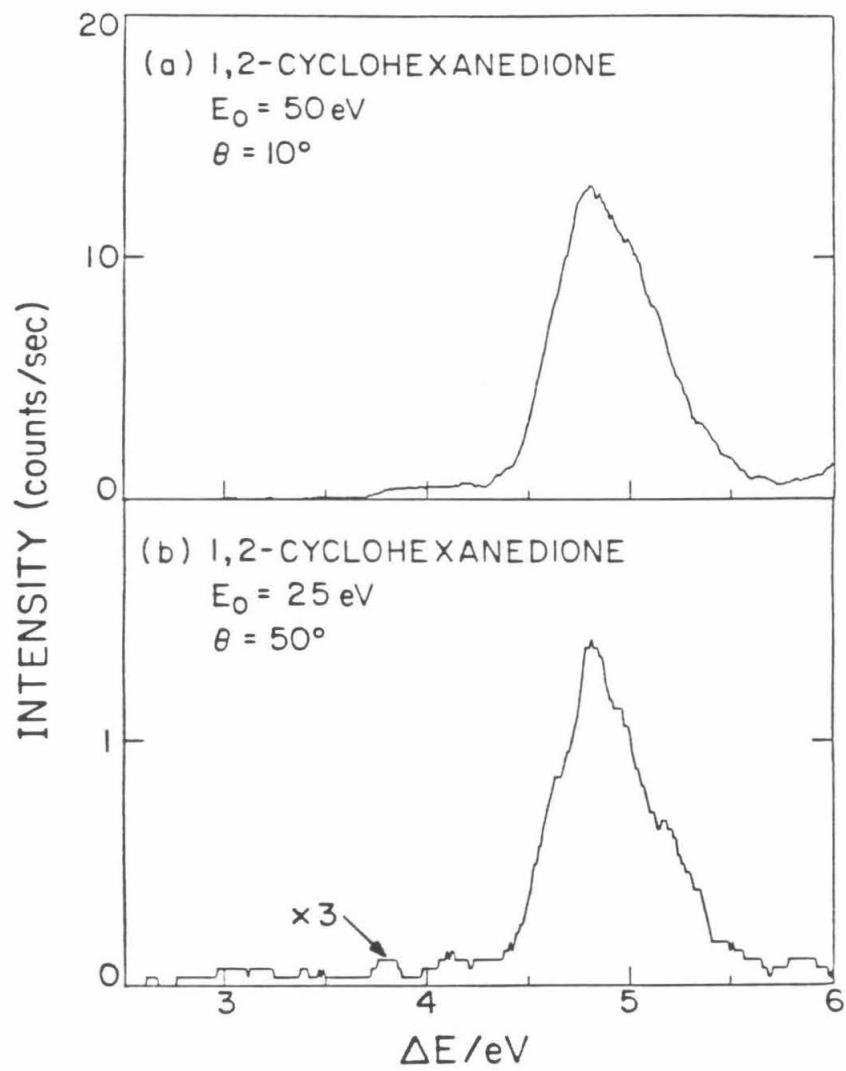


FIGURE 6.

